J Comput Neurosci
DOI 10.1007/s10827-010-0296-6

Control of neural synchrony using channelrhodopsin-2: a computational study

Sachin S. Talathi · Paul R. Carney · Pramod P. Khargonekar

Received: 8 September 2010 / Revised: 3 November 2010 / Accepted: 18 November 2010

Abstract In this paper, we present an optical stimulation based approach to induce 1:1 in-phase synchrony in a network of coupled interneurons wherein each interneuron expresses the light sensitive protein channelrhodopsin-2 (ChR2). We begin with a transition rate model for the channel kinetics of ChR2 in response to light stimulation. We then define "functional optical time response curve (fOTRC)" as a measure of the response of a periodically firing interneuron (transfected with ChR2 ion channel) to a periodic light pulse stimulation. We specifically consider the case of unidirectionally coupled (UCI) network and propose an open loop control architecture that uses light as an actuation signal to induce 1:1 in-phase synchrony in the UCI network. Using general properties of the spike time response curves (STRCs) for Type-1 neuron model (Ermentrout, Neural Comput 8:979-1001, 1996) and fOTRC, we estimate the (open loop) optimal actuation signal parameters required to induce 1:1 in-phase synchrony. We then propose a closed loop controller architecture and a controller algorithm to robustly sustain stable 1:1 in-phase synchrony in the presence of unknown deviations in the network parameters. Finally, we test the performance of this closed-loop controller in a network of mutually coupled (MCI) interneurons.

Keywords Synchrony · Optical stimulation · Time response curve · Arnold Tongue · Optogenetics · Channelrhodopsin-2

Action Editor: Carson C. Chow

S. S. Talathi (✉) · P. R. Carney
Department of Pediatrics, University of Florida, Gainesville, FL 32611, USA
e-mail: talathi@ufl.edu, sachin.talathi@gmail.com

S. S. Talathi · P. R. Carney
J Crayton Pruitt Family Department of Biomedical Engineering, University of Florida, Gainesville, FL 32611, USA

P. R. Carney
e-mail: carnepr@peds.ufl.edu

P. P. Khargonekar
Department of Electrical and Computer Engineering, University of Florida, Gainesville, FL 32611, USA
e-mail: ppk@ufl.edu

1 Introduction

Neural synchrony refers to the pattern of precisely coordinated dynamics of large numbers of heterogeneously connected networks of neurons within a given region of the brain or between multiple brain regions, leading to the generation of macroscopically observable brain rhythms (Buzsaki 2006). It is believed to be the critical mechanism by which the brain can integrate information across different sensory modalities including in various combinations: the haptic, visual, olfactory and auditory senses to create a coherent representation of object properties (Uhlhaas and Singer 2006). Studies of visuo-motor integration in cat visual cortex (Roelfsema et al. 1997) have also demonstrated an important role for neural synchrony in facilitating dynamic and flexible interaction between the sensory and motor areas to allow for versatility of sensory-motor coordination. Studies on human subjects using non-invasive recording techniques such as EEG have further demonstrated that neural synchrony is associated with cognitive functions that require large-scale

Published online: 21 December 2010

integration of distributed neural activity (Varela et al. 2001). In addition, there is growing evidence from literature to support the hypothesis that neural synchrony is a critical component of the temporal coding strategies for information processing in the brain (Uhlhaas et al. 2010).

As a result, a number of scientific studies have focused on the mechanisms of neural synchrony in the brain cortical networks (Fisahn et al. 1998; vanVreeswijk et al. 1994; Ernst et al. 1995; Chow et al. 1998). Early computational studies by Wang and Rinzel (1992), demonstrated that synaptically coupled interneurons can exhibit in-phase synchrony in their firing activity which led to the hypothesis that interneurons play a significant role in the generation of synchronous brain activity (Traub et al. 1996; Whittington et al. 1995). Subsequent theoretical and experimental studies have confirmed the role for interneurons in synchrony (Swadlow et al. 1998; Beierlein et al. 2000; Galarreta and Hestrin 2001; Lewis and Rinzel 2003; Skinner et al. 2005). These studies lead to the general conclusion that while homogeneous networks of fast spiking interneurons can produce synchrony, the synchrony is very sensitive to heterogeneity in network parameters. Recent work by our group and others have demonstrated that the sensitivity to heterogeneity can be mitigated through a number of biological mechanisms including spike timing dependent plasticity (Zhigulin et al. 2003; Talathi et al. 2008), signal propagation delays (Crook et al. 1997; Talathi et al. 2010) and electrical coupling (Bennett and Zukin 2004). While it is clear that a number of different biological mechanisms exist to induce synchrony in brain networks, very few studies have focused on neural stimulation based approaches to induce synchrony in brain networks.

Optogenetics is a rapidly developing novel optical stimulation technique that employs light activated ion channels to excite or suppress impulse activity in neurons with high temporal and spatial resolution (Deisseroth et al. 2006). This technique holds enormous potential to externally control activity states in neuronal networks. It is, however, unclear as to how optical stimulation will interfere with the intrinsic network dynamics shaped by the neurons and their synaptic interactions. In this paper, we investigate *whether and how optical stimulation can be used to achieve neural synchrony in the presence of significant heterogeneity in the network parameters*. We specifically consider a simple unidirectionally coupled network of two interneurons (UCI network) as a computational test-bed for this study. Each neuron in the UCI network expresses light sensitive ion channel channelrhodopsin-2 (ChR2). We then systematically study open-loop and closed-loop control strategies to induce 1:1 in-phase synchrony in the UCI network. We conclude by presenting numerical simulation results for the performance of the closed loop controller in a network of mutually coupled interneurons (MCI network).

The manuscript is organized as follows: We first present the mathematical model for the fast-spiking interneuron, the synapse and the channel kinetics of the light activated ChR2. We introduce the notion of functional optical time response curve (fOTRC) in analogy with spike time response curves (STRCs). This fOTRC construct allows us to obtain a discrete non-linear map for the evolution of the time difference in the spike times of the coupled neurons in the UCI network in the presence of periodic light pulse stimulation. We use this discrete map to determine the open loop control parameters for the light pulse actuation signal that can trigger 1:1 in-phase neural synchrony in the UCI network. The open loop control design is then modified to a closed loop feedback controller design to make the neural synchrony in the closed loop system robust to unknown perturbations in the network parameters. Finally we test the performance of this controller when the UCI network is modified to incorporate feedback synaptic coupling.

2 Methods

2.1 Model neuron and synapse

We consider a single compartment fast-spiking interneuron model of Wang and Buzsaki (1996), that consists of a fast sodium channel, delayed rectifier potassium channel and a leak channel. In addition, we include an ion channel for the light activated protein ChR2. The dynamical equation for the model neuron is given as:

$$\begin{aligned} C\frac{dV(t)}{dt} &= I_{DC} + g_{Na}m_{\infty}^{3}h(t)(E_{Na} - V(t)) \\ &\quad + g_{K}n^{4}(t)(E_{K} - V(t)) + g_{L}(E_{L} - V(t)) \\ &\quad + I_{\mathrm{ChR2}}(t) + I_{S}(t) \end{aligned} \tag{1}$$

where $C = 1\ \mu\mathrm{F/cm}^2$. We denote by $V(t)$ the membrane potential. The external DC current denoted by I_{DC} is set such that the neuron spikes with intrinsic period $T_0(I_{DC}) \propto 1/\sqrt{I_{DC} - I_0}$, where I_0 is the bifurcation point for the neuron to transition to regular spiking mode. Also, $I_S(t) = g_s S(t)(E_I - V(t))$ is the inhibitory synaptic current from the presynaptic neuron (V_{pre}). Note that g_s represents the strength of the synaptic

connection. We use E_r, r = Na, K, L, to denote the reversal potentials of the sodium and potassium ion channels and the leak channel respectively while E_I denotes the reversal potential of the inhibitory synapse. Moreover, g_r, r = Na, K, L represents the conductance of sodium, potassium and the leak channel respectively. The current flowing through the light activated ChR2 ion channel is denoted by I_{ChR2}. Channel kinetics for I_{ChR2} are described in Section 2.2. The steady state activation for sodium current is given by $m_\infty = \alpha_m/(\alpha_m + \beta_m)$. The inactivation variable for sodium channel $h(t)$ and the activation variable for potassium current $n(t)$ satisfies the following first order kinetic equation: $\frac{dX(t)}{dt} = \phi(\alpha_X(V(t))(1 - X(t)) - \beta_X(V(t))X(t))$, where $X(t) = h(t), n(t)$ with $\phi = 5$. The functions α_X and β_X are given in Table 1. The quantity $S(t)$ denotes the fraction of bound receptors and satisfies the following first order kinetic equation, (Abarbanel et al. 2003; Talathi et al. 2008),

$$\dot{S}(t) = \frac{S_0\left(V_{\text{pre}}(t)\cdot\theta(t)\right) - S(t)}{\hat{\tau}\left(S_I - S_0\left(V_{\text{pre}}(t)\cdot\theta(t)\right)\right)}$$

where $\theta(t) = \sum_i \Theta(t - t_i).\Theta((t_i + \tau_R) - t)$. $\Theta(X)$ is the heaviside function satisfying $\Theta(X) = 1$ if $X > 0$ else $\Theta(X) = 0$, and t_i is the time of the ith presynaptic neuronal spike ($V_{\text{pre}}(t)$). The kinetic equation for $S(t)$ involves two time constants, $\tau_R = \hat{\tau}(S_I - 1)$, the docking time for the neurotransmitter and $\tau_D = \hat{\tau}S_I$, the undocking time constant for the neurotransmitter binding. Finally, $S_0(\theta)$ is the sigmoidal function given by, $S_0(\theta) = 0.5(1 + \tanh(120(\theta - 0.1)))$.

2.2 Model for channel kinetics of ChR2

We adopt a four-state transition rate model as shown in Fig. 1 for the channel kinetics of ChR2 (Nikolic et al. 2009). This model simulates the photocurrent kinetics for the light activated ChR2 channel through two sets of intratransitional states: $C1 \leftrightarrow O1$, which is more dark adapted and $C2 \leftrightarrow O2$, which is more light adapted as shown in Fig. 1. In the absence of optical stimulation, ChR2 is assumed to be in state C1. In the light adapted state, however, ChR2 molecules are distributed across all four states, with increasing preference to be in state O2 as the duration of optical illumination increases. Following light absorption, the ChR2 molecules transition to the state O1. For a given level of optical excitation, there exists equilibrium between states O1 and C1. Also, as the duration of illumination increases, there is a transition to the state O2. The O2 state exists in equilibrium with the state C2, which then slowly (seconds) converts back to the state C1 following the termination of the optical signal. This process can be described through the following set of rate equations:

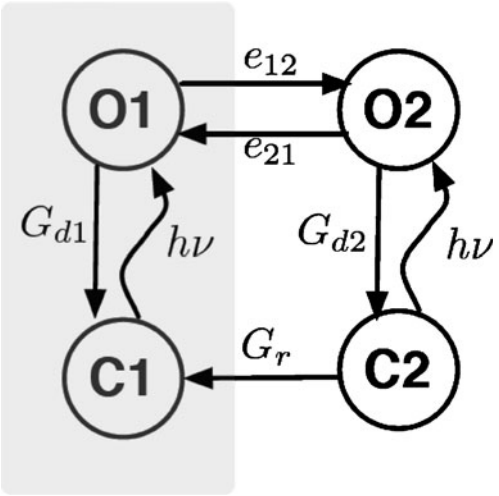

Fig. 1 Schematic diagram of the four-state model for ChR2 channel kinetics (adapted from Nikolic et al. 2009)

$$\begin{aligned}
\frac{dC1}{dt} &= G_r C2 + G_{d1} O1 - \epsilon_1 F p C1 \\
\frac{dO1}{dt} &= \epsilon_1 F p C1 - (G_{d1} + e_{12})\, O1 + e_{21} O2 \\
\frac{dO2}{dt} &= \epsilon_2 F p C2 - (G_{d2} + e_{21})\, O2 + e_{12} O1 \\
\frac{dp}{dt} &= \frac{S_0(\theta_{\text{optical}}) - p}{\tau_{\text{ChR}}}
\end{aligned} \tag{2}$$

where $C1$, $C2$ and $O1$ and $O2$ represent the fraction of ChR2 molecules in closed and open states respectively, such that $C1 + C2 + O1 + O2 = 1$. The number of photons absorbed by ChR2 molecules per unit time when light of intensity I (mW/mm^2) at wavelength of λ (nm) is applied is given by $F = \frac{0.0006 I\lambda}{w_{\text{loss}}}$. The multiplication

Table 1 Transition rates for the activation and inactivation variables of the ion channels

$\alpha_m = \frac{-0.1(V(t)+35)}{e^{-0.1(V(t)+35)} - 1}$	$\beta_m = 4e^{-(V(t)+60)/18}$
$\alpha_h = 0.07e^{-(V(t)+58)/20}$	$\beta_h = \frac{1}{e^{-0.1(V(t)+28)} + 1}$
$\alpha_n = \frac{-0.01(V(t)+34)}{e^{-0.1(V(t)+34)} - 1}$	$\beta_n = \frac{0.125}{e^{-(V+44)/88}}$

factor of 0.0006 is the conversion factor assuming the retinal cross-section $\sigma_{\text{ret}} \approx 1.2 \times 10^{-20}$ m^2 and w_{loss} represents the loss in original light flux from light absorption or scattering in the media (Hegemann et al. 2005). The constants G_{d1} and G_{d2} represent the transition rates for $O1 \rightarrow C1$ and $O2 \rightarrow C2$ respectively, G_r represents the transition rate for thermal conversion of C2 to C1 following the termination of the photostimulation, and e_{12} and e_{21} represent the transition rates between O1 and O2 respectively. The quantal efficiency for ChR2 in the dark adapted and the light adapted closed states is denoted by ϵ_1 and ϵ_2 respectively. The symbol θ_{optical} denotes the optical stimulation protocol, τ_{ChR} is the activation time constant of the ChR2 ion channel and p is the activation rate function for ChR2 ion channel (Nikolic et al. 2009). The function S_0 is defined in Section 2.1. The photocurrent entering the neuron membrane from this light activated ion channel is then given as

$$I_{\text{ChR2}} = g_{\text{ChR2}} \, (O1 + \gamma \, O2) \, (V - E_{\text{ChR2}}), \tag{3}$$

where g_{ChR2} is the maximal conductance measured in mS/cm^2, V is the neuron membrane potential, $E_{\text{ChR2}} = 0$ mV, is the reversal potential and γ measures the relative contribution of the two open states to the total conductance of the channel.

2.3 Time response curves

We define spike time response curves (STRCs) for an intrinsically firing interneuron (period T_0) as a measure of the degree of perturbation in the neuron's firing cycle induced by a synaptic input (Oprisan and Canavier 2001). We quantitatively define the jth order STRC Φ_{sj} as:

$$\Phi_{sj}(\delta t) = \frac{T_{sj}(\delta t) - T_0}{T_0} \tag{4}$$

where $T_{sj}(\delta t)$ is the period of jth firing cycle resulting from synaptic perturbation arriving at time δt and the subscript "s" represents synaptic perturbation. We assume that the first firing cycle $j = 1$ starts at time $t = 0$ and $0 \leq \delta t < T_0$. A synaptic perturbation can either advance or delay the occurrence of an impending spike depending on the bifurcation character of the neuron (Ermentrout 1996) and the type of synaptic perturbation (excitatory vs. inhibitory). The number of firing cycles for which the effect of synaptic perturbation lasts depends on the synaptic parameters: the synaptic rise time τ_R, the synaptic decay time τ_D, the reversal potential of the synapse E_R, and the synaptic conductance g_s. For example, Talathi et al. (2010) have shown that for the case with shunting synapse ($E_R = -55$ mV), $\Phi_{sj} = 0 \, \forall \, j > 3$ and

$$\Phi_{s1} \neq 0 \; \& \; \Phi_{s2} \neq 0 \text{ when } 0 \leq \delta t < T_0$$

$$\Phi_{s3} \neq 0 \text{ when } \delta t \rightarrow T_0$$

while for the case of fast-hyperpolarizing synapse ($E_R = -75$ mV), $\Phi_{sj} = 0 \, \forall \, j > 2$ and

$$\Phi_{s1} \neq 0 \text{ when } 0 \leq \delta t < T_0$$

$$\Phi_{s2} \neq 0 \text{ when } \delta t \rightarrow T_0$$

An example of STRCs estimated for an interneuron receiving synaptic perturbation through a fast inhibitory synapse and a fast shunting synapse is shown in Fig. 2.

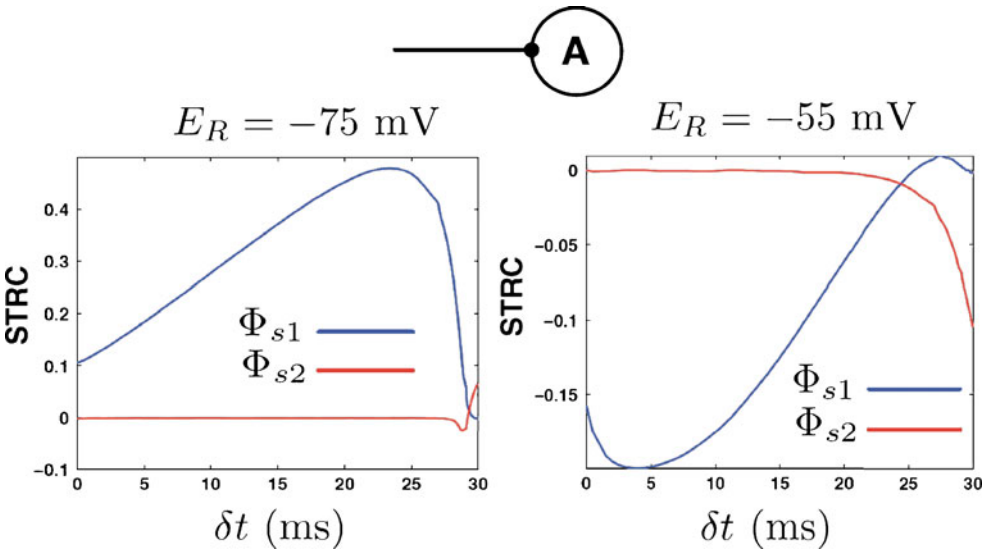

Fig. 2 Example of the STRCs for a fast spiking interneuron that receives synaptic perturbation through a fast-GABAA mediated inhibitory ($E_R = -75$ mV) and shunting synapse ($E_R = -55$ mV) respectively. The synaptic parameters are: $g_s = 0.15$ mS/cm^2, $\tau_D = 2$ ms, $\tau_R = 0.1$ ms. $I^{DC} = 0.5$ μA/cm^2, so that the neuron is intrinsically spiking with period $T_0 = 31.05$ ms

We now define the functional optical time response curve (fOTRC) as a measure of asymptotic perturbation in the firing cycle of an interneuron that results from repeated optical stimulation with light pulse of width W and intensity I that is low enough so as to not induce a neuronal action potential (see Cui et al. (2009) for a similar definition for repeated synaptic perturbations). We quantitatively define fOTRC as:

$$\Phi_{\nu}^{\infty}(\delta t) = \lim_{n\to\infty} \frac{T_{\nu}^{n}(\delta t) - T_0}{T_0} \tag{5}$$

where $T_{\nu}^{n} = t_{n+1} - t_n$ is the period of the nth firing cycle in the presence of repeated optical stimulation with light pulse that arrives at time δt following each action potential (see the schematic diagram in Fig. 3(a) and the subscript "ν" represents light perturbation. In Fig. 3(b) we show the fOTRC, obtained computationally, for optical stimulation with light pulse of intensity $I = 1$ mW/cm^2 and color coded as function of the width W and the perturbation time δt. The following two observations can be made from Fig. 3(b): (1) for a fixed perturbation time δt, as the width of light pulse is increased, fOTRC decreases indicating an increasing effect on the period of spiking cycle of the neuron; and (2) the maximum perturbation time $\delta t_{\max}^{W}$, which results in a stable value for fOTRC, decreases as the pulse width is increased. Perturbations occurring at time $\delta t \geq \delta t_{\max}^{W}$ interfere with the impending spike resulting in failure of fOTRC to converge to an asymptotic value.

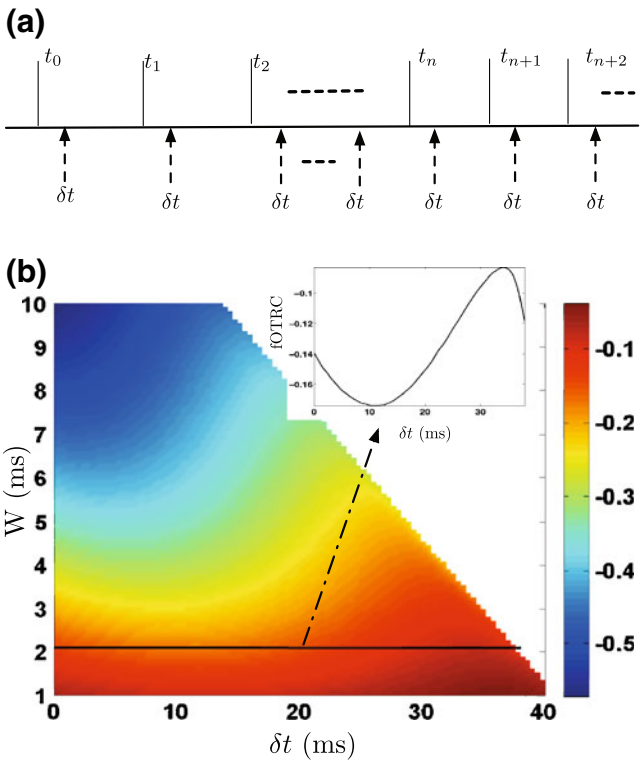

Fig. 3 (**a**) Schematic diagram of the optical stimulation protocol for determining the functional optical time response curve (fOTRC). (**b**) fOTRC color coded as function of the width W of the optical pulse of intensity H = 1 mW/cm^2 and the perturbation time δt. The region in white corresponds to the case when W large for a given delay δt, such that fOTRC does not reach a steady state value

Unless otherwise mentioned, all the simulations were performed using fixed time step 4th order Runge–Kutta method for differential equations with time step $\delta t = 0.05$ ms, on a 2GHz Intel Core Duo Mac OS X. The source code that generated the figures presented in the Results section is available for download from http://www.neurology.peds.ufl.edu/endl/.

3 Results

3.1 Estimating the model parameters for ChR2 channel kinetics

We begin by first determining the parameters in the four state transition rate model in order to quantitatively capture the mono-exponential transition period from peak to plateau current (τ_{in}) and the decay time of the ChR2 channel current kinetics (τ_{off}) for both the wild-type ChR2 and mutation thereof labelled E123T (Gunaydin et al. 2010). The model parameters were estimated to match the three key data points $\{\tau_{\text{in}}^{1000}, \tau_{\text{off}}^{1000}, \tau_{\text{off}}^{2}\}$ for each ChR2 variant (wild type and E123T) available from published literature by Gunaydin (2010), where τ_{in}^{1000} is the transition period from peak to plateau current in the presence of light pulse of 1 s in duration, τ_{off}^{1000} is the decay time after the 1 s light pulse is terminated, and τ_{off}^{2} is the decay time following the termination of a 200 ms light pulse. The intensity of the light pulse for each of these protocols was set at $I = 50$ mW/cm^2 and the wavelength $\lambda = 475$ nm. The details on the parameter estimation problem under the constraints given above is beyond the scope of present work and will be presented elsewhere. In Table 2 we list the estimated model parameters for both the wild-type and the E123T mutation of ChR2. In Fig. 4a we show the channel kinetics of the model for the voltage-clamp recordings in the presence of optical stimulation with a 700-ms and 2-ms light pulse (intensity $I = 50$ mW/cm^2 and the wavelength $\lambda = 475$ nm) (compare the results to Figs. 1d and 2d in Gunaydin et al. (2010)). In Fig. 4b we show the neuron membrane potential for the whole cell current clamp recordings in response to 10- Hz optical stimulation ($I = 50$ mW/cm^2; $\lambda = 475$ nm) with 2 ms light pulse. As suggested in Gunaydin et al. (2010),

Table 2 Parameters of the four state model to mimic the channel kinetics of wild type and ET123 mutation of ChR2

	Wild-type	E123T
G_{d1} (ms^{-1})	0.084	0.1779
G_{d2} (ms^{-1})	0.1254	0.2362
e_{12} (ms^{-1})	0.0297	0.0696
e_{21} (ms^{-1})	0.0184	0.0268
G_r (ms^{-1})	0.004	0.004
g_{ChR2}(mS/cm^2)	0.75	0.233
τ_{ChR2} (ms)	1.3	1.3
ϵ_1	0.8535	4.6125
ϵ_2	0.025	2.1969

the E123T mutation with fast channel kinetics eliminates the extra spike and the plateau potential that is observed in the membrane potential in the presence of wild type ChR2 mutation.

3.2 Analysis of 1:1 synchrony in the UCI network

Here we describe the intrinsic properties of the UCI network in terms of its ability to sustain 1:1 synchrony in absence of external stimulation. In Fig. 5(a) we show the schematic of the UCI network comprising of an intrinsically firing (period T_0^A) interneuron A interacting with an intrinsically firing interneuron B (period T_0^B) through a fast-$GABA_A$ mediated inhibitory synapse (with synaptic parameters: $g_s = 0.15$ mS/cm^2, $E_R = -75$ mV, $\tau_D = 2$ ms, $\tau_R = 0.1$ ms). The DC currents in A and B are different and are related via the heterogeneity parameter H as:

$$I_{DC}^B = I_{DC}^A \left(1 + \frac{H}{100}\right) < I_{DC}^A$$

such that $T_0^B > T_0^A$. For all the results presented below, unless otherwise mentioned, $I_{DC}^A = 0.5$ $\mu A/cm^2$, corresponding to intrinsic period $T_0^A \approx 31.05$ ms.

We will now briefly explain how STRCs can be used to analytically estimate the range of heterogeneity over which the UCI can exhibit 1:1 synchrony (Oprisan and Canavier 2001; Talathi et al. 2008). As discussed in Oprisan and Canavier (2001), Talathi et al. (2008), our goal is to determine the stability of phase locked state of 1:1 synchrony between the two coupled neurons. Let t_i^A $(i = 1, 2, \cdots)$ and t_j^B $(j = 1, 2, \cdots)$ represent the spike times for neurons A and B respectively. We define the mean period $\langle T^X \rangle = \lim_{m\to\infty} \frac{t_m^X}{m}$, $(X = A, B)$ and the time difference $\delta_n = t_n^B - t_m^A \geq 0$ between the nearest spike times of the two neurons. The index m represents the spike time of neuron A such that $t_{n-1}^B < t_m^A \leq t_n^B$. The two neurons are said to be in 1:1 synchrony if mean firing periods $\langle T_A \rangle = \langle T_B \rangle = T$ and δ_n approaches $\delta_s < T$. The two neurons are said to be locked in 1:1 in-phase synchrony if $\delta_s = 0$. In Fig. 5(b), we plot δ_n (shown in

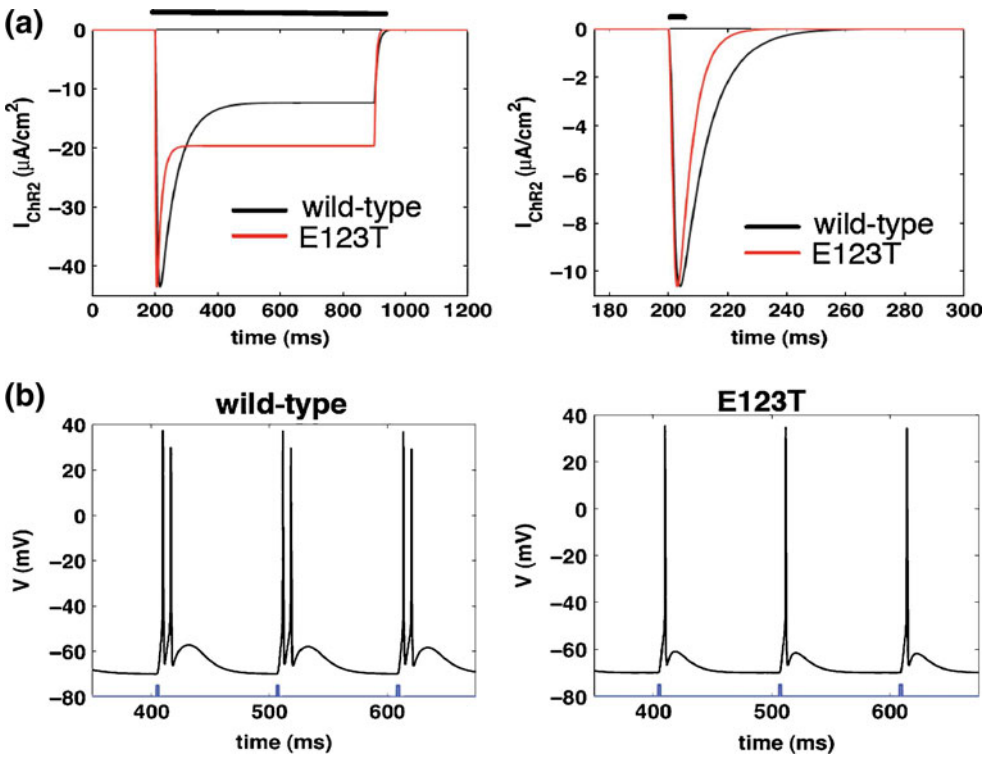

Fig. 4 (**a**) Voltage clamp (−100 mV) response of the four state model with parameters for the wild-type (*black*) and E123T mutation (*red*) when stimulated with optical pulse of 700 ms and 2 ms pulse-width respectively. The *think black line* in the figure represents the time when optical stimulation is present (**b**) Current clamp response of the interneuron expressing wild-type and E123T mutation in response to 10 Hz optical stimulation. $H = 50$ mW/cm^2, $\lambda = 475$ nm, $V_{rest} = -70$ mV

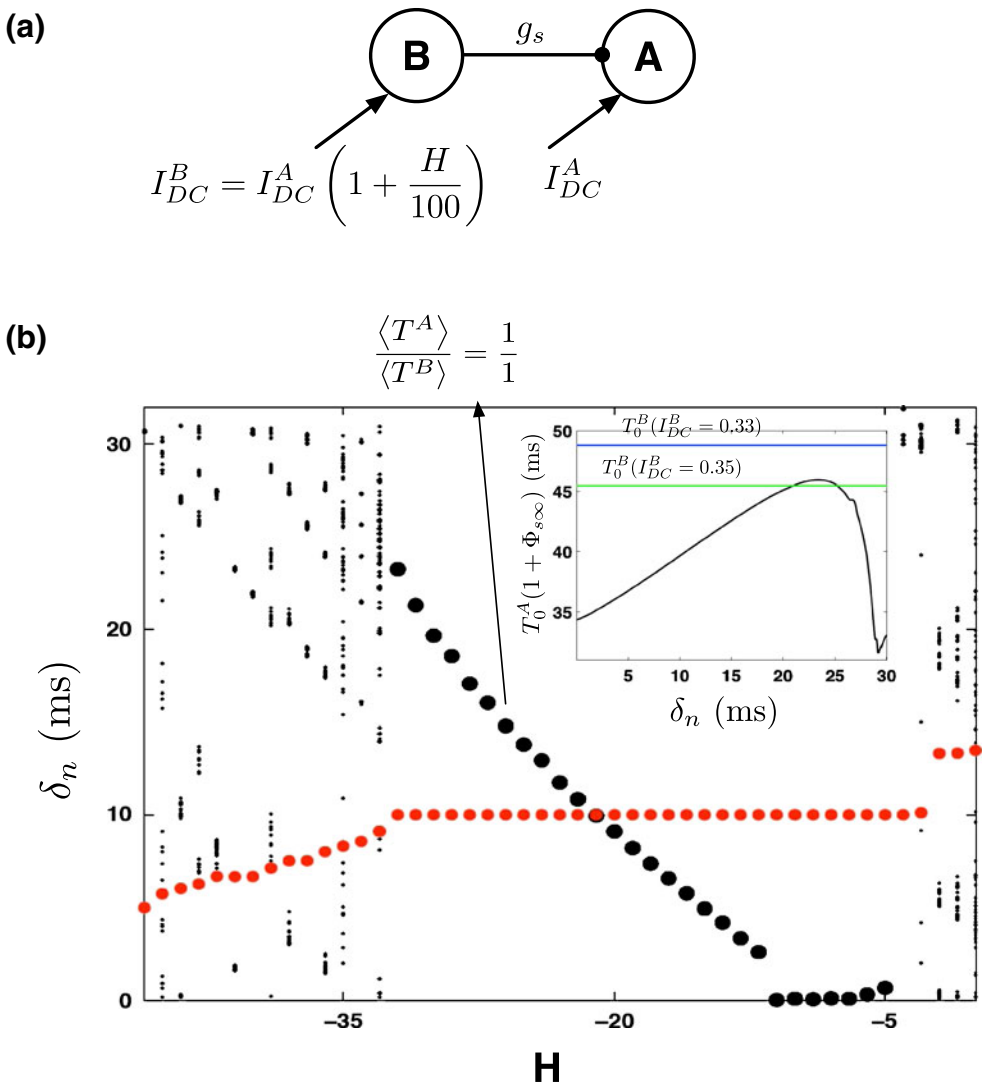

Fig. 5 (**a**) Schematic diagram of the UCI network. The bottom figure demonstrates the schematic of spike times of the neurons in the UCI network, when they are phase locked in 1:1 synchrony (**b**) Plot of the time difference δ_n between the spike times of neuron's A and B is plotted (shown in *black*) as function of heterogeneity H. Overlaid in *red dots*, we plot the ratio $\frac{\langle T^A \rangle}{\langle T^B \rangle}$ between the mean firing periods of the two neurons in the UCI network. Inset shows an example for the calculation of stable fixed point for Eq. (5). With $H = -30\%$ ($I^B_{DC} = 0.35$ μA/cm^2), solution to Eq. (6) exists with a stable fixed point at $\delta_s \approx 21$ ms. With $H = -34\%$ ($I^B_{DC} = 0.33$ μA/cm^2), Eq. (6) has no solution corresponding to the case when the two neurons cannot lock in 1:1 synchrony

black) as function of H. We also plot $10\frac{\langle T^A \rangle}{\langle T^B \rangle}$ (red dots in Fig. 5(b)) as function of H. We see that the two neurons can lock in 1:1 synchrony for a finite range ($-32 \leq H \leq -5$) of values for the heterogeneity H. However, only for $-9 < H < -7$ are the two neurons able to lock in 1:1 in-phase synchrony with $\delta_s \approx 0$.

Following earlier works (Oprisan and Canavier 2001; Talathi et al. 2008), for the case of UCI network with hyperpolarizing synapse ($E_R = -75$ mV), the stability of δ_s can be determined by analyzing the nonlinear map for the evolution of δ_n, which is given as:

$$\delta_{n+1} \approx \delta_n + T^B_0 - T^A_0 (1 + \Phi_{s\infty}(\delta_n)) \tag{6}$$

where $\Phi_{s\infty}(x) = \Phi_{s1}(x) + \Phi_{s2}(x)$ (we note that for the case of the UCI network with shunting synapse, the contribution from higher order STRC terms is significant and Eq. (6) is no longer valid (Talathi et al. 2010)). The fixed point δ_s of Eq. (6) can be obtained by solving the following equation:

$$T^A_0(1 + \Phi_{\infty s}(\delta_s)) = T^B_0 \tag{7}$$

The stability of the δ_s requires $0 < \frac{d\Phi_{s\infty}}{dx}|_{x=\delta_s} < \frac{2}{T^A_0}$. For the specific case of $H = -30\%$ i.e., $I^B_{DC} = 0.35$ μA/cm^2, we see from Fig. 5(b) inset that the stable fixed point solution to the nonlinear map in Eq. (6) exists at $\delta_n \approx 21$ ms and the two neurons are phase locked in 1:1 synchrony (as confirmed through numerical simulations of Eq. (1) for the UCI network with $\delta_s \approx 21$ ms). For $H = -34\%$ i.e., $I^B_{DC} = 0.33$ μA/cm^2, there is no solution to Eq. (7) and therefore for this value of heterogeneity in the UCI network, the two neurons cannot lock into synchronous state.

3.3 Open loop control architecture for inducing 1:1 in-phase synchrony in the UCI network

Our goal is to design an optical stimulation based controller that can induce stable 1:1 in-phase synchrony, i.e., $\delta_s = 0$ is a stable fixed point, in the UCI network for a broad range of H. For this purpose, we use the nonlinear map for the evolution of δ_n. We propose an open loop controller that continuously stimulates neuron B via a light pulse with parameters: delay τ, width W, and low intensity ($I = 1\text{mW/cm}^2$) that is such that the timing of an impending spike is modulated but the stimulation itself does not induce an action potential spike. The schematic of the controller is shown in Fig. 6(a).

In the presence of optical stimulation, the nonlinear map for the evolution of δ_n is obtained as follows. Following from the definition of fOTRC (see Eq. (5)), and the schematic in Fig. 6(a), we have for neuron B, $t^B_{n+1} = t^B_n + T^B_0\left(1 + \Phi^{\infty B}_{\nu}(\tau, W)\right)$ Now, following from earlier works (Oprisan and Canavier 2001; Talathi et al. 2008), for neuron A receiving hyperpolarizing inhibitory synaptic input we have, $t^A_{n+1} = t^A_n + T^A_0(1 + \Phi_{s\infty}(\delta_n))$, where again $\Phi_{s\infty}(x) = \Phi_{s1}(x) + \Phi_{s2}(x)$. The discrete map for the evolution of δ_n is then given as:

$$\delta_{n+1} = \delta_n + T^B_0(1 + \Phi^{\infty B}_{\nu}(\tau, W)) - T^A_0(1 + \Phi_{s\infty}(\delta_n)) \tag{8}$$

The fixed point δ_s of Eq. (8) satisfies

$$1 + \Phi_{\infty s}(\delta_s) = \frac{T^B_0}{T^A_0}(1 + \Phi^{\infty B}_{\nu}(\tau, W)) \tag{9}$$

The local stability of the equilibrium point $\delta_s = 0$ again requires $0 < \frac{d\Phi_{\infty s}}{dx}|_{x=\delta_s} < \frac{2}{T^A_0}$. We note that this stability condition is independent of the control parameters for the open loop control design considered above. It is clear from Eq. (9) that in order to achieve stable 1:1 in-phase synchrony the optical stimulation parameters, i.e., the width W and the delay τ of light pulse should be such that

$$\Phi^{\infty B}_{\nu}(\tau, W) = \frac{T^A_0}{T^B_0}(\Phi_{\infty s}(0) + 1) - 1 \tag{10}$$

The open loop control parameters W and τ that can induce stable 1:1 in-phase synchrony in the UCI network therefore satisfy the constraint

$$E = \left| 1 + \Phi^{\infty B}_{\nu}(\tau, W) - \frac{T^A_0}{T^B_0}(1 + \Phi_{s\infty}(0)) \right| = 0 \tag{11}$$

In Fig. 6b.1 and b.2, we plot E as a function of τ and W for the case when the neurons are expressed with the wild type and the E123T mutation of ChR2 respectively. The curve in blue represents the optimal set of open-loop control parameters $\{\tau^*(H), W^*(H)\}$ that satisfy Eq. (11). In terms of the controllers ability to induce 1:1 in-phase synchrony in the UCI network we see that it is more sensitive to the width of light pulse.

In Fig. 6(c), we demonstrate the open loop controller in action for a specific case of the UCI network comprising of interneurons transduced with E123T mutation of ChR2. We numerically solve Eq. (1) for neuron model and Eq. (2) for channel kinetics of ChR2 and observe the time evolution of the firing times of the two neurons in the network in the presence of the open loop controller. The initial UCI network configuration is such that $H = -30\%$. As a result, in the absence of optical stimulation, the network exhibits 1:1 synchrony with $\delta_s \approx 21$ ms (see Fig. 5(b)). When the open loop controller is turned on, neuron B receives repeated light pulse stimulation with parameters $\{\tau^* = 3.92,\ W^* = 5.5\}$, such that the constraint in Eq. (11) is satisfied. As can be seen from Fig. 6(c), following an initial transient period after the controller is turned on, the time difference $\delta_n \to 0$ and the UCI network is locked in 1:1 in-phase synchrony.

Next, in order to determine whether optical stimulation with the right control parameters can indeed enhance the domain of 1:1 in-phase synchrony, in Fig. 6(d) we plot δ_n as function of H for UCI network in the presence of open loop controller with optimal control parameters. The figure is generated as follows: for a given value of H, we solve Eq. (11) (fminsearch in matlab) to identify $\{\tau^*, W^*\}$. The open loop controller is turned on with these computed controller parameters. Then we numerically measure the asymptotic value of δ_n. When comparing the resulting plot of the time difference with those presented in Fig. 5(b), we make the following two observations: (1) The domain of 1:1 synchrony is widened with the UCI network now being able to lock in 1:1 synchrony for values of $H < -6$ %. (2) 1:1 synchrony is in-phase with $\delta_n \to \delta_s \approx 0$ for the entire range of heterogeneity values when the two neurons in the UCI network are locked in 1:1 synchrony. Thus, with an open loop optical stimulation based controller, the UCI network is able to synchronize in 1:1 in-phase synchrony for a wide range of heterogeneity which is not possible intrinsically for the UCI network.

So far, we have assumed that the value of H is known in designing the open loop controller parameters. This is a significant limitation of open loop control. Indeed, the open loop controller is not robust to unknown changes on the value of H as shown next.

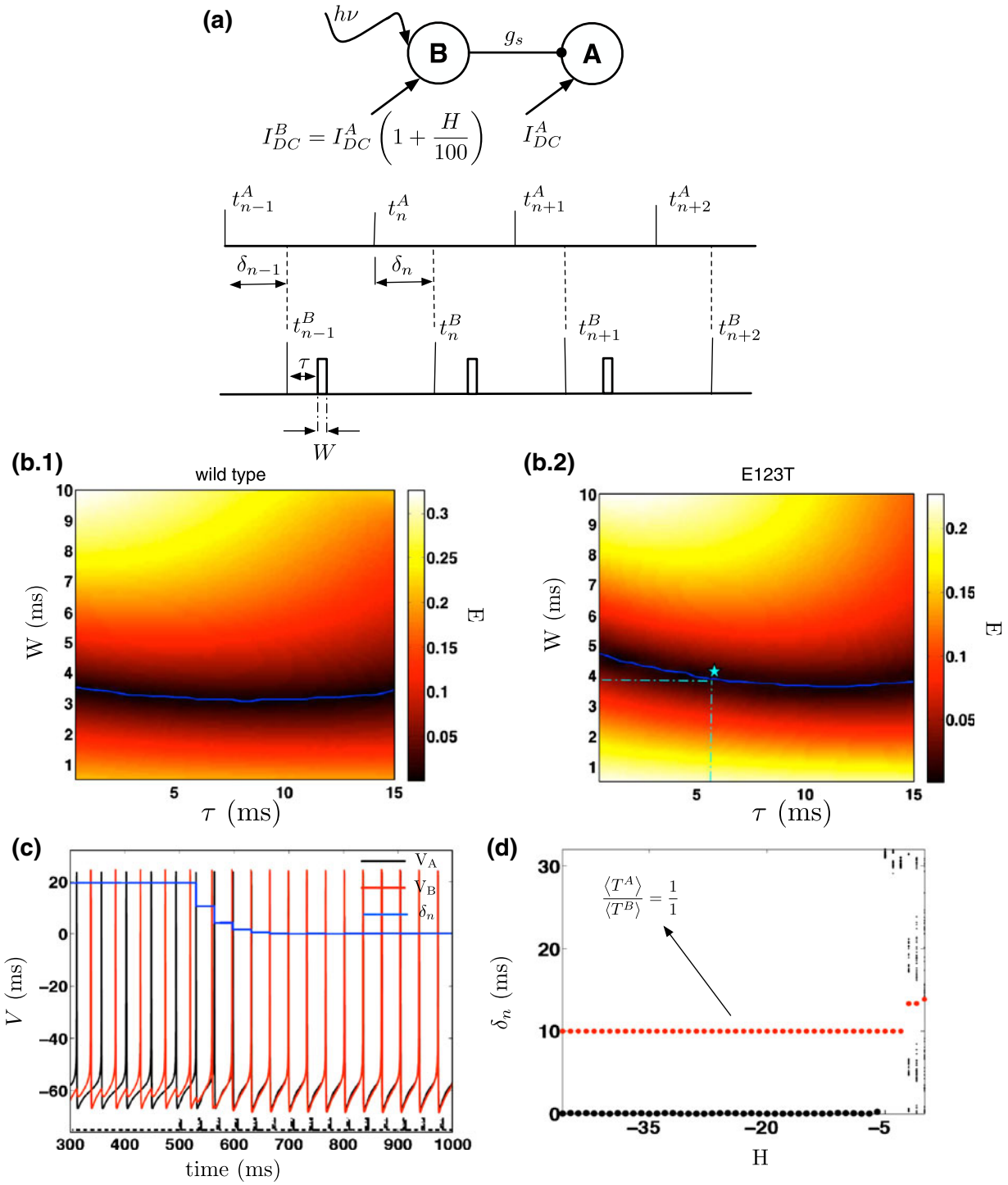

Fig. 6 (**a**) Schematic diagram of the UCI network in the presence of optical stimulation for open-loop control of 1:1 in-phase synchrony. The *bottom* figure demonstrates the schematic of spike times of the two neurons and the application of optical stimulation pulse in the UCI network. (**b**) The plot of function E in Eq. (12), as function of the optical stimulation parameters; the width W and the delay τ for the case when the neurons express wild type ChR2 (b.1) and E123T mutation (b.2). $E = 0$, corresponds to the case when the two neurons in the UCI network are locked in 1:1 in-phase synchrony. (**c**) Example demonstrating open-loop control in action. The controller is turned on at time $t = 500$ ms. The UCI network parameters are $I^A_{DC} = 0.5$ μA/cm^2, $H = -30\%$, $g_s = 0.15$ mS/cm^2, $E_R = -75$ mV, and $\tau_D = 2$ ms. The neurons in the network are expressed with E123T mutation of ChR2. The controller parameters are $\tau = 5.5$ ms and $W = 3.92$ ms. (**d**) Scatter plot of the time difference δ_n between the spike times of neuron's A and B is plotted (shown in *black*) as function of heterogeneity H in the presence of open-loop controller with parameters such that $E = 0$. Overlaid in red dots, we plot the ratio $\frac{\langle T^A \rangle}{\langle T^B \rangle}$ between the mean firing periods of the two neurons in the UCI network

3.4 Closed loop control architecture to enhance robustness of 1:1 in-phase synchrony in the UCI network

In the last section, we presented an open loop control architecture and controller parameters to induce 1:1 in-phase neural synchrony in the UCI network. The parameters of the controller satisfy the constraints in Eq. (11) for a given value of heterogeneity in the UCI network. In order to demonstrate the sensitive dependence of the open-loop controller performance on the heterogeneity value, in Fig. 7, we show the plot of δ_n for the UCI network using the open loop controller with fixed parameters $\{\tau^* = 5.5$ ms,$W^* = 3.92$ ms$\}$ estimated for the specific case $H = -30\%$ as discussed in the last section. We see that the open loop controller only induces 1:1 in-phase synchrony for $H^* = -30\%$, the specific case for which the controller was designed, and a small range of heterogeneity values around $H^* = -30\%$. In addition, the range of heterogeneity over which the UCI network can exhibit 1:1 synchrony is reduced as compared to the case when no optical stimulation is present (see Fig. 5). At the same time open loop optical stimulation induces higher order synchrony states, i.e., 3/2, 5/3, 2/1, not observed in the UCI network in absence of optical stimulation (detailed analysis for the role of optical stimulation in generating these higher order synchrony states is beyond the scope of present paper and will be pursued in future research).

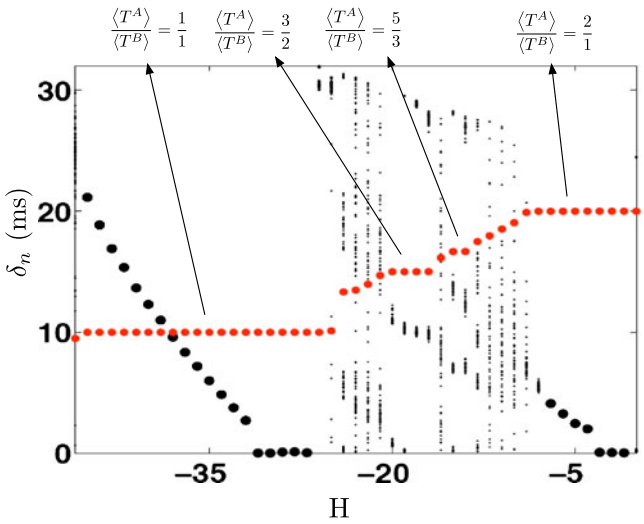

Fig. 7 Plot of the time difference δ_n between the spike times of neuron's A and B is plotted (shown in *black*) as function of heterogeneity H in the presence of open-loop controller with optical stimulation parameters set at $\tau = 5.5$ ms and $W = 3.92$ ms, corresponding the case when $H = -30\%$. Overlaid in *red dots*, we plot the ratio $\frac{\langle T^A\rangle}{\langle T^B\rangle}$ between the mean firing periods of the two neurons in the UCI network

The results from Figs. 6d and 7 suggest that while the open loop architecture can induce 1:1 in-phase synchrony with the appropriate choice of optical stimulation parameters, the open loop controller is very sensitive to the UCI network parameters and any perturbations will results in the failure to establish 1:1 in-phase synchrony. This conclusion is not unexpected as it is well known from basic control theory that open loop control is not robust against variations in system parameters. We have therefore developed a closed-loop feedback controller architecture so as to allow the parameters of optical stimulation to depend on the use of δ_n as a feedback signal. The schematic of this control architecture is shown in Fig. 8(a). A general mathematical description of the controller is as follows:

$$\begin{aligned} x_{n+1} &= f(x_n, \delta_n) \\ u_n^1 &= \tau^* + h_1(x_n, \delta_n) \\ u_n^2 &= W^* + h_2(x_n, \delta_n) \end{aligned} \tag{12}$$

with the constraint: $0 < u^1, u^2 \leq 15$. As before, τ^* and W^* are the open loop control parameters satisfying Eq. (11) for a given *nominal* value of heterogeneity H^* in the UCI network. The controller is a general discrete-time nonlinear system with state vector x and state-trasition map f and output maps h_1, h_2. The closed loop controller modifies the open-loop settings τ^* and W^*. A specific simple controller design will now be given below.

We will use a simple proportional plus integral (PI) controller given by:

$$\begin{aligned} x_{n+1} &= x_n + g(\delta_n) \\ u_n^1 &= \tau^* + a(\delta_n + x_n) \\ u_n^2 &= W^* + b\,(\delta_n + x_n) \end{aligned} \tag{13}$$

The function $g(\delta_n)$ is a continuous and differentiable function of δ_n and satisfies the following constraint:

$$g(\delta_n) = 0 \begin{cases} \text{if } \delta_n = 0; \\ \text{if } \delta_n = T_n^B = T_n^A = T; \end{cases} \tag{14}$$

The first constraint implies that $g = 0$ when the two neurons are firing in-phase. The second constraint corresponds to the periodic boundary condition, where T_n^A and T_n^B represent the instantaneous period of the two neurons in the nth firing cycle. These constraints imply that the control input becomes zero if the two neurons fire in synchrony.

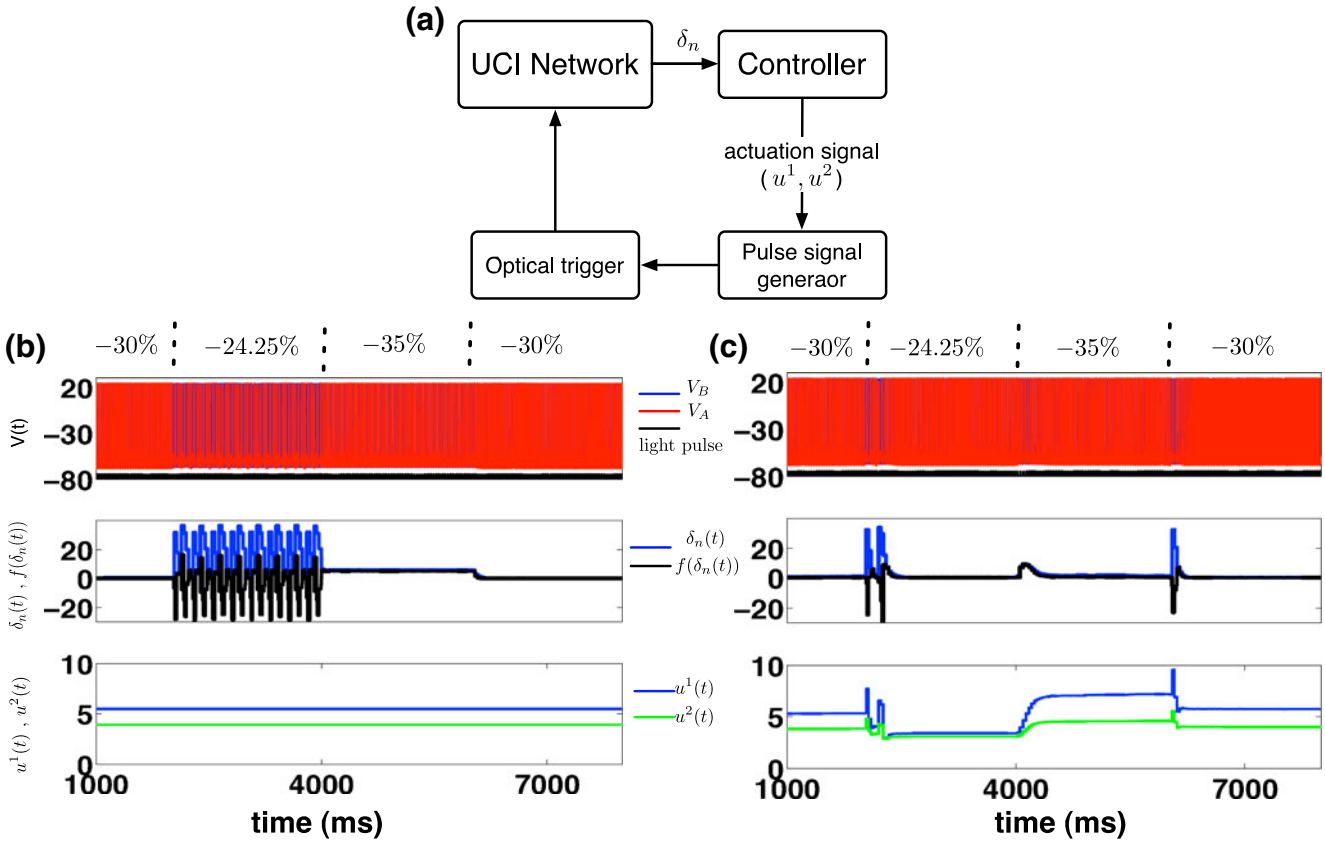

Fig. 8 (**a**) Schematic diagram of the closed-loop control implementation for control of 1:1 in-phase synchrony in the UCI network. (**b**) Example demonstrating the sensitivity of the open loop controller to perturbations in the UCI network parameters. The open loop control parameters (τ^* and W^*) are the same as in Fig. 6(c), while the parameters a, and b are each set to 0. (**c**) Example demonstrating the closed loop controller in action. The controller is able to maintain $\delta_n \approx 0$, even in the presence of sudden perturbations in the parameters of the UCI network. The closed loop controller parameters are $a = 0.25c$ and $b = 0.1c$ with $c = 0.3$. In both cases (**b**) and (**c**), the network perturbations are obtained as follows: at time $t = 2{,}000$ ms, H is abruptly increased from -30 to -24.25%. At time $t = 4{,}000$ ms, H is abruptly decreased from -24.25 to -35%. At time $t = 6{,}000$ ms, H is changed back to -30%

In Figs. 8(b, c) we present the results from application of this closed loop controller with $g(\delta_n) = \delta_n \sin(\frac{4\pi\delta_n}{T_n^B + T_n^A})$. The UCI network parameters are similar to those considered in Fig. 6(c) with $H^* = -30\%$ and the optimal optical pulse parameters $\{\tau^* = 5.5$ ms, $W^* = 3.92$ ms$\}$. We again numerically solve Eqs. (1) and (2) for the UCI network in the presence of optical stimulation with the light pulse parameters determined by the closed loop controller in Eq. (13). For all the calculations presented below, we set $a = 0.25c$ and $b = 0.1c$, with c being a design parameter. We choose $a > b$, because the optical stimulation based controller is more sensitive to variations in the width W of the light pulse in comparison to variations in the delay τ. For the case considered in Fig. 8(b), we have $c = 0$; simulating the scenario when the closed loop feedback is turned off. For the case considered in Fig. 8(c), the feedback loop is turned on and the closed loop control parameter is set at $c = 0.3$. At time $t = 2{,}000$, H is abruptly changed to $H = -24.25\%$. This corresponds to the case when the UCI network with open loop control parameters set at -30%, can no longer exhibit 1:1 synchrony (see Fig. 7) and therefore δ_n oscillates without settling into steady state value δ_s. At time $t = 3{,}500$ the heterogeneity is again abruptly changed to $H = -35\%$. This situation corresponds to the case when the UCI network with open loop control parameters set at -30% is phase locked in 1:1 synchrony with $\delta_s \approx 5$ ms (see Fig. 7). Finally at time $t = 6{,}000$, the heterogeneity is changed back to $H = -30\%$ corresponding to the case when the UCI network with open loop control parameters set at -30% exhibits 1:1 in-phase synchrony. In the absence of closed loop feedback, we see from Fig. 8(b) that the network is unable to sustain 1:1 in-phase synchrony with fluctuations in the heterogeneity in the network. However, as can be seen from Fig. 8(c), the closed

loop controller with feedback, dynamically modulates the parameters of optical pulse, such that following a short transient period after each abrupt change in heterogeneity value, the UCI network is able to return to the state of stable 1:1 in-phase synchrony.

Following from Eqs. (8) and (13), the nonlinear map for the evolution of the time difference δ_n in the presence of the closed loop controller is given as:

$$\begin{aligned}
\delta_{n+1} &= \delta_n + T_n^B - T_n^A \\
x_{n+1} &= x_n + \delta_n . \sin\left(\frac{4\pi\delta_n}{T_n^A + T_n^B}\right) \\
u_n^1 &= \tau^* + a(\delta_n + x_n) \\
u_n^2 &= W^* + b\,(\delta_n + x_n)
\end{aligned} \tag{15}$$

where, $T_n^A = T_0^A\,(1 + \Phi_{s\infty}(\delta_n))$ and $T_n^B = T_0^B\left(1 + \Phi_{\nu}^{\infty B}(u_n^1, u_n^2)\right)$. Equation (15) represents a two dimensional nonlinear map $\Delta_{n+1} = \vec{f}\,(\Delta_n)$, where $\Delta_n = \{\delta_n, x_n\}$, for the evolution of the time difference in the firing times (δ_n) of the two neurons in the presence of closed loop optical stimulation (x_n) with parameters $\{u^1, u^2\}$. 1:1 in-phase synchrony implies the existence of stable fixed point solution $\delta_s = 0$.

In order to determine whether the nonlinear map presented in Eq. (15) is able to successfully reproduce the numerical simulation results presented in Fig. 8, we plot the time series for evolution of δ_n, x_n, T_n^B, T_n^A, u_n^1 and u_n^2 for the cases when the closed loop controller is turned off (Fig. 9(a)) and when the controller is turned on (Fig. 9(b)). We see that the nonlinear map can successfully reproduce the results of the full numerical simulation of the UCI network.

We will now analyze the stability of this nonlinear discrete-time system given by Eq. (15), viewed as a mathematical representation of the closed loop system consisting of the UCI network and the closed loop controller for the specific case when $H = -24.25\%$. The parameters of the controller are the same as described in Fig. 8(c), i.e., $a = 0.25c$, $b = 0.1c$ with $c = 0.3$ and $\tau^* = 5.5$ ms, and $W^* = 3.92$ ms. From Eq. (15) we see that the fixed point for the nonlinear map is given as $\Delta_s = \{0, x_s\}$, where x_s satisfies the constraint:

$$x_s = \frac{u_s^1 - \tau^*}{a} = \frac{u_s^2 - W^*}{b} \tag{16}$$

and u_s^1 and u_s^2 represent optical stimulation parameters that satisfy the constraint:

$$T_s^A(0) = T_s^B(u_s^1, u_s^2) \tag{17}$$

We solve Eq. (17) (fmincon in matlab) under the constraint given in Eq. (16) to obtain $u_s^1 \approx 3.23$, $u_s^2 \approx 3.012$ and $x_s \approx -30.26$. The fixed point for the nonlinear map $\Delta_s \approx \{0, -30.26\}$. Local stability of the closed loop equilibrium point Δ_s can be determined using tools from linear stability analysis for discrete-time dynamical systems (Strogatz 2001; Khalil 2001) by calculating the eigenvalues λ_j (j = 1...2) of the Jacobian matrix $\frac{\partial \vec{f}\,(\Delta_n)}{\partial \Delta_n}|_{\Delta_s}$. Stability requires $|\lambda_j| < 1$. We numerically

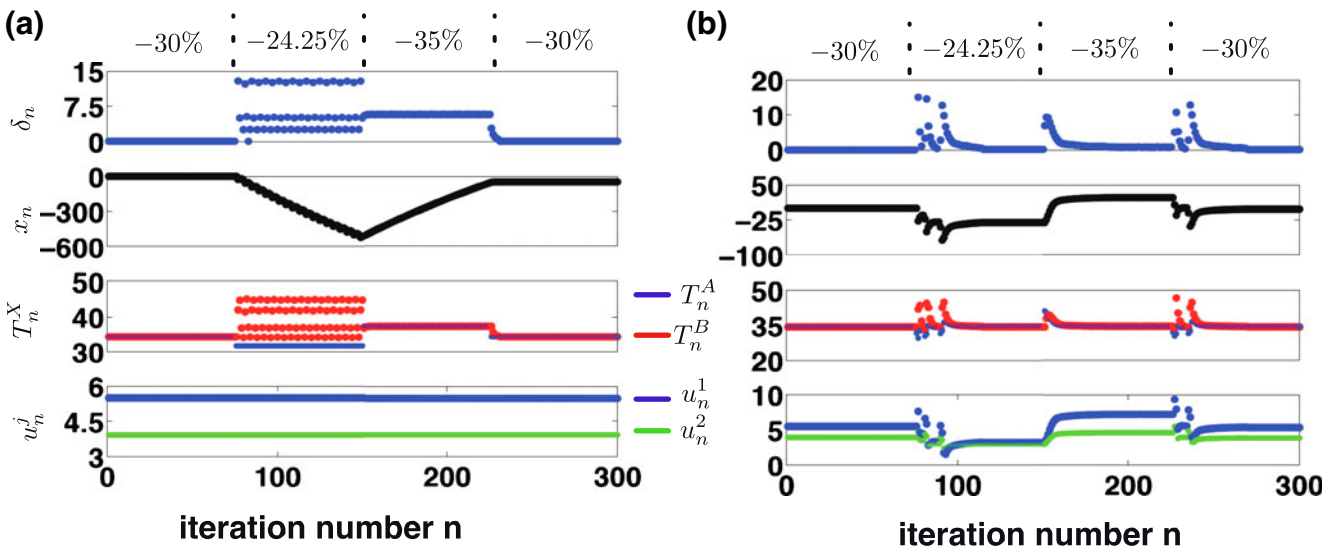

Fig. 9 (**a**) Evolution of the time difference δ_n, the controller variable x_n, the instantaneous period T_n^X (X = A,B) and the optical pulse parameters u_n^j (j = 1,2) determined through the nonlinear map in Eq. (13) when the closed loop controller is turned off ($a = 0.25c$,$b = 0.1c$ with $c = 0$). (**b**) Evolution of these variables when the closed loop controller is turned on ($a = 0.25c$,$b = 0.1c$ with $c = 0.3$)

estimate the eigen values for the Jacobian as: {0.79+.3i, 0.79−.3i}. Thus, the closed loop controller, for the choice of control parameter given above, is able to sustain locally stable 1:1 in-phase synchrony in the UCI network.

We will now use the Eq. (15) to determine the bound on the value for c as a function of H for which the UCI network coupled to a closed loop controller will exhibit stable 1:1 in-phase synchrony. For each value of H and c, we evolve the nonlinear map to determine whether the trajectory of $\Delta_n \rightarrow \Delta_s$. In order to demonstrate the difference in the evolution of the trajectory of Δ_n for the case when the discrete map evolves to a stable fixed point Δ_s, vs. the case when it does not, in Fig. 10 we show the evolution of $\{\delta_n, x_n\}$ for the cases: (a) $H = -24.25$, $c = 0.3$ and (b) $H = -24.25$ and $c = 1.05$. We see that $c = 1.05$ is beyond the range of closed loop control parameters allowed for the discrete map to trigger stable in-phase synchrony in the UCI network with $H = -24.25\%$. We perform the above calculation for all $-40 \leq H \leq -20$. The result of this analysis is summarized in Fig. 11. From the results, we can conclude that the maximum range of variability in the heterogeneity H around H^* can be sustained with a closed loop controller with parameter set at $c = 0.5$.

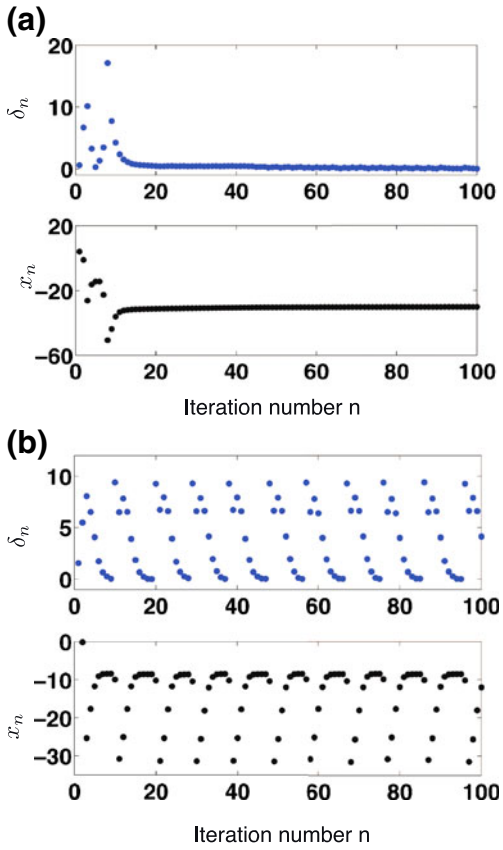

Fig. 10 Evolution of the nonlinear map (Eq. (13)) with parameters: $\tau^* = 5.5$ ms, $W^* = 5.5$ ms, $H = -24.25\%$. (**a**) The trajectory of Δ_n when $c = 0.3$ (**b**) The trajectory of Δ_n when $c = 1.05$

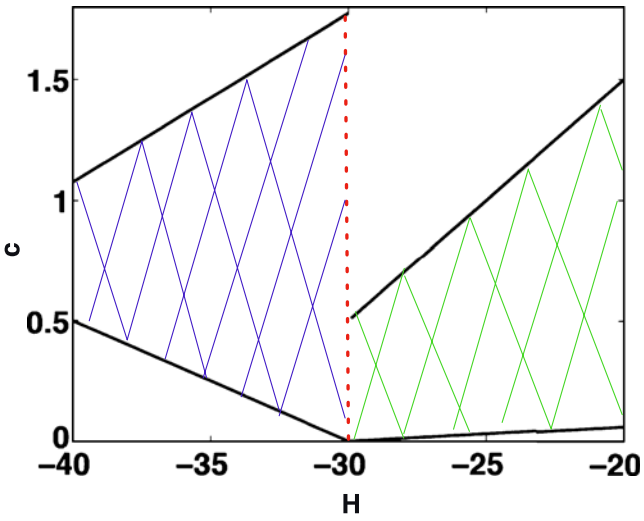

Fig. 11 The range for the value of the closed loop parameter c as function of heterogeneity H, for the UCI network with open loop control parameters: $\tau^* = 5.5$ ms, $W^* = 5.5$ ms. The *red dotted line* represents the default heterogeneity value for the UCI network. The regions shaded in *blue and green lines* correspond to the range of values of c for which the nonlinear map (Eq. (13)) exhibit stable fixed point Δ_s

3.5 Closed loop control of the UCI network in the presence of feedback synaptic coupling

In the final section, we address the issue of the influence of feedback coupling in the UCI network on the performance of the closed loop controller. We start with the specific UCI network with heterogeneity $H = -30\%$, optimal open loop parameters $\tau^* = 5.5$ ms, $W^* = 3.92$ ms and the closed loop parameter $c = 0.3$. Our analysis of the previous section suggests that the the UCI network will exhibit robust 1:1 in-phase synchrony. We now introduce feedback synaptic coupling from neuron A onto neuron B of strength $g_f = \frac{S}{100} g_s$. When $S = 0$, we get the UCI network and when $S = 100$, we get the MCI network wherein the strength of synaptic interaction between the two coupled neurons is equal. The schematic of the MCI is shown in Fig. 12(a). In Fig. 12(b), we show the plot of the time difference δ_n as a function of the strength of the feedback signal, in the presence of the closed loop controller. As expected, for weak feedback synaptic perturbations i.e., $S < 10$ the closed loop controller is able to sustain robust 1:1 in-phase synchrony in the network. However, for strong feedback coupling i.e., $S > 50$, this closed loop

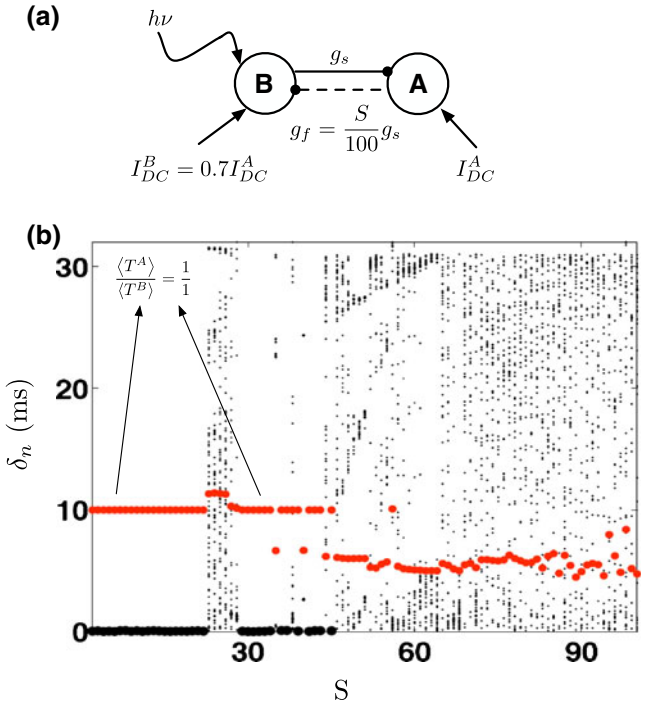

Fig. 12 (**a**) Schematic diagram of the network of mutually coupled interneurons. (**b**) Plot of the time difference δ_n between the spike times of neurons A and B is plotted (shown in *black*) as function the percent strength S of the feedback coupling g_f of the in the presence of closed-loop controller. The parameters are $H = -30\%$, $\tau^* = 5.5$ ms, $W^* = 3.92$ ms and $c = 0.3$

controller is unable to sustain 1:1 synchrony in the network. For intermediate strengths of feedback signal i.e., $10 < S < 50$, we see that while the closed loop controller is largely able to sustain 1:1 in-phase synchrony, there are regions of S values where the network does not exhibit 1:1 in-phase synchrony.

Here, we have designed and investigated a simple proportional plus integral controller for the UCI network and used it for the MCI network. The field of control theory offers a wealth of controller structures and design techniques that have the potential to assure better robustness and performance for the general problem of neural synchrony in neuronal networks. As such, the detailed mathematical analysis of the results presented in Fig. 12, and suitable modifications to the controller design to sustain 1:1 in-phase synchrony in the MCI network for a wide range of network parameters will be considered in a future publication.

4 Discussion

Optogenetics is an emerging technology with an unprecedented ability to probe neural circuitry *in vivo* at the spatial and temporal scales previously unachievable (Deisseroth et al. 2006; Boyden et al. 2005). While the technology is still nascent, in the last couple of years there has been a great surge in the interest in this novel tool to address fundamental neuroscience (Huber et al. 2008; Cardin et al. 2009) and neurological disease (Gradinaru et al. 2009; Tønnesen et al. 2009) related questions. In this paper, we conduct a computational study for the utility of optogenetic technique for active control of inhibition induced neural synchrony in brain networks. This study is motivated from the knowledge that synchronous firing activity within networks of fast spiking soma inhibiting interneurons is known to play an important role in the generation of gamma rhythms in the brain (Bartos et al. 2007). These rhythms contribute to cognitive functions such as memory formation and sensory processing and are disturbed in certain psychiatric disorders such as autism (Colwyn 2005) and schizophrenia (Symond et al. 2005). A possible modality of therapy for these illnesses can therefore be through novel brain stimulation techniques that attempt to selectively induce inhibitory neuronal synchrony and thereby restore gamma rhythms in the brain.

We specifically study the problem of control of neural synchrony in a simple unidirectionally coupled network of heterogeneously firing interneurons interacting through a fast-$GABA_A$ mediated inhibitory synapse (UCI network). The choice of a "relatively" simple network for control is motivated for the following reasons: (1) there is no prior work on the use of optogenetic stimulation for neural synchrony. In fact, there is very little prior work on mathematical analysis of optogenetic stimulation for neuronal systems. The case of two neuron feed-forward network is complex enough (set of 9-nonlinear ordinary differential equations) yet, amenable to mathematical analysis for the problem of controller design and (2) over last decade a number of researchers have focused on the role for interneuronal synchrony in the generation of gamma rhythms (Wang and Rinzel 1992; Wang and Buzsaki 1996). In particular, many researchers have focused on the sensitive dependence of interneuronal synchrony on the hetererogenity in the intrinsic neuronal dynamics. Many of these investigations use the setting of two interacting neurons (vanVreeswijk et al. 1994; White et al. 1998; Jeong and Gutkin 2007; Talathi et al. 2008).

While most research has focused on intrinsic mechanisms that allow coupled interneurons to synchronize, here we ask the specific question: can external optical stimulation (as opposed to intrinsic neuronal and synaptic properties such as plasticity, electrical coupling, delays etc.) overcome heterogeneity and

generate robust in-phase synchrony? We have precisely answered this question and to the best of our knowledge, this is the first study to systematically investigate the utility for optogenetics tools to design a controller for the specific task of control of neural synchrony in brain networks. While it is beyond the scope of present work, we hope that in future, the techniques developed in this work, for example, fOTRC, can be utilized to develop optogenetics based control strategies for inducing neural synchrony in a more realistic interneuronal network such as those considered by Bartos et al. (2007).

We begin by first constructing a deterministic four-dimensional transition rate model to simulate the kinetics of ChR2 in response to optical stimulation. This model is then incorporated into the Hogdkin–Huxley framework to simulate the effect of optical stimulation on neuronal dynamics. We then introduce the concept of functional optical time response curve (fOTRC), which quantifies the response of neuron to repeated optical stimulation respectively. This construct is analogous to the concept of STRC. An important point worth noting here is that fOTRC is calculated under the assumption that the intensity of light pulse in the optical stimulation is low enough so as to not induce an action potential spike, but merely perturb the timing of an impending action potential spike. Time response curves such as STRC and fOTRC are effective experimental tools for the study of neuronal network synchrony because they can be easily measured experimentally without the need for a detailed biophysical model for neuronal dynamics (Netoff et al. 2005).

We utilize these time response curves to design an open loop architecture for control of in-phase neural synchrony in the UCI network. The basic idea behind the design of the controller is to utilize optical stimulation to activate the ChR2 ion channel which in turn can selectively enhance the excitability of the underlying neuron by depolarizing its membrane potential. The optimal open loop parameters of light pulse (the stimulation time τ and the pulse width W) for optical stimulation are selected to satisfy the constraint that the asymptotic period of the driver neuron receiving optical stimulation matches the the instantaneous period of the driven neuron in the UCI network. We demonstrate that optical stimulation with optimal parameters not only enhances the domain of 1:1 synchrony but the two neurons in the network can sustain 1:1 in-phase synchrony for a wider range of heterogeneity in the intrinsic firing rates of the coupled neurons. We then modify the open loop scheme to incorporate closed loop feedback control architecture, which has the ability to dynamically modulate the parameters of the optical stimulation signal dependent on the state of UCI network. The closed loop control architecture with a suitable choice of controller parameters is able to sustain 1:1 in-phase neural synchrony in the network even in the presence of relatively large and unknown variations in the network heterogeneity. Using the time response curves we are able to derive a nonlinear map for the evolution of time difference in the spike time of the two coupled neurons, which is then used to determine the bounds on the value of the closed loop control parameters required to continually sustain 1:1 in-phase synchrony in the network. Finally we demonstrate that the performance of the closed-loop controller does not diminish in the presence of weak synaptic feedback signal.

In summary, the utility for the tools from the mathematical field of control theory and engineering to study problems in computational neuroscience, in particular neural synchrony, is relatively nascent (Schiff 2009). At the same time, the possibility of controlling pathological brain synchrony in neurological diseases has spurred interest in the control community to device novel control algorithms, that are based on intrinsic neural populations dynamics (Danzl et al. 2010). As such, in future we expect increased collaborations among computational neuroscientists, control theorists and biomedical engineers to utilize modern technology such as optogenetics to develop intelligent strategies for control of brain activity with therapeutic implications for brain related diseases.

Acknowledgements This research was supported through the intramural seed grant on Computational Biology from the University of Florida. SST and PRC were partially supported from the Wilder Center of Excellence for Epilepsy Research and the Childrens Miracle Network. PPK was partially supported by the Eckis Professor Endowment at the University of Florida. We acknowledge constructive feedback from Dr Willam Ogle, Dr Jason Frazier, Erin Boykin and Shivakeshavan Ratnadurai.

References

Abarbanel, H., Gibb, L., Huerta, R., & Rabinovich, M. (2003). Biophysical model of synaptic plasticity dynamics. *Biological Cybernetics, 89*, 214–226.

Bartos, M., Vida, I., & Jonas, P. (2007). Synaptic mechanisms of synchronized gamma oscillations in inhibitory interneuron networks. *Nature Reviews. Neuroscience*, 45–56.

Beierlein, M., Gibson, J. R., & Connors, B. W. (2000). A network of electrically coupled interneurons drives synchronized inhibition in neocortex. *Nature Neuroscience, 3*(9), 904–910. doi:10.1038/78809.

Bennett, M. V. L., & Zukin, R. S. (2004). Electrical coupling and neuronal synchronization in the mammalian brain. *Neuron, 41*(4), 495–511.

Boyden, E. S., Zhang, F., Bamberg, E., Nagel, G., & Deisseroth, K. (2005). Millisecond-timescale, genetically targeted optical control of neural activity. *Nature Neuroscience, 8*(9), 1263–1268. doi:10.1038/nn1525.

Buzsaki, G. (2006). *Rhythms of the brain*. Oxford University Press.

Cardin, J. A., Carlén, M., Meletis, K., Knoblich, U., Zhang, F., Deisseroth, K., et al. (2009). Driving fast-spiking cells induces gamma rhythm and controls sensory responses. *Nature, 459*(7247), 663–667. doi:10.1038/nature08002.

Chow, C., White, J., Ritt, J., & Kopell, N. (1998). Frequency control in synchronized networks of inhibitory neurons. *Journal of Computational Neuroscience, 5*, 407–420.

Colwyn, T., & Stuart, D. (2005). Disorganized rhythm and synchrony: Early signs of autism and rett syndrome. *Brain & Development, 27*(Suppl 1), S25–S34. doi:10.1016/j.braindev.2005.03.016.

Crook, S., Ermentrout, G., & Vanier, M. (1997). The role of axonal delay in the synchronization of networks of coupled cortical oscillators. *Journal of Computational Neuroscience, 4*(2), 161–172.

Cui, J., Canavier, C. C., & Butera, R. J. (2009). Functional phase response curves: A method for understanding synchronization of adapting neurons. *Journal of Neurophysiology, 102*(1), 387–398. doi:10.1152/jn.00037.2009.

Danzl, P., Nabi, A., & Moehlis, J. (2010). Charged balanced spike timing control for phase models of spiking neurons. *Discrete and Continuous Dynamical Systems, 28*, 1413–1435.

Deisseroth, K., Feng, G., Majewska, A. K., Miesenböck, G., Ting, A., & Schnitzer, M. J. (2006). Next-generation optical technologies for illuminating genetically targeted brain circuits. *Journal of Neuroscience, 26*(41), 10380–10386. doi:10.1523/JNEUROSCI.3863-06.2006.

Ermentrout, B. (1996). Type 1 membranes, phase resetting curves and synchrony. *Neural Computation, 8*, 979–1001.

Ernst, U., Pawelzik, K., & Geisel, T. (1995). Synchronization induced by temporal delays in pulse-coupled oscillators. *Physical Review Letters, 74*, 1570–1573.

Fisahn, A., Pike, F., Buhl, E., & Paulsen, O. (1998). Cholinergic induction of network oscillations at 40 hz in the hippocampus *in vitro*. *Nature, 394*, 186–189.

Galarreta, M., & Hestrin, S. (2001). Spike transmission and synchrony detection in networks of gabaergic interneurons. *Science, 292*(5525), 2295–2299. doi:10.1126/science.1061395.

Gradinaru, V., Mogri, M., Thompson, K. R., Henderson, J. M., & Deisseroth, K. (2009). Optical deconstruction of parkinsonian neural circuitry. *Science, 324*(5925), 354–359. doi:10.1126/science.1167093.

Gunaydin, L., Yizhar, O., Berndt, A., Sohal, V., Deisseroth, K., & Hegemann, P. (2010). Ultrafast optogenetic control. *Nature Neuroscience, 13*(3), 387–392. doi:10.1038/nn.2495.

Hegemann, P., Ehlenbeck, S., & Gradmann, D. (2005). Multiple photocycles of channelrhodopsin. *Biophysical Journal, 89*(6), 3911–3918. doi:10.1529/biophysj.105.069716.

Huber, D., Petreanu, L., Ghitani, N., Ranade, S., Hromádka, T., Mainen, Z., et al. (2008). Sparse optical microstimulation in barrel cortex drives learned behaviour in freely moving mice. *Nature, 451*(7174), 61–64. doi:10.1038/nature06445.

Jeong, H., & Gutkin, B. (2007). Synchrony of neuronal oscillations controlled by gabaergic reversal potentials. *Neural Computation, 19*, 706–729.

Khalil, H. (2001). *Nonlinear systems* (3rd ed.). Prentice Hall.

Lewis, T. J., & Rinzel, J. (2003). Dynamics of spiking neurons connected by both inhibitory and electrical coupling. *Journal of Computational Neuroscience, 14*(3), 283–309.

Netoff, T. I., Acker, C. D., Bettencourt, J. C., & White, J. A. (2005). Beyond two-cell networks: Experimental measurement of neuronal responses to multiple synaptic inputs. *Journal of Computational Neuroscience, 18*(3), 287–295. doi:10.1007/s10827-005-0336-9.

Nikolic, K., Grossman, N., Grubb, M., Burrone, J., Toumazou, C., & Degenaar, P. (2009). Photocycles of channelrhodopsin-2. *Photochemistry and Photobiology, 85*(1), 400–411. doi:10.1111/j.1751-1097.2008.00460.x.

Oprisan, S., & Canavier, C. (2001). Stability analysis of ring of pulse coupled oscillators: The effect of phase resetting in the second cycle after the pulse is important at synchrony and for long pulses. *Differential Equations and Dynamical Systems, 9*, 243–258.

Roelfsema, P., Engel, A., Konig, P., & Singer, W. (1997). Visuomotor integration is associated with zero time-lag synchronization among cortical areas. *Nature 385*(6612), 157–161.

Schiff, S. (2009). Kalman meets neuron: The emerging intersection of controltheory with neuroscience. In *Conf Proc IEEE Eng Med Biol Soc* (pp. 3318–3321).

Skinner, F. K., Chung, J. Y. J., Ncube, I., Murray, P. A., & Campbell, S. A. (2005). Using heterogeneity to predict inhibitory network model characteristics. *Journal of Neurophysiology, 93*(4), 1898–907. doi:10.1152/jn.00619.2004.

Strogatz, S. (2001). *Nonlinear dynamics and chaos with application to physics, biology, chemistry and engineering*. Westview Press.

Swadlow, H. A., Beloozerova, I. N., & Sirota, M. G. (1998). Sharp, local synchrony among putative feed-forward inhibitory interneurons of rabbit somatosensory cortex. *Journal of Neurophysiology, 79*(2), 567–582.

Symond, M. P., Symond, M. B., Harris, A. W. F., Gordon, E., & Williams, L. M. (2005). "Gamma synchrony" in first-episode schizophrenia: A disorder of temporal connectivity? *American Journal of Psychiatry, 162*(3), 459–65. doi:10.1176/appi.ajp.162.3.459.

Talathi, S., Hwang, D., Carney, P., & Ditto, W. (2010). Synchrony with shunting inhibition in a feedforward inhibitory network. *Journal of Computational Neuroscience, 28*(2), 305–321. doi:10.1007/s10827-009-0210-2.

Talathi, S., Hwang, D., & Ditto, W. (2008). Spike timing dependent plasticity promotes synchrony of inhibitory networks in the presence of heterogeneity. *Journal of Computational Neuroscience, 25*, 262–281.

Tønnesen, J., Sørensen, A. T., Deisseroth, K., Lundberg, C., & Kokaia, M. (2009). Optogenetic control of epileptiform activity. *Proceedings of the National Academy of Sciences of the United States of America, 106*(29), 12162–12167. doi:10.1073/pnas.0901915106.

Traub, R., Whittington, M., Stanford, I., & Jefferys, J. (1996). A mechanism for generation of long-range synchronous fast oscillations in the cortex. *Nature, 383*(6601), 621–624.

Uhlhaas, P. J., Roux, F., Rodriguez, E., Rotarska-Jagiela, A., & Singer, W. (2010). Neural synchrony and the development of cortical networks. *Trends in Cognitive Sciences, 14*(2), 72–80. doi:10.1016/j.tics.2009.12.002.

Uhlhaas, P. J., & Singer, W. (2006). Neural synchrony in brain disorders: Relevance for cognitive dysfunctions and pathophysiology. *Neuron, 52*(1), 155–168. doi:10.1016/j.neuron.2006.09.020.

vanVreeswijk, C., Abbott, L., & Ermentrout, B. (1994). When inhibition and not excitation synchronizes neural firing. *Journal of Computational Neuroscience, 1*(313—321).

Varela, F., Lachaux, J. P., Rodriguez, E., & Martinerie, J. (2001). The brainweb: Phase synchronization and large-scale

integration. *Nature Reviews. Neuroscience, 2*(4), 229–239. doi:10.1038/35067550.

Wang, X., & Buzsaki, G. (1996). Gamma oscillation by synaptic inhibition in a hippocampal interneuronal network model. *Journal of Neuroscience, 16*, 6402–6413.

Wang, X., & Rinzel, J. (1992). Alternating and synchronous rhythms in reciprocally inhibitory model neurons. *Neural Computation, 4*, 84–97.

White, A., Chow, C., Ritt, J., Trevino, C., & Kopell, N. (1998). Synchronization and oscillatory dynamics in heterogeneous, mutually inhibited neurons. *Journal of Computational Neuroscience, 5*, 5–16.

Whittington, M., Traub, R., & Jefferys, J. (1995). Synchronized oscillations in interneuron networks driven by metabotropic glutamate receptor activation. *Nature, 373*, 612–615.

Zhigulin, V. P., Rabinovich, M. I., Huerta, R., & Abarbanel, H. D. I. (2003). Robustness and enhancement of neural synchronization by activity-dependent coupling. *Physical Review, E, Statistical, Nonlinear and Soft Matter Physics, 67*(2 Pt 1), 021,901.

J Comput Neurosci
DOI 10.1007/s10827-008-0077-7

Spike timing dependent plasticity promotes synchrony of inhibitory networks in the presence of heterogeneity

Sachin S. Talathi · Dong-Uk Hwang · William L. Ditto

Received: 25 July 2007 / Revised: 15 January 2008 / Accepted: 16 January 2008

Abstract Recently Haas et al. (J Neurophysiol 96: 3305–3313, 2006), observed a novel form of spike timing dependent plasticity (iSTDP) in GABAergic synaptic couplings in layer II of the entorhinal cortex. Depending on the relative timings of the presynaptic input at time t_{pre} and the postsynaptic excitation at time t_{post}, the synapse is strengthened ($\Delta t = t_{post} - t_{pre} > 0$) or weakened ($\Delta t < 0$). The temporal dynamic range of the observed STDP rule was found to lie in the higher gamma frequency band ($\geq$40 Hz), a frequency range important for several vital neuronal tasks. In this paper we study the function of this novel form of iSTDP in the synchronization of the inhibitory neuronal network. In particular we consider a network of two unidirectionally coupled interneurons (UCI) and two mutually coupled interneurons (MCI), in the presence of heterogeneity in the intrinsic firing rates of each coupled neuron. Using the method of spike time response curve (STRC), we show how iSTDP influences the dynamics of the coupled neurons, such that the pair synchronizes under moderately large heterogeneity in the firing rates. Using the general properties of the STRC for a Type-1 neuron model (Ermentrout, Neural Comput 8:979–1001, 1996) and the observed iSTDP we determine conditions on the initial configuration of the UCI network that would result in 1:1 in-phase synchrony between the two coupled neurons. We then demonstrate a similar enhancement of synchrony in the MCI with dynamic synaptic modulation. For the MCI we also consider heterogeneity introduced in the network through the synaptic parameters: the synaptic decay time of mutual inhibition and the self inhibition synaptic strength. We show that the MCI exhibits enhanced synchrony in the presence of all the above mentioned sources of heterogeneity and the mechanism for this enhanced synchrony is similar to the case of the UCI.

Keywords Inhibitory synapses · Spike timing dependent plasticity · Synchronization · Networks · Heterogeneity

Action Editor: Carson C. Chow

S. S. Talathi (✉) · D.-U. Hwang · W. L. Ditto
J Crayton Pruitt Family Department of Biomedical Engineering, University of Florida, FL 32611, USA
e-mail: stalathi@bme.ufl.edu

D.-U. Hwang
e-mail: donguk.hwang@bme.ufl.com

W. L. Ditto
e-mail: william.ditto@bme.ufl.com

1 Introduction

It is generally accepted that inhibitory interneurons are important for synchrony in the neocortex. Several studies have reported a role for inhibitory interneurons in generating stable synchronous rhythms in the neocortex (Bernardo 1997; Jefferys et al. 1996; Michelson and Wong 1994; Whittington et al. 1995; Bragin et al. 1995). Cortical oscillations in the gamma frequency band (20–80 Hz), are thought to be involved in binding of object properties such as color and shape of a given object through synchronization, a process of great significance in the brain and its conscious perception of the surrounding world (Ritz and Sejnowski 1997).

The set of experimental findings and the importance of the binding property mentioned above has led to a

number of theoretical studies of synchrony among inhibitory interneurons (Ernst et al. 1995; vanVreeswijk et al. 1994; Wang and Rinzel 1992). The result of these studies can in general be summarized as: depending on the decay time of the inhibitory synaptic coupling, mutually coupled inhibitory neurons exhibit in-phase synchrony (zero phase difference) or out-phase synchrony (phase difference of π). However much of the above investigations did not explore the effects of heterogeneity in the intrinsic firing rates on synchronization nor did they take into account noise, which is invariably present in neuronal systems. In another set of theoretical investigations, White et al. (1998) explored the effects of small heterogeneities on the degradation of synchrony of fast spiking inhibitory neurons, and the mechanism by which the degradation occurs. They found that introduction of even small amounts of heterogeneity in the external dc current that drives the firing rate of the neuron, resulted in a significant reduction in the coherence of neuronal spiking. They attributed this loss in synchrony to the failure of a heterogeneous network to entrain the frequency of firing. It is important then to understand what mediates observed *in vivo* synchrony of inhibitory neuronal networks under biologically realistic conditions of noise induced unpredictability and intrinsic heterogeneity in the spiking rates of the neuronal ensemble.

In this paper we study the issue of sensitivity of synchrony to heterogeneity in neuronal firing rates, in the context of recently observed spike timing dependent plasticity in inhibitory synapses (iSTDP; Haas et al. 2006). We begin our analysis by considering a pair of unidirectionally coupled interneuron's (UCI) with dissimilar intrinsic firing rates. We study the influence of iSTDP on the synchronization properties of these two coupled neurons. We observe that iSTDP modulates the synaptic coupling strength such that the driven neuron fires synchronously in-phase with the driving neuron. The stability of this in-phase synchronous solution is then studied in terms of the stability of the fixed point of spike time evolution map for the coupled neurons using the spike time response method (Acker et al. 2004).

We then explore the function of iSTDP in *enhancing* synchronization between mutually coupled interneurons (MCI) with self inhibition in the presence of heterogeneity in the intrinsic firing rates. We consider the following set of heterogeneity in the MCI: (a) heterogeneity in external dc current, I^{DC}, (b) heterogeneity in the synaptic decay time, τ_D and (c) heterogeneity in the self inhibition strength, g_s.

Earlier work (Nowotny et al. 2003; Zhigulin et al. 2003) has explored the function of synaptic plasticity at an excitatory synapse in improving synchronization of a unidirectionally coupled neuronal network. They demonstrated that STDP of excitatory synapses with the property that the synaptic strength decreases when postsynaptic spike occurs after the presynaptic spike ($\Delta t = t_{\text{post}} - t_{\text{pre}} > 0$) and vice-versa, result in increased synchronization. In addition the role of gap junction coupling between interneurons in enhancement of synchronization has also been well studied (Skinner et al. 1999). It was shown in Kopell and Ermentrout (2004), that gap junction coupling plays a complementary role with respect to chemical synapses in synchrony of inhibitory neuronal network. The authors demonstrated that while, inhibition through GABAergic synapses is important for mitigating the effect of the initial conditions, it is the gap junction coupling that significantly improves synchronization in the presence of heterogeneity. *Our results in this work demonstrate that inhibitory plastic synapses can serve similar role by significantly improving synchronization in the presence of heterogeneity*.

The paper is organized as follows: In the methods section we present the mathematical model for the neuron, the synapse and the network studied. We then define the spike time response curve (STRC) for an isolated neuron with self inhibition. We then present the empirical iSTDP rule, observed by Haas et al. (2006) and use it in this paper to study the synchronization properties of the inhibitory network in the presence of heterogeneity. In the results section, we begin with the demonstration of the influence of iSTDP on synchronization of the two unidirectionally coupled interneurons. We then derive an analytic expression for the evolution of spike times for each neuron using STRC and then demonstrate how the iSTDP modulates the synaptic strength to synchronize the driven neuron to fire in-phase with the driving neuron for a broad range of heterogeneity in the firing rates. A similar enhancement in synchronization brought about by iSTDP is observed in the MCI with different intrinsic firing rates.

We have also done some investigation on the influence of noise in the presence of iSTDP on the synchronization property of the MCI. We considered two potential sources of noise through the milieu of the neuronal environment which might influence the dynamics of the network. The first source of noise considered was in the intrinsic firing frequency of each neuron and the second source of noise was considered in the modulation strength of the iSTDP. We found that even in the presence of mild noise, iSTDP plays a critical role in maintaining the synchronous state under heterogeneity. All the details on iSTDP induced

synchrony in the UCI and the MCI in the presence of noise will be presented in future work.

2 Methods

2.1 Model neuron

Each neuron is modeled based on Hodgkin Huxley framework as a single compartment model with fast sodium channel, delayed rectifier potassium channel and a leak channel. The parameters of the model are set such that it represents a cortical neuron model of type I (Ermentrout 1996). Each neuron is self inhibited through a GABAergic synaptic model which obeys second order kinetics. The dynamical equation for the model neuron is given by,

$$\begin{aligned} C\frac{\mathrm{d}V(t)}{\mathrm{d}t} &= I^{DC} + g_{\mathrm{Na}}m^3(t)h(t)(E_{\mathrm{Na}} - V(t)) \\ &\quad + g_{\mathrm{K}}n^4(t)(E_{\mathrm{K}} - V(t)) + g_{\mathrm{L}}(E_{\mathrm{L}} - V(t)) \\ &\quad + I_M(t) + I_S(t) \end{aligned} \tag{1}$$

where $C = 1\,\mu F/\mathrm{cm}^2$. $V(t)$ is the membrane potential, I^{DC}: external DC current drive, is set such that the neuron spikes at a given intrinsic frequency $F(I^{DC})$. $I_S(t) = g_s S_S(t)(E_I - V(t))$, is the synaptic current due to self inhibition and $I_M(t) = g_M(t)S_M(t)(E_I - V(t))$ is the synaptic current from external inhibition. g_s is the synaptic strength of self inhibition and $g_M(t)$ is the dynamic synapse, whose strength is determined by the inhibitory synaptic plasticity rule discussed below. E_r (r = Na, K, L) are reversal potentials of the sodium and potassium ion channels and the leak channel respectively. E_I, is the reversal potential of the inhibitory synapse. g_r (r = Na, K, L) represent the conductance of sodium, potassium and the leak channel respectively.

The gating variables $X = \{m, h, n\}$ satisfy the following first order kinetic equation: $\frac{\mathrm{d}X(t)}{\mathrm{d}t} = \alpha_X(V(t))(1 - X(t)) - \beta_X(V(t))X(t)$, where α_X and β_X are given by

$$\alpha_m = \frac{0.32(13-(V(t)-Vth))}{e^{\frac{(13-(V(t)-Vth))}{4.0}}-1} \qquad \beta_m = \frac{0.28((V(t)-Vth)-40)}{e^{\frac{((V(t)-Vth)-40)}{5}}-1}$$

$$\alpha_h = 0.128e^{\frac{17-(V(t)-Vth)}{18}} \qquad \beta_h = \frac{4}{e^{\frac{40-(V(t)-Vth)}{5}}+1}$$

$$\alpha_n = \frac{0.032(15-(V(t)-Vth))}{e^{\frac{(15-(V(t)-Vth))}{5}}-1} \qquad \beta_n = \frac{0.5}{e^{\frac{(V(t)-Vth)-10}{40}}}$$

with $V_{th} = -65$ mV.

$S_Y(t)$, ($Y = \{S, M\}$) gives the fraction of bound receptors and satisfy the following first order kinetic equation (Abarbanel et al. 2003),

$$\dot{S}_Y(t) = \frac{S_0(\theta(t)) - S_Y(t)}{\hat{\tau}(S_I - S_0(\theta(t)))}$$

where $Y = \{S, M\}$, and $\theta(t) = \sum_i \Theta(t - t_i).\Theta((t_i + \tau_R) - t)$. $\Theta(X)$ is the heaviside function satisfying $\Theta(X) = 1$ if $X > 0$ else $\Theta(X) = 0$ and t_i is the time of the ith presynaptic neuronal spike. In the case of self inhibition the presynaptic neuron is the same as the post synaptic neuron. The kinetic equation for $S(t)$ involves two time constants, $\tau_R = \hat{\tau}(S_I - 1)$, the docking time for the neurotransmitter and $\tau_D = \hat{\tau}S_I$, the undocking time constant for the neurotransmitter binding. Finally, $S_0(\theta)$ is the sigmoidal function given by, $S_0(\theta) = 0.5(1 + \tanh(120(\theta - 0.1)))$.

In Table 1 we list all the parameters for the model considered, unless otherwise stated in the text and figure captions.

All the model parameters given above are within physiological range and give high spike rates typical of the fast spiking interneurons (Lacaille and Williams 1990; McCormick et al. 1985).

All the simulations were done using 4th order Runge–Kutta method for differential equations with time step $\delta t = 0.01$ ms, on a 2 GHz Intel Core Duo Mac OS X. The source code is available from authors on request.

2.2 Spike time response curve (STRC)

As a measure of the influence of synaptic input on the firing times of a neuron, we define the spike time response curve (STRC) $\Phi(t, \tau_R, \tau_D, g, T^0) = T - T^0$ (Acker et al. 2004; Oprisan et al. 2004), where T^0 is the intrinsic period of spiking for a given neuron model obtained by driving the neuron with a fixed DC current I^{DC} and T is the time at which the neuron fires a spike after it has received a perturbation through synaptic input at time $t < T$, in its spiking cycle. The key to the computation of STRC is that the perturbation is through a model GABAergic input with synaptic parameters, τ_R: the synapse rise time, τ_D: the synaptic decay time and g: the synaptic strength. In general this input

Table 1 List of all the parameters for the model considered

Neuron model	E_{Na}	50 mV
	E_{K}	−95 mV
	E_{L}	−64 mV
	g_{Na}	215 mS/cm^2
	g_{K}	43 mS/cm^2
	g_{L}	0.813 mS/cm^2
Synapse model	E_I	−82 mV
	g_S	0.2 mS/cm^2
	g_M (static synapse)	0.1 mS/cm^2
	τ_R	0.2 ms
	τ_D	5 ms

need not be weak. The STRC is obtained numerically here using the direct method of STRC computation as shown in the schematic diagram of STRC calculation in Fig. 1(a). The neuron firing regularly with period T^0, is perturbed through inhibitory synapse at time t after the neuron has fired a spike at reference time zero. The spiking time for neuron is considered to be the time when the membrane voltage V, crosses a threshold (set to 0 mV in all the calculations presented here). As a result of this perturbation, the neuron fires the next spike at time T which is different from T^0, the time at which the neuron would have fired a spike in absence of any perturbation through inhibitory synapse. The STRC measures this shift in firing time of the neuron $T - T^0$ as a function of the time of perturbation in the neuronal firing period through the synaptic input. As shown in Fig. 1(b) the STRC is obtained by varying the perturbation time t, over the entire cycle of

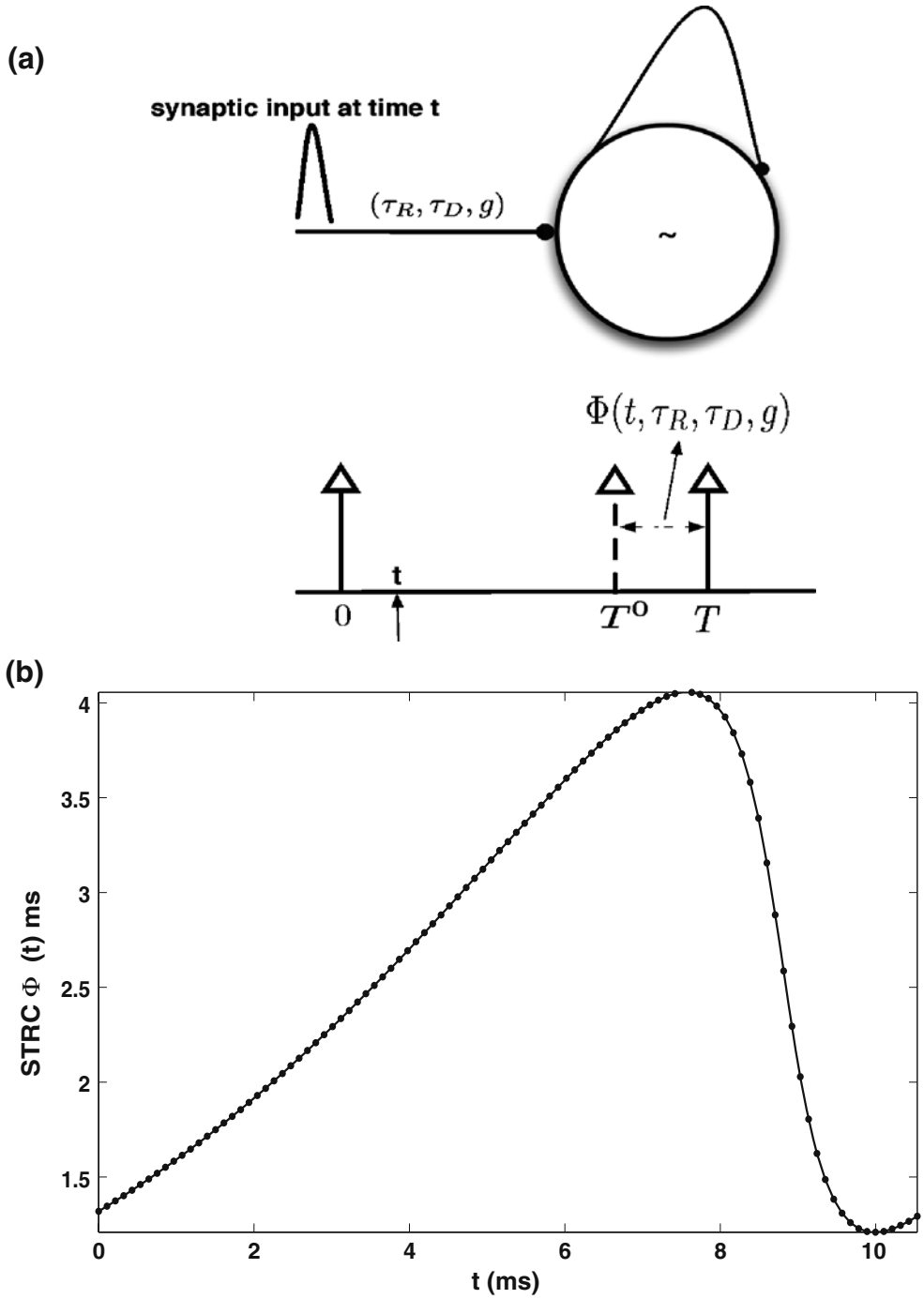

Fig. 1 Spike time response curve (STRC). (**a**) Schematic diagram demonstrating the perturbation effect of synaptic input to neuron firing at given period T^0. A perturbation is delivered to the neuron through the inhibitory synapse at time t after the last neuronal spike at reference time t. The perturbation results in the next spike of neuron occurring at time T which is different from the time of spike for neuron T^0 in the absence of any synaptic perturbation. The STRC measures this shift in spike time as function of the time t, when the perturbation is delivered (**b**) STRC of neuron firing with period $T^0 = 10.6$ ms. The synaptic parameters are: $\tau_R = 0.2$ ms, $\tau_D = 5$ ms, and $g = 0.1$ mS/cm^2

spiking ($T^0 = 10.6$ ms, for the example considered) and plotting Φ versus the perturbation time t. The synaptic parameters for computation in Fig. 1(b) are, $\tau_R = 0.2$ ms, $\tau_D = 5$ ms, $g = 0.2$ mS/cm^2 .

STRC is analogous to the phase response curve (PRC; Ermentrout 1996). Similar to the PRC for type I neurons, the STRC results in the subsequent spike of the neuron receiving an inhibitory input to be delayed in time. For brevity of notation, in all further calculations, unless otherwise mentioned, we suppress the dependence of Φ on τ_R, τ_D and define $\Phi(t, \tau_R, \tau_D, g) \equiv \Phi(t, g)$.

2.3 Spike timing dependent plasticity of inhibitory synapses

A spike timing dependent plasticity rule for inhibitory synapses (iSTDP) has been recently reported in Haas et al. (2006) and an empirical fit to the observed experimental data was obtained with the following functional form

$$\Delta g(\Delta t) = \frac{g_0}{g_{\text{norm}}} \alpha^\beta |\Delta t| \Delta t^{\beta-1} e^{-\alpha|\Delta t|} \tag{2}$$

where $\Delta t = t_{\text{post}} - t_{\text{pre}}$. t_{pre} is the time of presynaptic spike input arrival and t_{post} is the time of a spike generated by the postsynaptic neuron. g_0 is the scaling factor accounting for the amount of change in inhibitory conductance induced by the synaptic plasticity rule and is set to $g_0 = 0.02$ in all the calculations presented here. $g_{\text{norm}} = \beta e^{-\beta}$ is the normalizing constant. With parameter values $\alpha = 1$ and $\beta = 10$ (Haas et al. 2006), we obtain a window of ± 20 ms over which the efficacy of synaptic plasticity is non zero. In Fig. 2 we show the iSTDP rule fit with functional form given in Eq. (2). Four key properties of the iSTDP rule are summarized below:

1. $\Delta g(\Delta t) > 0$ for $\Delta t > 0$
2. $\Delta g(\Delta t) < 0$ for $\Delta t < 0$
3. $\Delta g(\Delta t) \approx 0$ for $\Delta t \approx 0$ and
4. $\Delta g(-\Delta t) = -\Delta g(\Delta t)$

Properties 1 and 2 above imply that a pre-synaptic spike occurring before post-synaptic excitation will always enhance the strength of inhibitory synaptic input and vice-versa. Property 3 imply that the synaptic strength of self inhibition is not modified by the spiking neuron as the pre and the post synaptic spikes for the self inhibitory synapse occur at the same time, i.e., $\Delta t = 0$. Property 4, emerges from our choice of same values for parameters α and β for both positive and negative Δt regions. We have also explored the effect of asymmetry

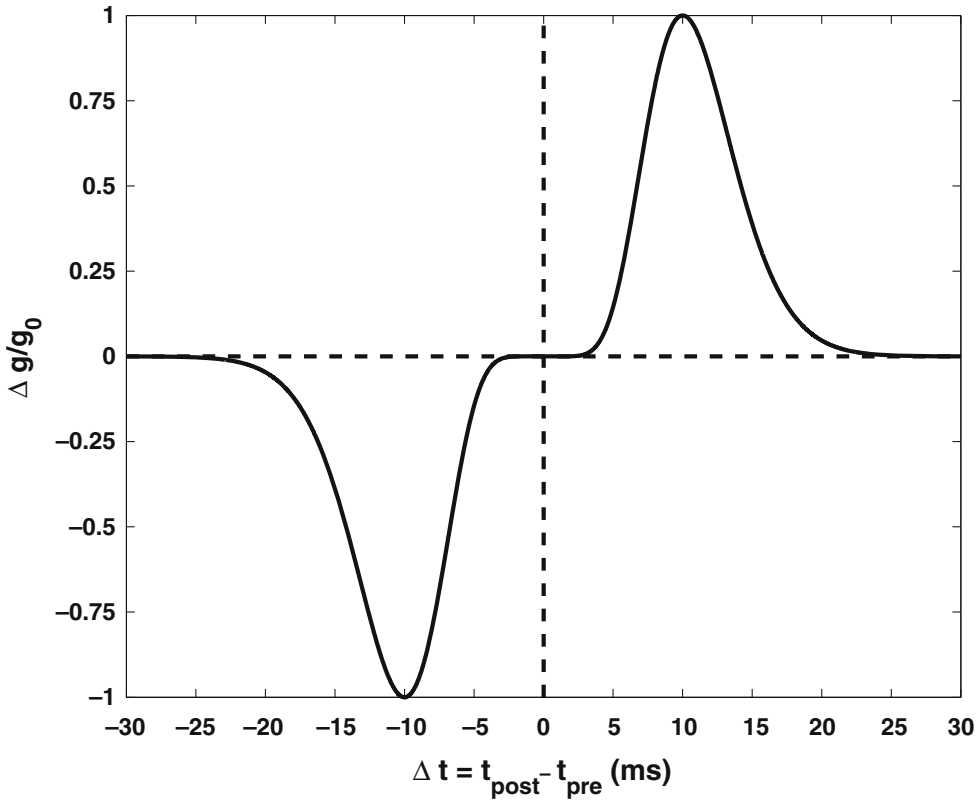

Fig. 2 STDP rule for inhibitory synapses. The parameters are $\alpha = 1$, $\beta = 10$ and $g_0 = 1$

in the empirical rule on the synchronization properties of the inhibitory network. We find that for level of asymmetry as presented in Haas et al. (2006), where for $\Delta t > 0$, $\alpha = 0.94$ and for $\Delta t < 0$, $\alpha = 1.1$, with $\beta = 10$, the enhancement in synchronization window through iSTDP remains essentially the same as presented in Fig. 6. In all the calcutions presented in this work, unless otherwise mentioned, the parameters for the empirical fit for iSTDP define in Eq. (2) are, $\alpha = 1$, $\beta = 10$ and $g_0 = 0.02$.

2.4 Inhibitory neuronal network

We consider a network of two neurons with self inhibition in (a) unidirectional coupling and (b) bidirectional coupling (mutual inhibition), configuration as shown in Fig. 3. Synchronization in the case of unidirectional coupling requires that the driven neuron (1) fires at a higher rate as compared to the driving neuron (2) because the effect of inhibition is to slow the firing rate of the inhibited neuron.

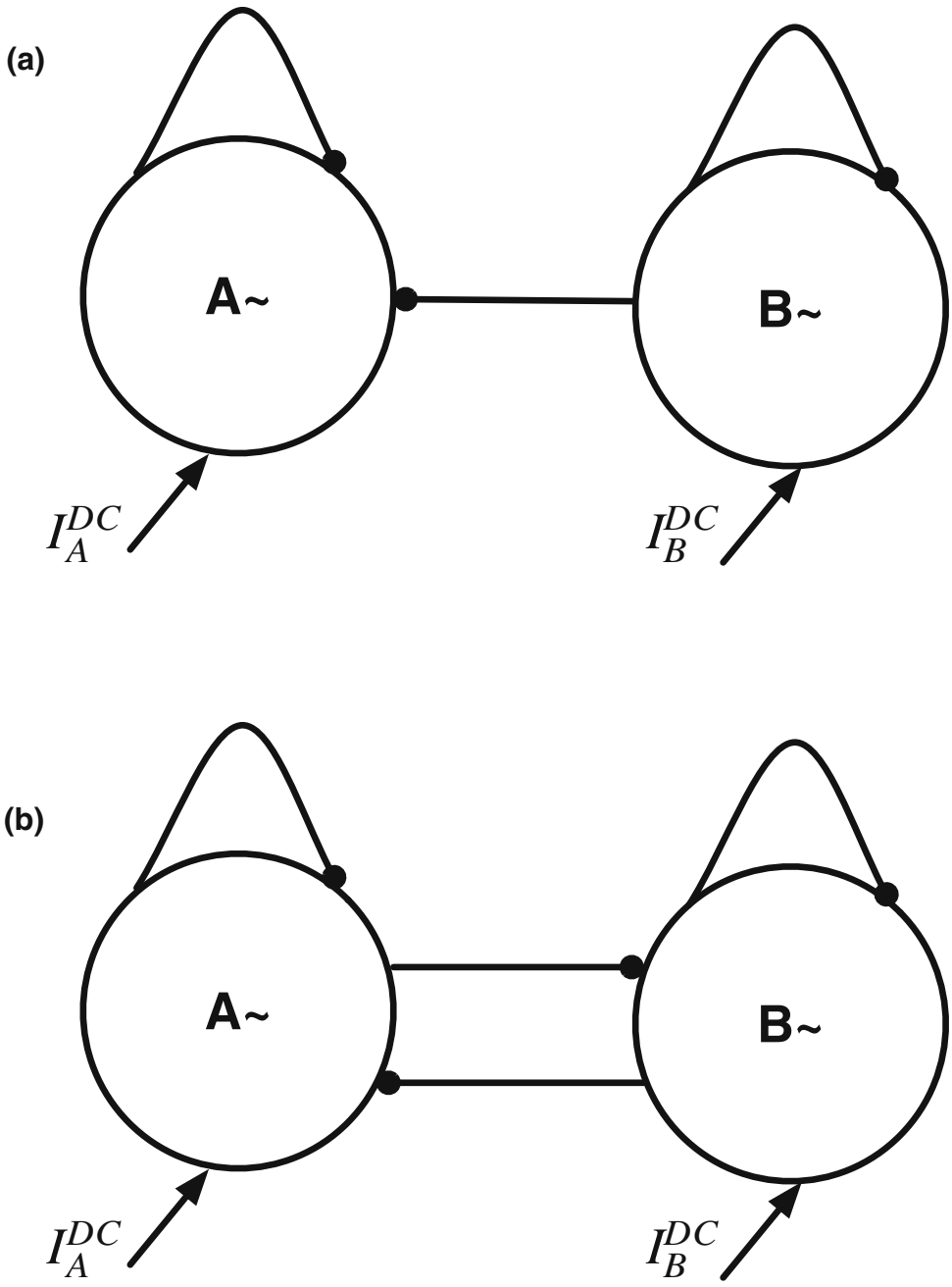

Fig. 3 Inhibitory neuronal network. (**a**) Unidirectional coupled interneurons (UCI), $I^A_{DC} > I^B_{DC}$; (**b**) mutually coupled interneurons (MCI), $I^A_{DC} \neq I^B_{DC}$. The $\sim$ in $(K\sim)$, $K \equiv \{A, B\}$, represents the fact that the strength of constant input drive I^{DC} is such that each neuron is driven above the threshold for spiking and has an intrinsic firing rate $F(I^{DC})$

3 Results

3.1 Single self inhibited neuron

We begin with the study of the firing characteristics of single self inhibited neuron dependent on the synaptic parameters: the rise time τ_R, the decay time τ_D and the strength of self inhibition, g_s. Spike based adaptation, dependent on self inhibition is considered for the following reasons,

- Biological neural networks often have local inhibitory interneurons which deliver feedback inhibition to the cells that activate those interneurons (Sheperd 1990).
- It has been shown by Traub et al. (2001), that the frequency in the gamma regime in a distributed network of inhibitory interneurons is highly dependent on synaptic decay time. This effect has been simulated through self inhibition in our model.
- The iSTDP learning rule considered in this work, has a zero at $\Delta t = 0$, which implies, the strength of self inhibition is not modulated through the iSTDP rule. As a result, the synchronization in the UCI and the MCI, is not modulated by changes in self-inhibition strength of through iSTDP. In addition, self-inhibition provides a control over frequency range of operation of the neuron through the synaptic parameters.

In Fig. 4, we show the frequency response of the neuron for the following set of synaptic parameters, $g_s = \{0.2, 0.5, 0.75, 1.0\}$ mS/cm^2, $\tau_R = \{0.1, 0.5, 1.1, 2.0\}$ ms and $\tau_D = \{5, 10, 25, 50\}$ ms. We see that while the biologically realistic time scales for synaptic rise time do not have a significant effect on the firing characteristics of the self inhibited neuron, the synaptic decay time and the strength of self inhibition do significantly decrease the firing frequency of the neuron for a fixed level of input drive I^{DC}. This results from the fact that for slower synaptic decay times the effect of inhibition persists longer. As a result the neuron takes longer time to recover from hyper-polarization to produce a spike again. Also if the strength of inhibition is high, the neuron is strongly inhibited and it takes a longer time to recover back to produce the next spike. Thus τ_D, the decay time of self inhibition and g_s, the synaptic strength of self inhibition determines the frequency regime of operation of the neuron. Heterogeneity in one of these parameters will significantly affect the synchronization properties of network of inhibitory neurons.

3.2 Spike time scheme for the analysis of iSTDP induced synchrony

For the analysis of iSTDP induced synchrony in the UCI and the MCI in the presence of heterogeneity using STRC, we adopt the following representation for spike times from neuron A and B:

Let $W_A = [w_A(1), w_A(2), \cdots w_A(i), \cdots w_A(N_A)]$, where $w_A(i) = t_A^i$ and t_A^i represents the time of ith spike from neuron A and N_A is the total number of spikes from neuron A. Similarly we define the set $W_B = [w_B(1), w_B(2), \cdots w_B(j), \cdots, w_B(N_B)]$ with $w_B(j) = t_B^j$, where t_B^j again represents the time of jth spike from neuron B. We now define a new set W_E comprising of all spike times from the coupled system (UCI/MCI) arranged in monotonically increasing order as follows, $W_E = W_A \oplus W_B = [w_E(1), w_E(2), \cdots w_E(N_A + N_B)]$. For example, if $t_A^1 < t_B^1 < t_A^2$, the first two elements in the set W_E are, $w_E(1) = t_A^1$ and $w_E(2) = t_B^1$ respectively. In the case when neurons A and B fires at the same time, we have for some i, and j, $t_A^i = t_B^j$. These two simultaneous spike events are added to W_E such that, for some n, $w_E(n) = t_A^i$ and $w_E(n+1) = t_B^j$. We next define two new sets, $\widetilde{W}_A$ and $\widetilde{W}_B$, which represents a modified spike time series for neurons A and B defined by, $\widetilde{W}_{A/B} = [\tilde{w}_{A/B}(1), \tilde{w}_{A/B}(2), \cdots \tilde{w}_{A/B}(N_A + N_B)]$,where each element $\tilde{w}_{A/B}(n)$ is obtained from $W_{A/B}$ and W_E as follows,

$$\tilde{w}_{A/B}(n) = \max\left(w_{A/B}(i) \leq w_E(n)\right) \quad \left(0 < i \leq N_{A/B}\right)$$

We now define an inter spike interval (ISI) time series $s(n)$, for the coupled system as $s(n) = w_E(n+1) - w_E(n)$. When the two neurons show in-phase synchrony with period T, we have $s(2n-1) = 0$ and $s(2n) = T$, $\forall\, n > 0$. For the case of dynamic synapse, the synaptic strength $g(t)$ is modulated by the pre-post synaptic spike pairs through iSTDP [Eq. (2)]. We define $g(t) = g(n)$ when $w_E(n) \leq t < w_E(n+1)$. In Fig. 5 we show the schematic diagram for the spike time scheme used for the analysis of the iSTDP induced synchrony as presented in this section.

3.3 iSTDP induced synchrony in the UCI

3.3.1 Numerical simulations

We consider two self inhibited neurons with unidirectional coupling [Fig. 3(a)] in the presence of heterogeneity in their intrinsic firing rates introduced through

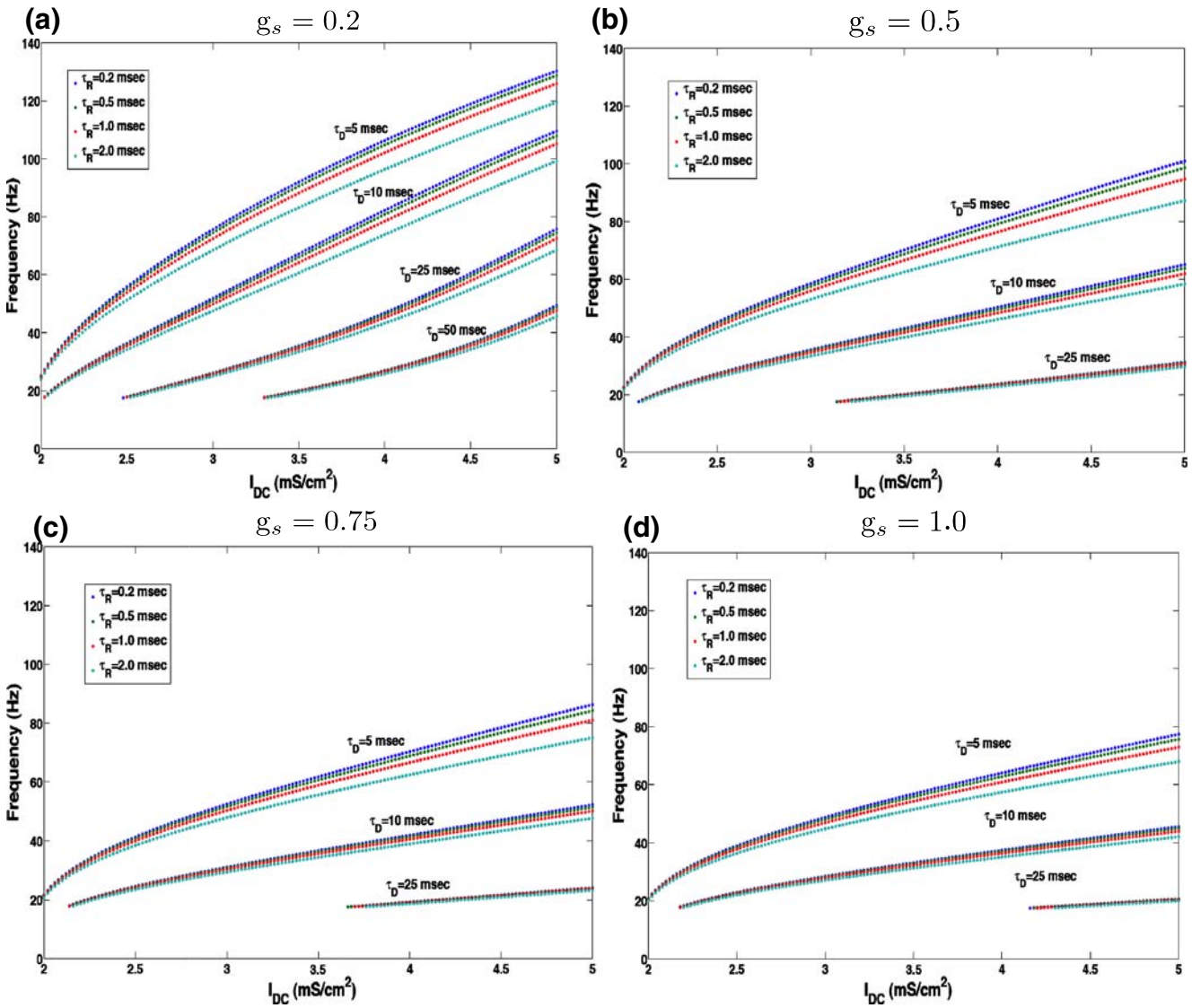

Fig. 4 Frequency response of single self inhibited neuron as function of the input current I^{DC}, for given synaptic parameters of self inhibition: The synaptic decay time τ_D, The synaptic rise time τ_R and the strength of self inhibition g_s. In each case,{a,b,c,d} all the parameters for neuron model are constant, however we vary the strength of self inhibition as, g_s={0.1,0.5,0.75,1.0} mS/cm^2 respectively. See online publication for the color version of this figure

different external drive (I^{DC}) and study the synchronization properties of the coupled neurons in the context of dynamic synapse. We set $I_B^{DC} = 2.5$ μA/cm^2, such that neuron B is firing at frequency of $F(I_A^{DC}) =$ 56 Hz, giving an intrinsic period of $T_B^0 \approx 17.85$ ms. We define heterogeneity

$$H = 100\frac{I_A^{DC} - I_B^{DC}}{I_A^{DC} + I_B^{DC}}$$

where I_A^{DC} is the steady input current in neuron A. When $I_A^{DC} \approx I_B^{DC}$, the heterogeneity $H \approx 0$ and if all other neuronal parameters are identical, the two neurons have identical firing rates. For $I_A^{DC} \gg I_B^{DC}$, $H \approx$ 100 and the two neurons are maximally heterogeneous in terms of their firing rates. For all the simulations below, unless otherwise mentioned, the initial conditions on the membrane potentials, $V_A(t = 0) = -75$ mV and $V_B(t = 0) = -65$ mV. We have also run numerical simulations for a number of different initial conditions on the membrane potential and found that the iSTDP induced synchronous state is the global attractor of the coupled system. Also, all the spike times required by the synaptic update rule and the STRC calculations were obtained as the time when the membrane voltage of neuron rose through a threshold of 0 mV.

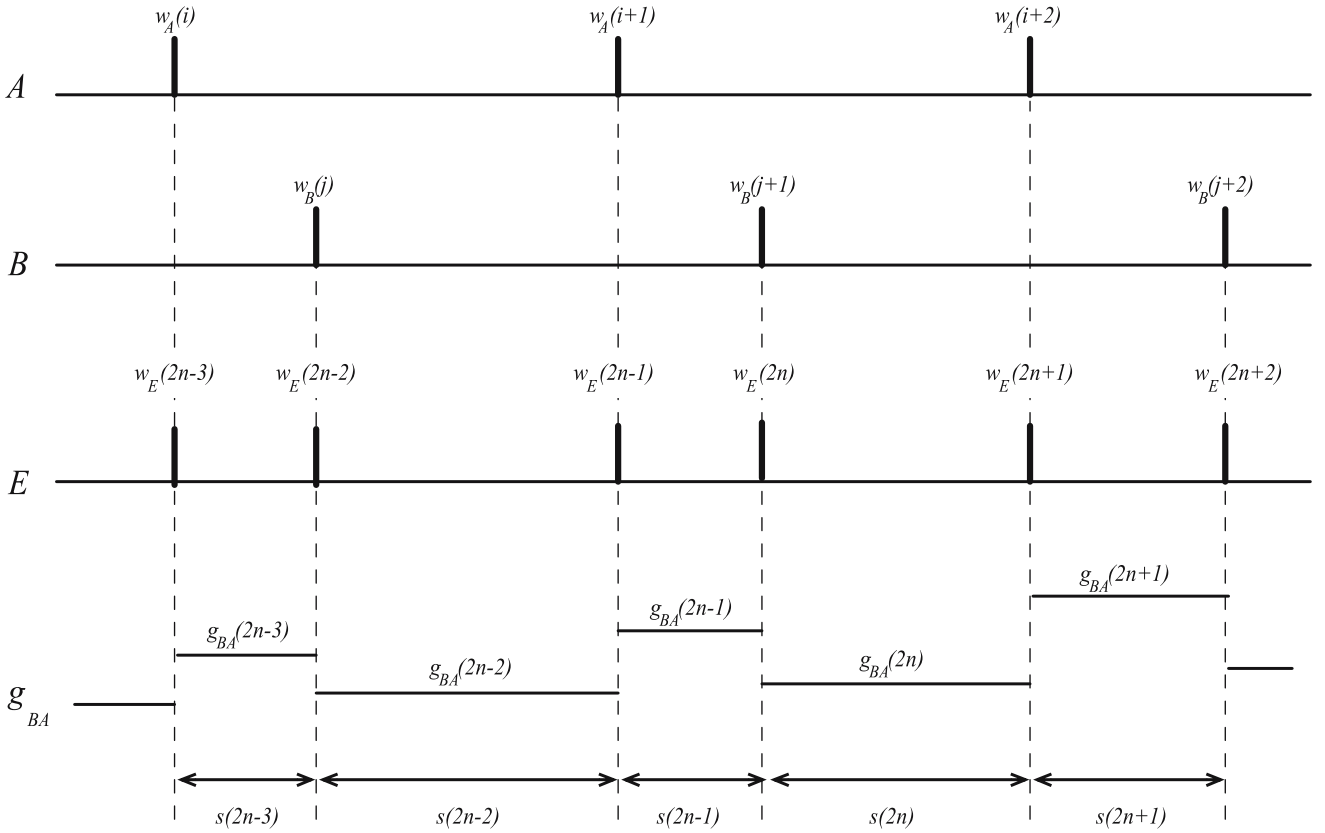

Fig. 5 The set W_A. W_B, W_E corresponding to the spike times of neuron A, neuron B and the coupled system are shown. We also show the inter-spike interval s between the spikes in the coupled system and the evolution of the dynamic synapse g_{BA} modulated by the iSTDP rule

We now consider two situations: one in which the conductance of the inhibitory synapse from B to A, g^S_{BA} is static, with $g^S_{BA} = 0.1$ mS/cm^2 (g_{ij} is the conductance of inhibitory synapse from neuron i onto neuron j), and a second situation in which the inhibitory synaptic strength is dynamic and is governed by the iSTDP rule given in Fig. 2, such that

$$g_{BA}(n) = g_{BA}(n-1) + \Delta g(\tilde{w}_A(n) - \tilde{w}_B(n)) \tag{3}$$

where $g_{AB}(n)$ is synaptic strength from B to A for duration, $w_E(n) \leq t < w_E(n+1)$ (see Results, Section 3.2).

In defining the synaptic update rule defined above, we make two key assumptions

- The iSTDP update is considered to be dependent only on the two nearest spike neighbors, and the effects of spike pairs is assumed to sum linearly, following the conditions under which (Haas et al. 2006) experimentally observed the iSTDP. We ignore multi-spike interactions, which have been shown to play a significant role in STDP of excitatory synapses (Froemke and Dan 2002) and also any dependence of iSTDP on the frequency of firing of the pre-synaptic neuron.
- The iSTDP update is assumed to happen instantaneously, as a result we ignore the delay that exists between the pairing of the pre and post-synaptic spikes and the resultant induction of synaptic modification as suggested by the experiments.

The implication of above assumptions regarding the iSTDP update rule, are explored in more details in the discussion section. We begin with the initial synaptic strength $g_{BA}(t=0) \equiv g_{BA}(0) = g^S_{BA} = 0.1$ mS/cm^2. In order to determine synchrony in the firing of the UCI, in Fig. 6(a) we plot the ratio of the period for spiking for neuron B (the driver neuron) T^0_B to the average period for spiking for neuron A, $\langle T_A \rangle$ as a function of heterogeneity H, for the two cases considered above: Static synapse, and Dynamic synapse, modulated by iSTDP rule defined in Eq. (2). We see that in the case of static synapse, neuron B is able to entrain neuron A to fire at its frequency for mild levels of heterogeneity H (from about 2 to 12). But as the heterogeneity increases beyond $H \approx 12$, neuron B with a static synapse is no

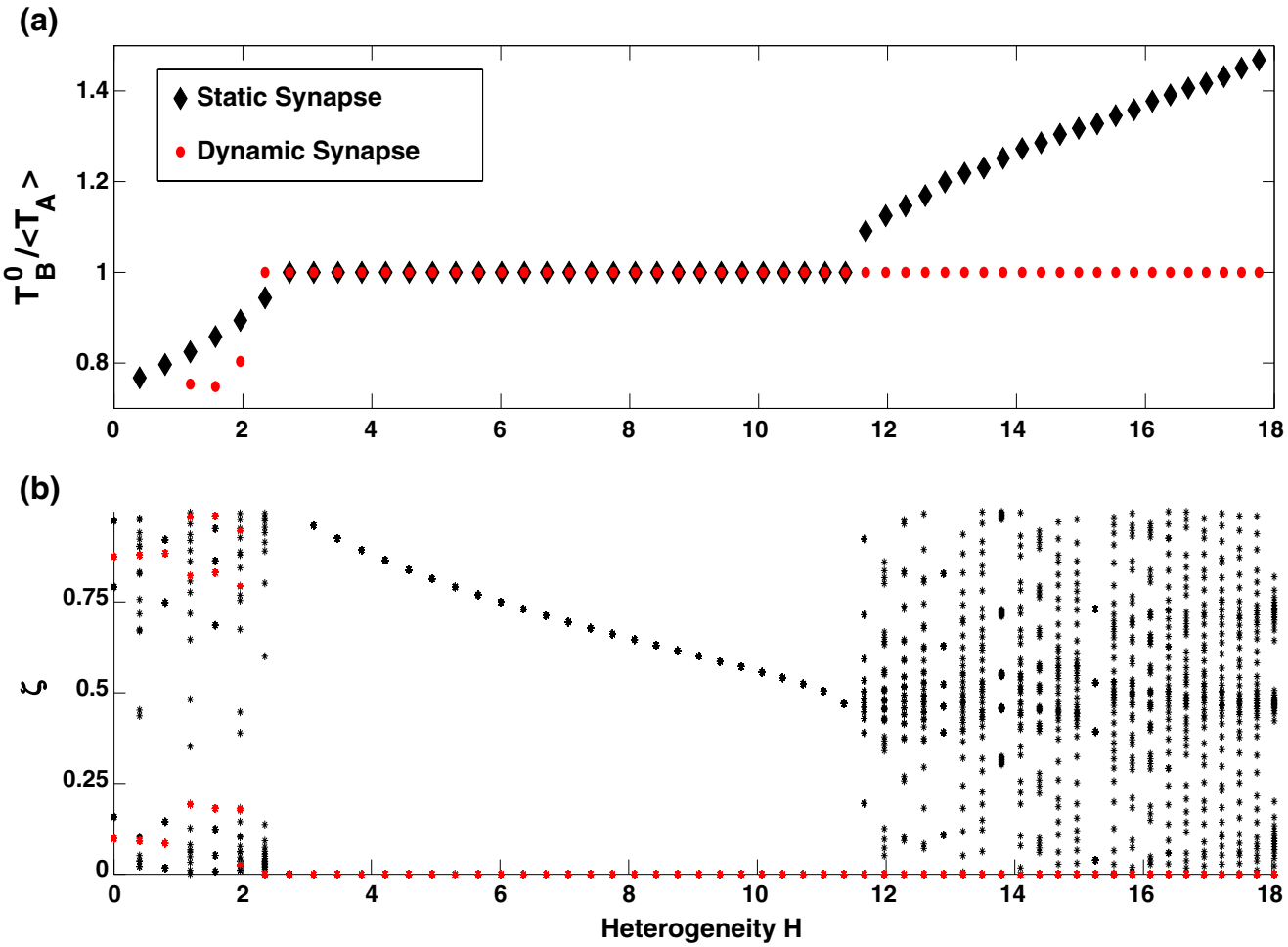

Fig. 6 Synchronization in the UCI with static (*black*) and dynamic synapse (*red*). (**a**) The ratio of average spiking period of each neuron of the UCI is plotted as function of heterogeneity H. (**b**) The generalized phase difference ζ is plotted as function of heterogeneity H. See online publication for the color version of this figure

longer able to entrain neuron A to fire at its frequency and the two neurons fire asynchronously.

In Fig. 6(b), we show the scatter plot of the phase difference, $\zeta(n)$, between the two coupled neurons as function of heterogeneity H. We define the general phase difference $\zeta(n)$ at $w_E(n)$ as

$$\begin{aligned}\zeta(n) &= \frac{w_A(i)-w_B(j)}{w_B(j+1)-w_B(j)} \\ &\quad \text{with } (w_B(j) \le w_A(i) = w_E(n) < w_B(j+1)) \\ &= \frac{w_B(j)-w_A(i)}{w_A(i+1)-w_A(i)} \\ &\quad \text{with } (w_A(i) \le w_B(j) = w_E(n) < w_A(i+1)). \quad (4)\end{aligned}$$

For the case of the UCI, Fig. 3(a), $\langle T_B \rangle = T_B^0$. We see that in the static synaptic case, the two neurons phase lock in 1:1 synchrony, with a finite phase difference ζ for a certain range of heterogeneity values ($2 < H < 12$). However with dynamic synapse, the region of 1:1 synchrony is enhanced to cover a larger range of heterogeneity and in addition, for the set of synaptic parameters considered, the two neurons always exhibit in-phase synchrony, i.e., $\zeta = 0$. As an example of such a scenario, we show in Fig. 7(a) the time series of membrane voltage of the two neurons firing asynchronously for heterogeneity of $H = 12.28$ ($I_A^{DC} = 3.2\ \mu\text{A/cm}^2$ and $I_B^{DC} = 2.5\ \mu\text{A/cm}^2$).

In the case of dynamic synapse, iSTDP is able to modulate the synaptic strength g_{BA}, such that even for increasing heterogeneity in firing frequency of neuron A, neuron B is still able to entrain the driven neuron A, to fire synchronously with neuron B. iSTDP modulates the synaptic strength to a final stable configuration at which the two neurons fire in-phase, resulting in $\tilde{w}_A(n) - \tilde{w}_B(n) \approx 0$. The particular form of the iSTDP rule ($\Delta g(\Delta t = 0) = 0$) then implies that the synaptic strength no longer changes and the network reaches a

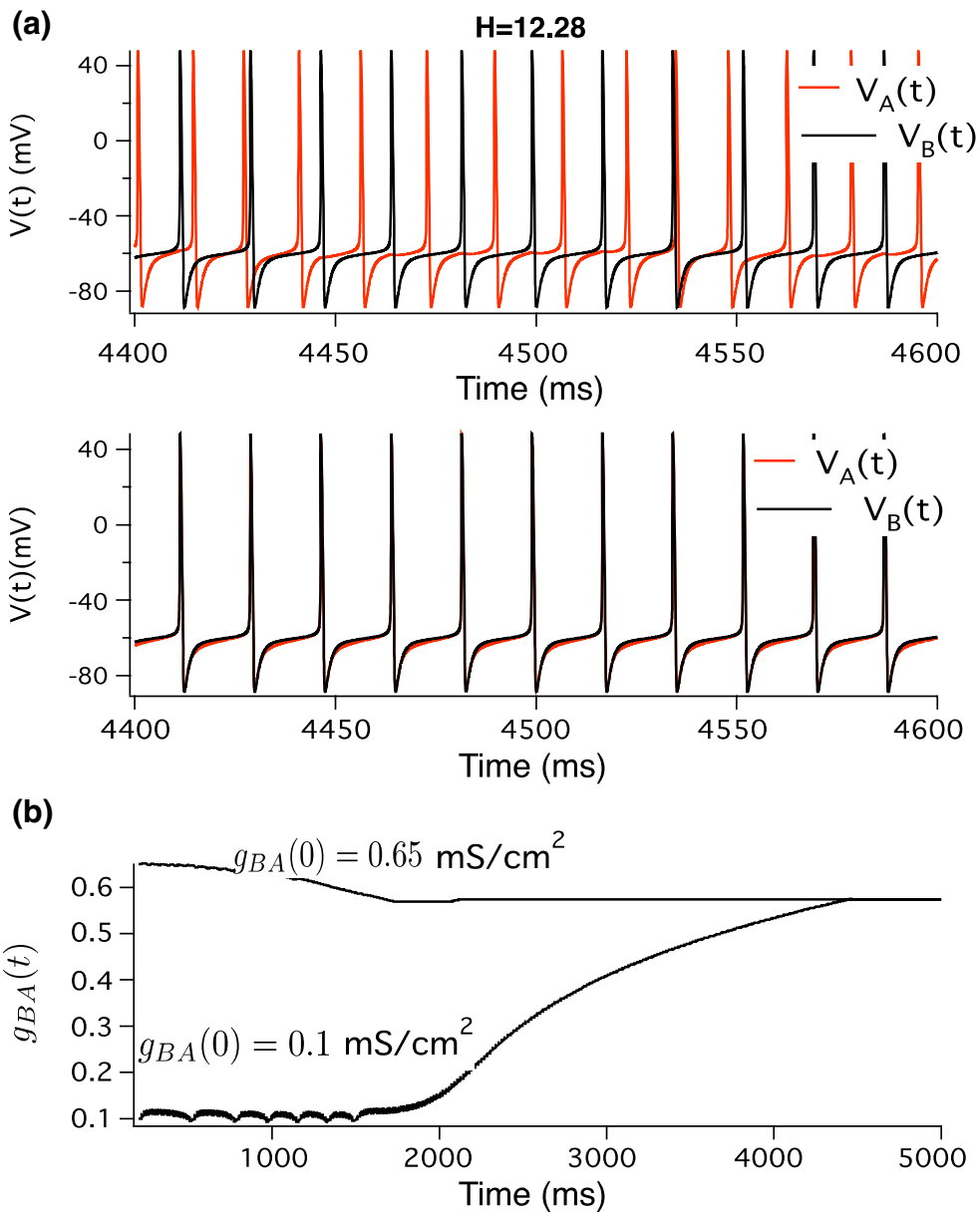

Fig. 7 (**a**) The time series of each neuron in the UCI is plotted for a given level of heterogeneity, $H = 12.28$ in the intrinsic drive I^{DC} to each neuron with (**a**) static synapse and (**b**) dynamic synapse, modulated through iSTDP. (**c**) The plot of evolution of the dynamic synaptic strength to final steady state configuration for a given heterogeneity $H = 12.28$, starting from two different initial conditions, $g_{BA}(0) = 0.1$ and $g_{BA}(0) = 0.65$ mS/cm^2 respectively. See online publication for the color version of this figure

final stable state when the two neurons are entrained to fire synchronously. In Fig. 7(b) we show the time evolution of membrane voltage of the two neurons A and B, firing synchronously in-phase for heterogeneity of H=12.28, when the inhibitory synaptic strength has evolved to a final steady state configuration. In Fig. 7(c) we show an example of evolution of the inhibitory synaptic strength through iSTDP from two different initial conditions to final steady state configuration, resulting in the in-phase synchrony of the UCI. Note that for initial strength $g_{BA}(0) = 0.1$ mS/cm^2, the synaptic strength oscillates around this value for a long time until eventually it monotonically increases to the final steady state value at which the two neurons are locked in in-phase synchrony. The oscillation in synaptic strength and the monotonic increase further on, represent two distinct states of the UCI which will be explored in details below.

3.3.2 Stability analysis of UCI synchrony by STRC

In order to understand the mechanism of synchrony in the UCI we use the method of STRC to derive a map for the evolution of the time difference $s(n)$. In order to simplify the analysis we assume that the two neurons fires alternatively, specifically neuron A fires at

$t_E(2n-1)$, while neuron B fires at $t_E(2n)$, $\forall\ n > 0$. For a given fixed inhibitory synaptic strength, g^S_{BA}, if $\Phi_A(t, g_{BA})$ is the STRC for neuron A, we have (Fig. 5)

$$\begin{aligned} w_E(2n+1) - w_E(2n-1) &= T^0_A + \Phi_A\big(w_E(2n) \\ &\quad - w_E(2n-1), g^S_{BA}\big) \\ &= T^0_A + \Phi_A\big(s(2n-1), g^S_{BA}\big) \end{aligned} \tag{5}$$

Also by definition of $s(2n)$, we have

$$\begin{aligned} w_E(2n+1) - w_E(2n-1) &= (w_E(2n+1) - w_E(2n)) \\ &\quad + (w_E(2n) - w_E(2n-1)) \\ &= s(2n) + s(2n-1). \end{aligned} \tag{6}$$

Similarly, since neuron B fires with period of T^0_B, we have

$$s(2n+1) + s(2n) = T^0_B \tag{7}$$

Then from Eqs. (5), (6) and (7), we have

$$s(2n+1) = T^0_B - T^0_A - \Phi_A\left(s(2n-1), g^S_{BA}\right). \tag{8}$$

The steady state solution to above equation can be obtained by solving for the fixed point s^* of odd sequence of the evolution map for $s(2n+1)$, defined by $s(2n+1) = s(2n-1) = s^*$. We then obtain

$$\Phi_A\left(s^*, g^S_{BA}\right) = T^0_B - T^0_A \tag{9}$$

The stability of the fixed point s^* requires, $0 < \frac{d\Phi(t,g)}{dt}|_{t=s^*} < 2$. In Fig. 8(a), we show the STRC for neuron A in the static synapse case with $g^S_{BA} = 0.1$ mS/cm^2 for heterogeneity $H = 12.28$ ($I^{DC}_A = 3.2$ and $I^{DC}_B = 2.5$ μA/cm^2). For this case, with the static strength of mutual inhibition set at $g^S_{BA} = 0.1$ mS/cm^2, Equation (9) has no solution since there is no intersection between the STRC $\Phi_A(t, g^S_{BA})$ and the line $T^0_B - T^0_A$, as can

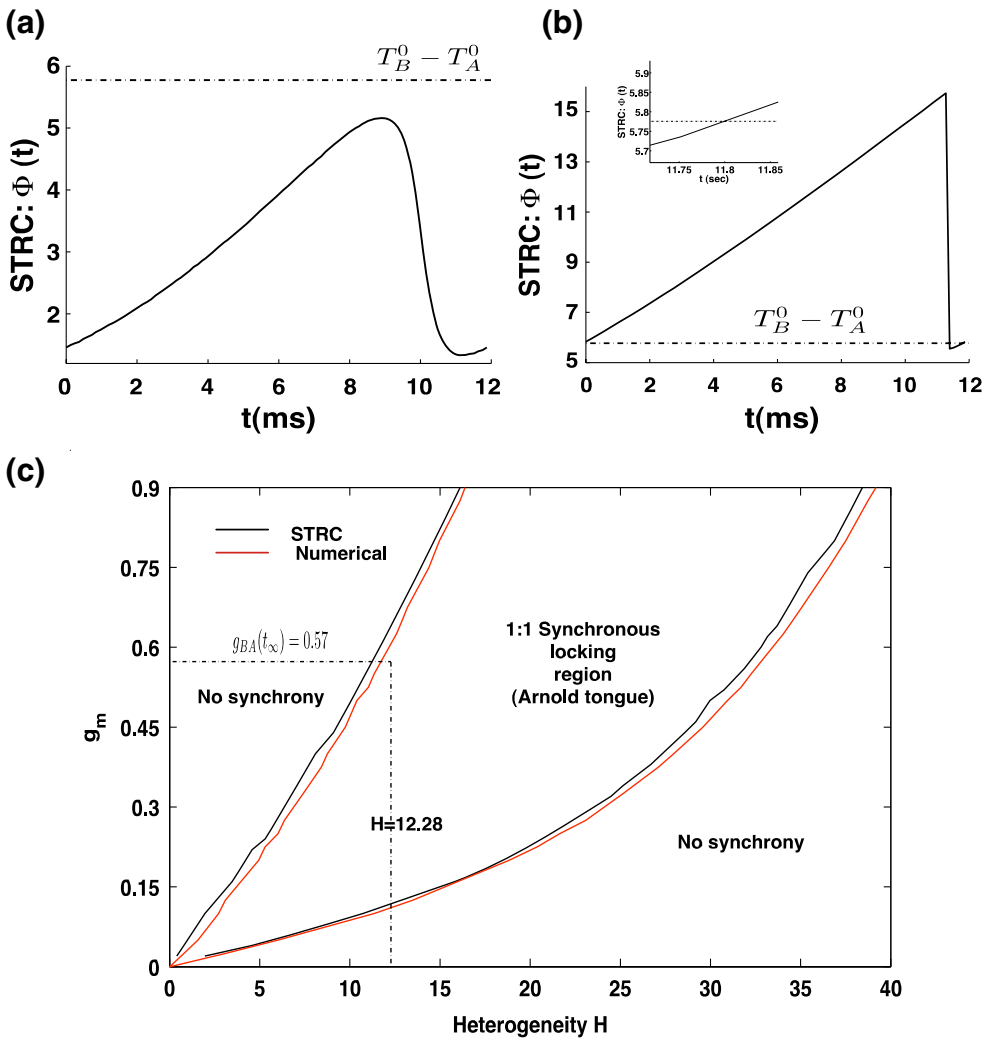

Fig. 8 (**a**) The STRC for neuron A, when the strength of synaptic inhibition $g_{BA} = 0.1$ mS/cm^2. (**b**) The STRC for neuron A, when the strength of the synaptic inhibition $g_{BA} = 0.57$ mS/cm^2, representing the final steady state value when the two neurons in the UCI are locked in in-phase synchrony. (**c**) The 1:1 synchronous regime for the UCI s determined through STRC (*black*) and numerical simulations of the model for the UCI (*red*). See online publication for the color version of this figure

be seen from Fig. 8(a) and therefore the two neurons cannot lock in synchronous state.

In Fig. 8(b), we similarly show the STRC computed with dynamic synapse in the asymptotic state when the system has locked into in-phase synchronous solution and the inhibitory synaptic strength $g_{BA}(t)$ has reached a final stable value, $g_{BA}(t=\infty) \equiv g_{BA}(\infty) = 0.57$. We see that the solution to Eq. (9) exists as the STRC curve $\Phi_A(t, g_{BA}(\infty))$ intersects the line $T_B^0 - T_A^0$ at $s^* = 11.8$ and the condition for stability for this fixed point is also satisfied.

In above example we considered a specific example for the synaptic strength, $g_{BA} = 0.1$ mS/cm^2 and determined that the lack in the existence of stable fixed point solution to Eq. (9), results in the absence of synchrony between the firing of the two coupled neurons in the UCI. We also showed that iSTDP modulated synaptic strength in the asymptotic state ($g_{BA}(\infty) = 0.57$ mS/cm^2) provides a unique stable solution to the Eq. (9), and the two coupled neurons in the UCI fire in in-phase synchrony.

3.3.3 Arnold tongue of UCI

We next solve Eq. (9) for different levels of heterogeneity H, thereby modulating T_A^0 to determine the set of inhibitory synaptic strength g_{BA} which will result in unique stable solution for Eq. (9) to exist. The solution to Eq. (9) is obtained by estimating the STRC using the direct method for STRC computation as explained in the methods section, for each value of the inhibitory synaptic strength g_{BA}, and determining, whether there exists a stable fixed point solution to Eq. (9). In Fig. 8(c) we present the results of these calculations. For given H, the curve in black gives the lower and upper bound on the set of inhibitory synaptic strengths, for which a unique stable solution for Eq. (9) exists. For example with H=10, the range of values for g_{BA} which result in an unique stable solution to exist for Eq. (9) is $0.09 < g_{BA} < 0.49$. For this range of values for inhibitory synaptic strength g_{BA}, at $H = 10$ the driver neuron B is able to entrain the driven neuron A to oscillate in synchrony with it. This region of synchronous 1:1 locking between the two coupled neurons is analogous to the classical Arnold tongue (Kurths et al. 2001) obtained for synchrony between two coupled nonlinear oscillators. Arnold tongues are typical signature of synchrony in coupled nonlinear oscillators. In general the width of synchrony between two heterogeneous neural oscillators (heterogeneity in intrinsic firing period of the oscillators) is dependent on the strength of coupling between the driver and the driven oscillator. Arnold tongues provide a two dimensional visualization of this dependence of the width of synchrony on the strength of coupling between the two oscillators. Naturally in the absence of any coupling the two oscillators are firing at their intrinsic oscillation frequency and the width of synchrony is zero. As the strength of coupling is increased, the width of synchrony increases, resulting in an tongue shaped two dimensional area. In Fig. 8(c), this general feature of Arnold tongue is represented by the area bounded by the two black curves, obtained through STRC by solving Eq. (9) as discussed above.

In Fig. 8(c), shown in red is a similar bound on the levels of heterogeneity leading to synchronous oscillation in the UCI, obtained by numerically integrating Eq. (1), for the dynamics of evolution of the two coupled neurons. The curves in red are obtained by fixing the firing period of the driver neuron B at T_B^0 and varying the intrinsic firing period for neuron A, T_A^0 by changing the dc current I_A^{DC}, thereby varying the level of heterogeneity H in the firing of the two coupled neurons, and then determining the synaptic strength g_{BA}, that will result in $\frac{T_B^0}{<T_A>} \approx 1$, so that the two neurons are locked in 1:1 synchrony. We find the results of numerical simulation match the results from STRC calculations in Fig. 8(c). We also see that for $H = 12.28$, the asymptotic value $g_{BA}(t)$ obtained through the modulation of the synapse from B to A through iSTDP is $g_{BA}(\infty) = 0.57$ mS/cm^2 which is in the region of 1:1 synchrony for the two coupled neurons. We therefore conclude that iSTDP modulates the synaptic strength g_{BA} such that Eq. (9) is satisfied and the two coupled neurons lock into 1:1 synchronous in-phase oscillation.

3.3.4 In-phase synchrony in the UCI induced by iSTDP

iSTDP however not only modulates $g_{BA}(t)$ such the two neurons are locked in 1:1 synchrony, but the strength is modulated such that the two neurons exhibit in-phase synchrony with the phase difference ζ being identically zero irrespective of H and initial $g_{BA}(0)$, as can be seen from Fig. 6(b). In order to understand the function of iSTDP in producing this in-phase synchrony between the two coupled neurons, we consider the following two scenarios with the case, $H = 12.28$ and $g_{BA}(0) = 0.1$ mS/cm^2 as an example. The initial strength of g_{BA} is outside and below the region of 1:1 synchronous locking for the two coupled neurons for given heterogeneity, as can be seen in Fig. 9.

In this situation, with $H > 0$, neuron A is firing at a higher rate than neuron B. Therefore more often than not, neuron A will fire more than once for every period of firing of neuron B. Each firing of neuron A (the postsynaptic neuron), results in corresponding increase in synaptic strength g_{BA} through iSTDP. For

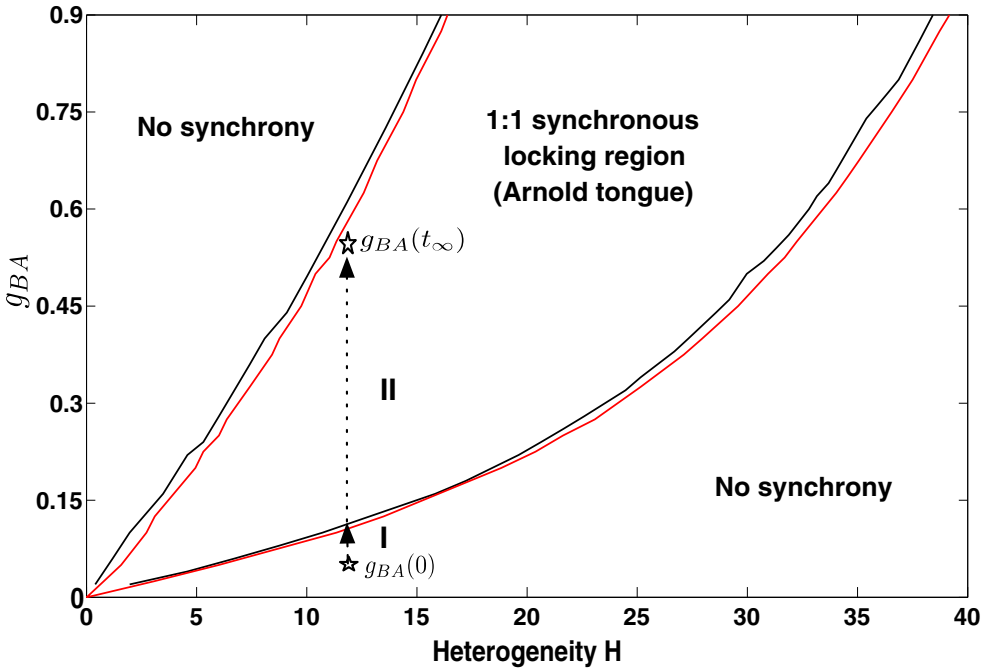

Fig. 9 Path to 1:1 in-phase synchrony. Modulation of synaptic strength to go from non-synchronous region to the Arnold tongue (I) and further modulation of the synapse to lead to stable in-phase synchrony (II). See online publication for the color version of this figure

every spike of neuron B, however only the last spike of neuron A will contribute to the decrease in the synaptic strength g_{BA} through iSTDP. This is because we consider only the nearest spike pair interaction in updating the synaptic strength at any given point in time. Overall, however with $H > 0$ and g_{BA} outside the Arnold tongue region, the probability of firing of neuron A is greater than that of neuron B and the synapse from g_{BA} increases in strength approaching the Arnold tongue from below.

In order to understand the evolution of the synaptic strength g_{BA} from a value inside the Arnold tongue to the final stable fixed point $g_{BA}(\infty)$ (Fig. 9), by iSTDP, we derive a two dimensional map for the evolution of synaptic strength and the time lag between the firing of the two neurons. Under the assumption that once the synapse have evolved to the region within the Arnold tongue, the two neurons are phase locked in synchrony, i.e., $\langle T_A \rangle \approxeq T_B^0$ and the locked state remains quasi-static as the synaptic strength evolves, the map for evolution of the quasi-static stable state s^* is obtained from Eq. (9) as,

$$\begin{aligned}
&\Phi_A\left(s^*(2n+1), g_{BA}(2n+1)\right) \\
&\quad = T_B^0 - T_A^0 \implies s^*(2n+1) \\
&\quad = (\Phi_A)^{-1}\left(T_B^0 - T_A^0, g_{BA}(2n+1)\right)
\end{aligned} \tag{10}$$

The synaptic strength $g_{BA}(n)$ is modulated through iSTDP every time a spike event occurs either from neuron A or from neuron B. According to the iSTDP update rule as given in Eq. (3) we have,

$$\begin{aligned}
g_{BA}(2n+1) &= g_{BA}(2n) + \Delta g(\tilde{w}_A(2n+1) - \tilde{w}_B(2n+1)) \\
&= g_{BA}(2n-1) + \Delta g(\tilde{w}_A(2n) - \tilde{w}_B(2n)) \\
&\quad + \Delta g(\tilde{w}_A(2n+1) - \tilde{w}_B(2n+1)) \\
&= g_{BA}(2n-1) + \Delta g\left(w_E(2n-1) - w_E(2n)\right) \\
&\quad + \Delta g(w_E(2n+1) - w_E(2n)) \\
&= g_{BA}(2n-1) - \Delta g(s^*(2n-1)) + \Delta g(s^*(2n)) \\
&\approx g_{BA}(2n-1) - \Delta g(s^*(2n-1)) \\
&\quad - \Delta g(s^*(2n-1) - T_B^0) \\
&\equiv g_{BA}(2n-1) + G_{\text{eff}}(s^*(2n-1), T_B^0)
\end{aligned} \tag{11}$$

where $G_{\text{eff}}(s, T) = -\Delta g(s) - \Delta g(s - T)$, combines the effect of spike times of each neuron A and B in modulating the synaptic strength through iSTDP.

In deriving Eq. (11), we have used the assumption of the quasi-stationarity of the locked state of the time lag s^* inside the Arnold tongue, resulting in $s^*(2n) \approx T_B^0 - s^*(2n-1)$, which results in the period of oscillation of neuron A being the same as that of the period of firing of neuron B.

Equations (10) and (11), thus give a recursive map for the evolution of the synaptic strength $g_{BA}(2n+1)$ and the time lag, $s^*(2n+1)$ between the spiking of the two coupled neurons, after the synaptic strength has evolved to a value inside the Arnold tongue. Starting

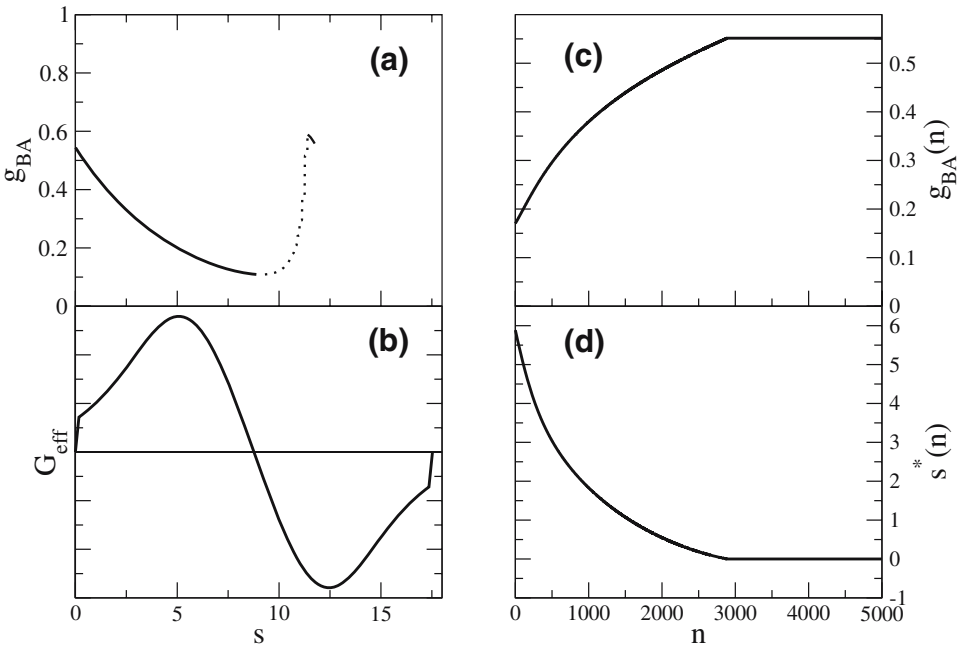

Fig. 10 Two dimensional map for the evolution of the synaptic strength within the Arnold tongue: (**a**) g_{BA} vs stable (*solid*) and unstable (*dotted*) fixed points s. (**b**) G_{eff} as a function of s. (**c**)and (**d**) shows temporal evolution of $g_{BA}(n)$ and $s^*(n)$ for the UCI with heterogeneity $H = 12.28$

from initial condition $g_{BA}(1)$ and $s^*(1)$, from Eq. (11), we determine $g_{BA}(3)$. Using the value of $g_{BA}(3)$, in the function Φ_A^{-1}, we determine $s^*(3)$ and so on.

In Fig. 10(a) and (b), we show $(\Phi_A)^{-1}$ and G_{eff} for the case $H = 12.28$. $(\Phi_A)^{-1}$ was obtained numerically from the set of STRC curves (Φ_A) computed for various s^* and g_{BA}. For given g_{BA}, we located s^* where the curve $\Phi_A(s^*, g_{BA})$ intersects line $T_B^0 - T_A^0$ by using linear interpolation. We found that there are always one stable and one unstable root, if there is intersection between $\Phi_A(s^*, g_{BA})$ and the line $T_B^0 - T_A^0$. We can therefore numerically find $(\Phi_A)^{-1}$ for stable and unstable s^* separately. In Fig. 10(a) we show, for given g_{BA}, where these stable and unstable s^* are located.

For a given $T_B^0 - T_A^0$, as g_{BA} increases due to iSTDP, the amplitude of STRC increases, as can be seen from Fig. 8(a) and (b). The solution to Eq. (10) then appears through saddle node bifurcation resulting in synchronous locking of the two coupled neurons at a stable time lag s^*. This is shown in Fig. 10(a). Once the two neurons are locked in 1:1 synchrony with a stable time lag, s^*, as we can see from Eq. (11), and Fig. 10(b), the synaptic strength g_{BA} increases resulting in a new stable state s^*, until recursively reaching the final asymptotic state of 1:1 in-phase synchrony with s^* identically zero. As the two neurons fire in-phase the synaptic strength no longer evolves and the coupled neurons are locked in 1:1 in-phase synchrony. Figure 10(c) and (d) shows the recursive evolution in the synaptic strength g_{BA} and the corresponding evolution of the time lag s^*, as given from Eqs. (10) and (11) to the final asymptotic values, $s^* = 0$ and $g_{BA}(t = \infty) = 0.57$ mS/cm^2.

It should be noted that the convergence to 1:1 synchrony between the two coupled neurons comes from generally observed properties of synchrony between two coupled oscillators and the convergence to stable in-phase synchrony are the consequence of global properties of iSTDP and the STRC for the type I neuron model considered.

3.3.5 Synchrony in the UCI and dependence on initial synaptic strength

The analysis presented above began with the assumption of the initial coupling strength $g_{BA}(0)$ being below the Arnold tongue for given heterogeneity levels considered. In such situations, in general the neuron A is firing at frequency greater than neuron B and as mentioned earlier, the synapse g_{BA} will on average increase in strength such that the synaptic strength evolves to the domain of Arnold tongue. However, if we begin with initial condition $g_{BA}(0)$ outside and above the Arnold tongue, the situation might be different. For example, for given heterogeneity level, and the initial synaptic strength outside and above Arnold tongue, the synapse might be able to modulate the firing rate of neuron A, enough such that the neuron A might fire at the same rate of neuron B or might even fire slowly. The synaptic strength according to the iSTDP rule might then evolve such the synapse might not enter 1:1 locking region at

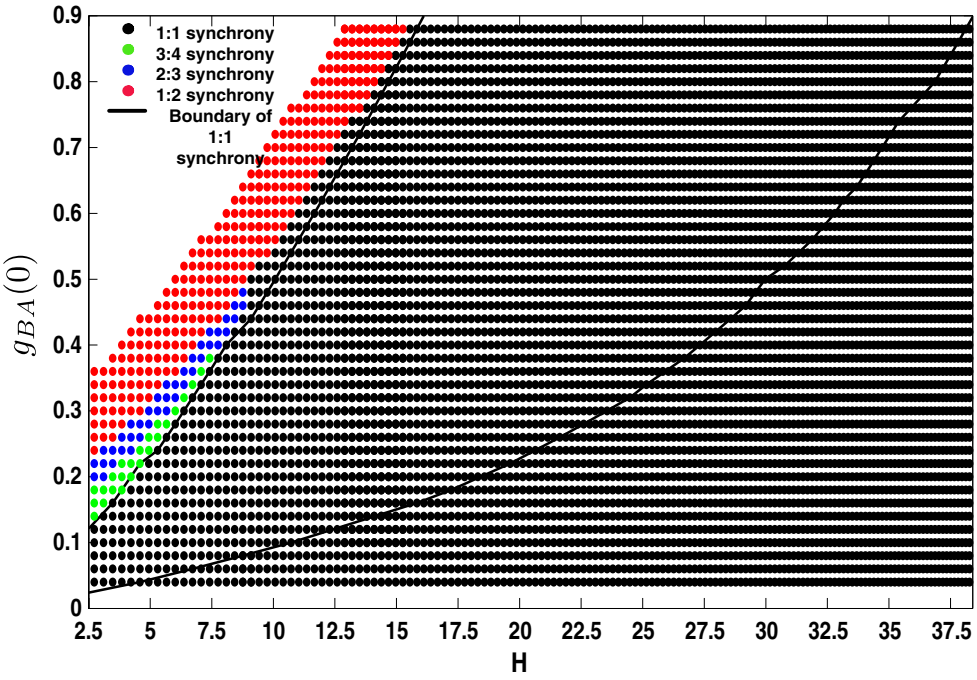

Fig. 11 Steady state reached by the UCI through the dynamic modulation of the synaptic strength, as function of the initial synaptic strength $g_{BA}(0)$ for given heterogeneity H. See online publication for the color version of this figure

all. In order to understand the evolution of dynamics under these conditions, in Fig. 11 we plot the ratio of $T_B^0/ < T_A >$ for the two coupled neurons, in the dynamic case, for a given initial strength of $g_{BA}(0)$ and given heterogeneity H.

We can see from Fig. 11, as predicted by our theoretical analysis with the two dimensional coupled map above, for all initial levels of synaptic strength below or within the Arnold tongue the coupled system evolves to 1:1 in-phase synchrony. However for initial levels of synaptic strength outside and above the Arnold tongue, we see that the system evolves in general to p:q (p,q ϵ $\mathbb{Z}$) synchrony. In addition we can also see from Fig. 11 that for low levels of heterogeneity, if the initial synaptic strength is too high neuron B inhibits neuron A from firing and no synchrony results.

3.4 iSTDP induced synchrony in the MCI

We next consider the network of two self inhibited neurons mutually coupled to each other through inhibition [Fig. 3(b)]. It has been shown earlier by White et al. (1998), that such a network with identical properties can synchronize in-phase for entire range of parameters I^{DC}, τ_D, for a given fixed value of self inhibition. However, the synchronization fails if one introduces slight heterogeneity in the firing of the two coupled neurons.

We examine this particular scenario as presented above for unidirectional coupling, in the context of dynamic synapse. We consider heterogeneity introduced through different external drive (I^{DC}), through different decay time of synaptic inhibition (τ_D) and finally through different strength of self inhibition g_s. We again compare the two situations: static synapse synchrony versus dynamic synapse synchrony. For static case we set, $g_{AB}^S = g_{BA}^S = 0.1$ mS/cm^2. For the case of dynamic synapse we have, $g_{BA}(n) = g_{BA}(n-1) + \Delta g(\tilde{w}_A(n) - \tilde{w}_B(n)))$ and $g_{AB}(n) = g_{AB}(n-1) + \Delta g(\tilde{w}_B(n) - \tilde{w}_A(n)))$. We again consider only the nearest neighbor interaction in modulating the synaptic strength. In Fig. 12(a) we plot the ratio of the average firing period of neuron B, $< T_B >$ to that of neuron A, $< T_A >$ as function of heterogeneity H introduced through different external drive, for the static and the dynamic synapse case. We see that the dynamic synaptic modulation by STDP results in p:q (p,q ϵ $\mathbb{Z}$) for all heterogeneity levels considered. In particular we see an enhanced window of 1:1 and 2:1 synchronization induced by dynamic synapse as seen in Fig. 8(b). This implies an increased probability of observing coherence in the firing pattern of the MCI even in presence of mild heterogeneity as has been reported in many *in vivo* experimental data (Eckhorn et al. 1988; Gray et al. 1989). In Fig. 12(b), we again show the scatter plot of the general phase difference ζ, as defined in Eq. (4). We again see that STDP modulates the synaptic strength such that the two neurons, either phase lock with zero phase lag (in the case of 1:1 synchrony) or the phase

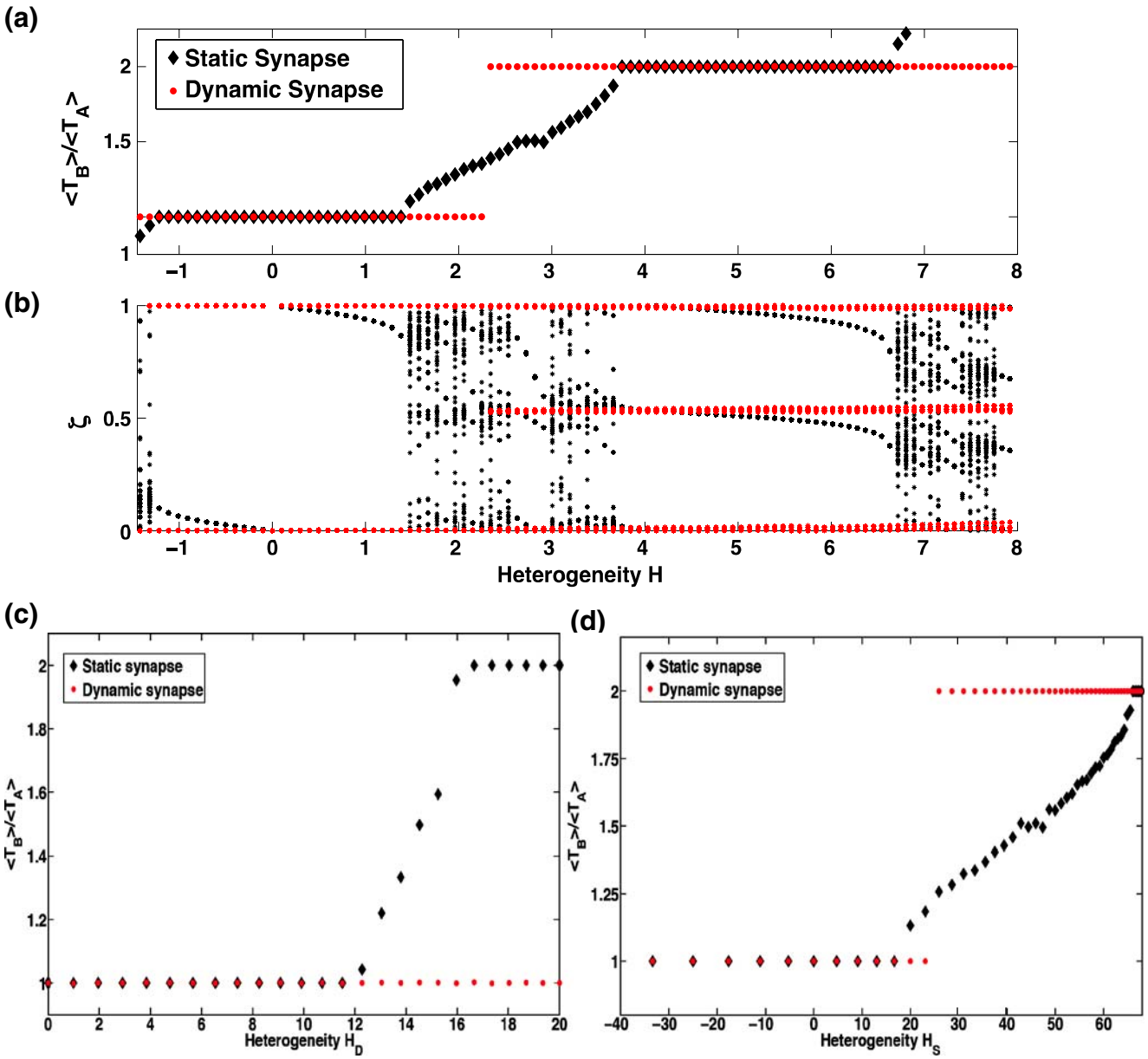

Fig. 12 Synchronization between pair of self inhibited neurons with mutual inhibition. (**a**) Heterogeneity is introduced through different input drive I^{DC}. (*1*) gives the ratio of average firing period of the two coupled neurons as function of heterogeneity H, for the case with static (*black*) and dynamic (*red*) synapse. (*2*) gives the plot of general phase difference ζ for the MCI as function of heterogeneity H. (**b**) The ratio of average firing period of the two coupled neurons in the MCI is plotted as function of heterogeneity H_S introduced through different level of self inhibition on the neurons. (**c**) The ratio of average firing period of the two coupled neurons in the MCI is plotted as function of heterogeneity introduced through different synaptic time constant τ_D. See online publication for the color version of this figure

difference oscillates between antiphase and in-phase synchrony, (2:1 frequency locking).

In Fig. 12(c), we plot the ratio of firing period of the two coupled neurons, as function of heterogeneity introduced through different synaptic decay time of the inhibition. For the results presented in this figure, we set $I_A = I_B = 2.5\ \mu\text{A/cm}^2$, $g_s = 0.1\ \text{mS/cm}^2$, the decay time for inhibitory synapse from B to A, $\tau_D^{BA} = 5$ ms and we define heterogeneity in synaptic decay time as

$$H_D = 100\frac{\tau_D^{AB} - \tau_D^{BA}}{\tau_D^{AB} + \tau_D^{BA}}$$

(τ_D^{ij} is the synaptic decay time for synapse from neuron i to neuron j). Heterogeneity in firing rate of the two

neurons is introduced by different synaptic decay time as, larger the decay time of synapse, longer is the inhibition and the neuron tends to fire at slower rate. We again see that the dynamic synapse is able to modulate the strength of inhibition on each neuron, such that the two neurons are able to synchronize over a broader range of heterogeneity in the synaptic decay time.

We finally consider a source of heterogeneity introduced by different self inhibition strength g_s. We define heterogeneity in self inhibition

$$H_S = 100\frac{g_S^B - g_S^A}{g_S^B + g_S^A}$$

The parameters for the MCI in this configuration are, $I_A^{DC} = I_B^{DC} = 2.5$ μA/cm^2, $\tau_D = 5$ ms, $\tau_R = 0.1$ ms and $g_S^A = 0.1$ mS/cm^2. In Fig.12(d), we show the results comparing synchrony between the two coupled neurons with static synapse and dynamic synapse. Again the coupled neurons with dynamic synapse show a greater robustness in synchrony as compared to the static case.

In order to understand synchrony in the MCI, with dynamic modulation of both synaptic strength g_{AB} and g_{BA}, we numerically simulated the MCI with the evolution rule applied to the synapse from slower firing neuron B to the faster firing neuron A, g_{BA} as in the unidirectional case studied above, and fixed the synaptic strength in opposite direction g_{AB} fixed at moderately lower strength. Depending on the initial condition on the synaptic strength g_{BA}, the two neurons either phase locked in in-phase 1:1 synchrony or the system evolved to 2:1 synchrony. We thus conclude that synchrony in the MCI is brought about by the modulation of the synapse from the slower neuron to the faster neuron and that the modulation in the synapse from faster neuron to the slower neuron, simply controls the firing rate of the slower neuron and prevents the effective inhibition of the slower neuron by the faster neuron.

4 Discussion

In this work we have analyzed the functional significance of spike timing dependent plasticity, recently observed for inhibitory synapses (Haas et al. 2006) in synchronizing a pair of neurons with self inhibition in two coupling configurations: (a) uni-directional coupling and (b) bi-directional coupling. We begin with the study of a single self inhibited neuron and show how the firing frequency of the neuron is dependent on the decay time of the synapse and the strength of the self synapse. Slower synaptic decay time results in prolonged influence of inhibition and it takes longer time for neuron to recover from inhibition to fire again, there by decreasing the firing frequency of neuron for the same level of input drive through I^{DC}. The presence of self inhibition which results in spike based adaptation in firing of the neuron was considered because it has been shown that the frequency in the gamma band in a distributed network of inhibitory neurons is highly dependent on the synaptic decay time. This effect can be simulated through self inhibition. Moreover the iSTDP learning rule, considered in this study has an interesting zero at $\Delta t = 0$ implying that iSTDP does not modulate the self inhibition synaptic strength. Thus the analysis of synchrony through STRC is unaffected by the presence of self inhibition. In addition (as can be seen from results in Section 3.1) the parameters of the self inhibition synapse, provide control over the frequency range of the operation of the neuron and provide an additional source of heterogeneity that might influence synchrony between mutually coupled interneurons.

Network of mutually coupled neurons with intrinsic heterogeneity in firing frequency has been studied earlier in White et al. (1998). These authors demonstrated that even a mild introduction of heterogeneity in the network results in disruption of synchrony in the network as the coupling not only has to align the phase for synchrony but also has to entrain the frequency of firing of the two neurons. They showed that synchrony is achieved only when inhibition is strong enough so that the firing period is dominated by the synaptic decay time. However a very strong inhibition results in loss of synchrony through suppression whereby the faster spiking neuron inhibits the slow neuron so much so that it stops firing.

In this work we show that a possible route to achieve stable synchronous oscillations in the presence of heterogeneity is through spike timing dependent plasticity of inhibitory synapses. Recently Haas et al. (2006), have reported spike timing dependent plasticity of inhibitory synapses (iSTDP) in layer II of the entorhinal cortex. In this work we have utilized the functional form for this recently observed synaptic plasticity rule to study its influence on the synchronization of inhibitory neuronal network in the presence of heterogeneity. The empirical fit to iSTDP data observed by Haas et al. (2006), is presented in Fig. 2. We have shown that in the presence of heterogeneity, the dynamic synapse through iSTDP results in significant enhancement of neural synchrony. The iSTDP modulates the synaptic strength such that the faster spiking neuron slows down through increase in inhibition on it and vice versa. We would like to

note that STDP of inhibitory synapses has also been observed in acute hippocampal slices (Woodin et al. 2003). The authors report a functional form for iSTDP in hippocampal slices that is symmetric with respect to the timing of the pre- and postsynaptic spikes and is non-zero at zero time delay, which is distinctly different from the functional form for iSTDP rule observed in the entorhinal cortex by Haas et al. (2006). The significance of this form of iSTDP in the enhancement of synchrony in inhibitory neuronal network remains to be explored.

In all our calculations for the dynamic modulation of the inhibitory synaptic strength and the theoretical analysis thereof, we have made two key assumptions for the update rule governed by iSTDP. We considered only the neighboring spike pair interaction for iSTDP and assumed that the effect of the iSTDP modulation sum linearly. This assumption allowed us to obtain an analytic expression for the evolution of the synaptic strength, after the two coupled neurons are phase locked and have evolved to the region within the arnold tongue. It has also been shown by Froemke and Dan (2002), that in the presence of natural spike trains, the contribution to synaptic modification is primarily through the timing of the first spike in each burst. It would be interesting to see how the dynamics of synchrony between the MCI would be affected through such multi-spike interaction. The second key assumption we made was that the iSTDP update happens instantaneously, thereby we ignore the actual delay of several minutes that exists between the pairing of the pre and post-synaptic spikes and the results induction of synaptic modification. Although our assumption of instantaneous iSTDP update implies that the synaptic modification has time scale much faster than the firing rate of the neuron, which is contrary to the observed experimental results, the mere introduction of delay in synaptic update, as seen in experiments, has no consequence for our results. In order to verify that it is indeed the case, we varied the intensity of change in synaptic strength through iSTDP by modulating g_0, such that the increment in the synaptic strength induced by iSTDP is much smaller in the UCI. We observed no changes in the results from our simulations.

In Fig. 6 we compared the synchrony in the UCI with heterogeneity in the presence and absence of dynamic synapse. We see that iSTDP results in 1:1 synchrony between the two neurons for all levels of heterogeneity considered. We analyzed this network synchrony with the method of STRC and demonstrate that iSTDP modulates the synaptic strength such that there exists a unique stable synchronous solution to Eq. (9) for the levels of heterogeneity considered. In addition, once the synaptic strength has evolved within the region of 1:1 synchronous locking, iSTDP further modulates the synaptic strength such that it approaches monotonically to a final stable configuration wherein the two neurons are locked in in-phase 1:1 synchrony. We also demonstrated, the influence of the initial synaptic strength in achieving the final 1:1 in-phase synchronous solution.

We next show through numerical simulations, that the enhancement in synchronization persists for mutually coupled pair of neurons in the presence of increasing levels of heterogeneity. For both intrinsic heterogeneity through different external drive and extrinsic heterogeneity through different decay time of the synapse and different strength of self inhibition, iSTDP is able to maintain synchrony between the coupled neurons. Although not presented in this work, the stability of the synchronous state for the MCI can also be studied using the STRC method (Acker et al. 2004).

This effect of the iSTDP in enhancement of synchrony in the UCI and the MCI in the presence of heterogeneity in the firing rates of the two coupled neurons is an interesting result from neuroscience perspective as it suggests that neural system through STDP is very robust against any external perturbation and that system always phase locks in in-phase synchrony. While such a robust state of neural synchrony is essential for memory consolidation, it might not be an optimal scenario for sensory information processing wherein sensory information is encoded in the form of a temporal code and a robust neural synchrony might result in loss of all sensory information.

We have also done numerical simulations with mild noise in the intrinsic firing rate of each coupled neuron and the iSTDP rule to study the influence of noise in the coupled system on the synchrony induced by iSTDP. We found that the synchrony remains enhanced with iSTDP for all the levels of heterogeneity considered. However under similar noise conditions, synchrony is completely lost with static synapse. Details on the influence of iSTDP learning on synchrony in the presence of noise will be presented in the forthcoming work.

Higher frequency synchronous oscillations have been reported experimentally in behaving animals (Ylinen et al. 1995). Our study above suggest that iSTDP might in fact work better at such high frequencies, in maintaining synchronous network oscillations. It has been suggested in Haas et al. (2006), that plasticity of inhibitory synapses may play an important role in balancing the effect of excitatory synapse preventing run away behavior typically observed in epileptogenesis. Also recently Abarbanel and Talathi (2006), used the model for STDP used in this work to design a neural circuitry for spike pattern recognition. In this work we

present yet another important function for STDP in inhibitory synapses: its role in maintaining synchrony in networks of coupled interneurons, under biologically realistic situation of mild heterogeneity and noise.

Acknowledgements This work was performed under the sponsorship of the Office of Naval Research (Grant N00014-02-1-1019) and the National Institute of Health Collaborative Research in Computational Neuroscience program (1R01EB004752).

References

Abarbanel, H., Gibb, L., Huerta, R., & Rabinovich, M. (2003). Biophysical model of synaptic plasticity dynamics. *Biological Cybernetics, 89*, 214–226.

Abarbanel, H., & Talathi, S. (2006). Neural circuitry for recognizing interspike interval sequences. *Physical Review Letters, 96*, 148104.

Acker, C., Kopell, N., & White, J. (2004). Synchronization of strongly coupled excitatory neurons: Relating network behavior to biophysics. *Journal of Computational Neuroscience, 15*, 71–90.

Benardo, L. (1997). Recruitment of GABAergic inhibition and synchronization of inhibitory interneurons in rat neocortex. *Journal of Neurophysiology, 77*, 3134–3144.

Bragin, A., Jando, G., Nadasdy, Z., Hetke, J., Wise, K., et al. (1995). Gamma (40–100 Hz) oscillations in the hippocampus of the behaving rat. *Journal of Neuroscience, 15*, 47–60.

Eckhorn, R., Bauer, B., Jordan, W., Brosch, M., Kruse, W., et al. (1988). Coherent oscillations: A mechanism of feature linking in the visual cortex. *Biological Cybernetics, 60,* 121–130.

Ermentrout, B. (1996). Type 1 membranes, phase resetting curves and synchrony. *Neural Compute, 8*, 979–1001.

Ernst, U., Pawelzik, K., & Geisel, T. (1995). Synchronization induced by temporal delays in pulse-coupled oscillators. *Physical Review Letters, 74*, 1570–1573.

Froemke, R., & Dan, Y. (2002). Spike-timing-dependent synaptic modification induced by natural spike trains. *Nature, 416*, 433–438.

Gray, C., Koenig P, Engel, K., & Singer, W. (1989). Oscillatory responses in cat visual cortex exhibit intercolumnar synchronization which reflect global stimulus properties. *Nature, 338*, 334–337.

Haas, J., Nowotny, T., & Abarbanel, H. (2006). Spike-timing-dependent plasticity of inhibitory synapses in the entorhinal cortex. *Journal of Neurophysiology, 96*, 3305–3313.

Jefferys, J., Traub, R., & Whittington, M. (1996). Neuronal networks for induced 40 Hz rhythms. Trends in *Neuroscience, 19*, 202–208.

Kopell, N., & Ermentrout, B. (2004). Chemical and Electrical synapses perform complementary roles in the synchronization of interneuronal networks. *Proceedings of the National Academy of Sciences, 101*, 15482–15487.

Kurths, J., Pikovsky, A., & Rosenblum, M. (2001). *Synchronization, a universal concept in non-linear science.* Cambridge University Press.

Lacaille, J., & Williams, S. (1990). Membrane properties of interneurons in stratum oriens-alveus of the CA1 region of rat hippocampus in vitro. *Neuroscience, 36*, 349–359.

McCormick, D., Connors, B., Lighthall, J., & Prince, D. (1985). Comparative electrophysiology of pyramidal and sparsely spiny stellate neurons of the neocortex. *Journal of Neurophysiology, 54*, 782–806

Michelson, H., & Wong, R. (1994). Syncrhonization of inhibitory neurones in the guinea-pig hippocampus in vitro. *Journal of Physiology, 477*, 35–45.

Nowotny, T., Zhigulin, V., Selverston, A., Abarbanel, H., & Rabinovich, M. (2003). Enhancement of synchronization in hybrid neural circuit by spike timing dependent plasticity. *Journal of Neuroscience, 23*, 9776–9785.

Oprisan, S., Prinz, A., & Canavier, C. (2004). Phase resetting and phase locking in hybrid circuits of one model and one biological neuron. *Biophysical Journal, 87*, 2283–2298.

Ritz, R., & Sejnowski, T. (1997). Synchronous oscillatory activity in sensory systems: New vistas on mechanisms. *Current Opinion in Neurobiology, 7*, 536–546.

Sheperd, G. (1990). *The synaptic organization of the brain.* New York: Oxford University Press.

Skinner, F., Zhang, L., Velazquez, P., & Carlen, P. (1999). Bursting inhibitory interneuronal networks: A role for gap-junctional coupling. *Journal of Neurophysiology, 81*, 1274–1283.

Traub, R., Kopell, N., Bibbig, A., Buhl, E. H., le Beau, F., et al. (2001). Gap junctions between interneuron dendrites can enhance synchrony of gamma oscillatios. *Journal of Neuroscience, 21*, 9478–9486.

vanVreeswijk, C., Abbott, L., & Ermentrout, B. (1994). When inhibition and not excitation synchronizes neural firing. *Journal of Computational Neuroscience, 1*, 313–321.

Wang, X., & Rinzel, J. (1992). Alternating and synchronous rhythms in reciprocally inhibitory model neurons. *Neural Computation, 4*, 84–97.

White, A., Chow, C., Ritt, J., Trevino, C., & Kopell, N. (1998). Synchronization and oscillatory dynamics in heterogeneous, mutually inhibited neurons. *Journal of Computational Neuroscience, 5*, 5–16.

Whittington, M., Traub, R., & Jefferys, J. (1995). Synchronized oscillations in interneuron networks driven by metabotropic glutamate receptor activation. *Nature, 373*, 612–615.

Wilkie, J. (2004). Numerical methods for stochastic differential equations. *Physical Review E, 70*, 017701.

Woodin, M., Ganguly, K., & Poo, M. (2003). Coincident Pre- and Postsynaptic activity modifies GABAergic synapses by postsynaptic changes in Cl Transporter activity. *Neuron, 39*, 807–820

Ylinen, A., Bragin, A., Nadasdy, Z., Jando, G., Szabo, I., et al. (1995). Sharp wave-associated high-frequency oscillation (200 Hz) in the intact hippocampus: network and intracellular mechanisms. *Journal of Neuroscience, 15*, 30–46.

Zhigulin, V., Rabinovich, M., Huerta, R., & Abarbanel, H. (2003). Robustness and enhancement of neural synchronization by activity-dependent coupling. *Physical Review E, 67.*

Neuroscience Letters xxx (2009) xxx–xxx

Contents lists available at ScienceDirect

Neuroscience Letters

journal homepage: www.elsevier.com/locate/neulet

Circadian control of neural excitability in an animal model of temporal lobe epilepsy

Sachin S. Talathi[a,c,*], Dong-Uk Hwang[a,c], William L. Ditto[e], Tom Mareci[c,d], Hector Sepulveda[a], Mark Spano[f], Paul R. Carney[a,b,c]

[a] J. Crayton Pruitt Family Department of Biomedical Engineering, University of Florida, Gainesville, FL 32611-6131, United States
[b] Departments of Pediatrics, Neurology, and Neuroscience, University of Florida, Gainesville, FL 32611-6131, United States
[c] McKnight Brain Institute, University of Florida, Gainesville, FL 32611-6131, United States
[d] Department of Biochemistry and Molecular Biology, University of Florida, Gainesville, FL 32611-6131, United States
[e] Harrington Department of Bioengineering, Arizona State University, Tempe, AZ 85287-9309, United States
[f] NSWC, Carderock Laboratory, W. Bethesda, MD 20817, United States

ARTICLE INFO

Article history:
Received 22 January 2009
Received in revised form 16 March 2009
Accepted 18 March 2009

Keywords:
Circadian rhythm
Epilepsy
Epileptogenesis
Latent period
Imbalance
Population spikes

ABSTRACT

We provide experimental evidence for the emerging imbalance in the firing activity of two distinct classes (type 1 and type 2) of population spikes recorded from the hippocampal area CA1 in an animal model of temporal lobe epilepsy. We show that during the latent period of epileptogenesis following status epilepticus inducing brain injury, there is a sustained increase in the firing rate of type 1 population spikes (PS1) with a concurrent decrease in the firing rate of type 2 population spikes (PS2). Both PS1 and PS2 firing rates are observed to follow a circadian rhythm and are in-phase in control rats. Following brain injury there is an abrupt phase shift in the circadian activity of the PS firing rates. We hypothesize that this abrupt phase shift is the underlying cause for the emergence of imbalance in the firing activity of the two PS. We test our hypothesis in the framework of a simple two-dimensional Wilson–Cowan model that describes the interaction between firing activities of populations of excitatory and inhibitory neurons.
Published by Elsevier Ireland Ltd.

"Balanced" networks in the brain have been proposed to account for a large variety of observations of cortical activity, including the representation of sensory information, decision-making and sleep and motor control [7]. A loss of balance in the neuronal network activity has been associated with the emergence of a number of neurological diseases including Parkinson's [15], Autism [18], Schizophrenia [22], and Tourette's syndrome [20]. Epilepsy, a neurological disorder of the brain in which patients suffer from recurrent seizures, is associated with an imbalance in the activity of excitatory and inhibitory populations of neurons in the brain, in favor of the former, leading to an abnormal hyper-synchronous state of the brain [4]. A number of *in vitro* studies have demonstrated the mechanism of this hyperexcitability at the synaptic level [8,11]. However, the functional implication of these synaptic changes leading to the progression of the brain to an epileptic state following brain injury in an *in vivo* system is still unknown.

Here we investigate the temporal dynamics of firing rates of high amplitude short time duration (100–200 ms) spatially localized patterns of spontaneous electrical activity referred to as *population spikes* (PS), recorded from the hippocampal CA1 area in an animal model of temporal lobe epilepsy. The PS are the macroscopic physiological features representing the integrated synaptic activity in the extracellular space generated by synchronous firing of populations of neurons in the brain [3,5]. Depending on the shape profile two distinct classes of PS were identified in neural recordings from the hippocampal CA1 area, labeled as type 1 PS (PS1) with a large negative excursion in the measured electrical activity and type 2 PS (PS2) with a large positive excursion in the measure electrical activity.

We observe that the firing rates of the two PS (defined as the number of spontaneous PS events observed per unit of time) exhibit circadian-like 24 h periodicity and are locked in-phase in control rats. However, during the latent period, defined as the time period following brain injury until the time of generation of first spontaneous epileptic seizures, while the firing rates of these PS are circadian, they are now locked in anti-phase. This phase shift is abrupt occurring within a few days post-brain injury and persists throughout the latent period. During the latent period we also observe an evolving imbalance in the firing rate of the two PS (quan-

* Corresponding author at: J. Crayton Pruitt Family Department of Biomedical Engineering, University of Florida, Gainesville, FL 32611-6131, United States.
Tel.: +1 352 846 2246.
E-mail address: sachin.talathi@gmail.com (S.S. Talathi).

0304-3940/$ – see front matter. Published by Elsevier Ireland Ltd.
doi:10.1016/j.neulet.2009.03.057

tified through an estimate of the drift in the baseline firing rate), such that there is a sustained increase in the firing rate of PS1 with a concurrent sustained decrease in the firing rate of PS2. We theorize that *this evolving imbalance may be implicated in the generation of the first spontaneous epileptic seizure following electrically induced status epilepticus*.

Based on these experimental findings, we hypothesize that the strength of the interactions between the populations of neurons in the hippocampus is dependent on their phase relative to the daily circadian cycle. Brain injury abruptly disturbs the circadian phase, which in turn triggers homeostatic mechanisms [9] producing changes in the interaction strength between the populations of hippocampal neurons which in turn modulates their firing activity. We refer to this as the "circadian-control" (CC) hypothesis. We suggest that this may underlie the cause for the emerging imbalance in the firing activity of the PS in the hippocampal CA1 area.

Our experiment used adult male Sprague Dawley rats ($n = 9$) of age 63 days and weighing between 200 and 265 g, which were implanted with 16 microwire recording electrodes (microelectrodes) bilaterally into the CA1 and the dentate gyrus regions of the hippocampus. In addition, a bipolar, twisted Teflon-coated stainless steel electrode was implanted into the right ventral hippocampus for the induction of brain injury [16]. The experimental details are given in the methods section of the supplementary material accompanying this manuscript. After 1 week of baseline recordings at a sampling rate of 12 kHz, rats ($n = 7$) were electrically stimulated for 30 min until sustained behavioral and electrographic seizures were observed. After the rats stopped seizing they entered a seizure-free latent period. Subsequently, rats were housed in a controlled environment with 24 h symmetric day–night cycle and monitored with continuous video and extracellular brain electrical activity recordings. Videos were screened daily for spontaneous seizures. At the end of the recording session, the rats were sacrificed and the intact brains were excised. The isolated intact brains were imaged with high-field magnetic resonance microscopy to confirm the location of the electrode placement within the CA1 region of the hippocampus [19,21]. In total 7 (E1–E7) rats were electrically stimulated into status epilepticus. A total of 3 rats (E1–E3) entered the chronic phase of epileptic seizures, following an epileptogenic phase with a minimum of a Racine grade 3 first spontaneous seizure. Data presented in this work is primarily derived from these 3 epileptogenic rats. Table 1 in the supplementary methods section summarizes the mean duration of epileptogenic phase and the Racine seizure grade for all the electrically stimulated rats. The rats (E4–E7) provided us with additional data-points to validate epileptogenic circadian modulation in firing activity of PS events following status epilepticus.

In Fig. 1A, we show a representative example of the extracellular activity recorded from the hippocampal CA1 area of an epileptogenic rat during the latent period. Overlaid on the trace, in squares and circles, we show the PS1 and PS2 events, respectively. In Fig. 1B and C, we show the mean shape profile of the PS1 activity and the mean shape profile of the PS2 activity detected from the same rat over a latent time period of 12 days of recordings using a modification of a well-known spike clustering algorithm [12].

The time evolution of the normalized firing rates of PS1 and PS2 from an age-matched control rat (C1) and during the latent period in an epileptogenic rat (E2) is shown in Fig. 2A–D. Key points worth mentioning from Fig. 2 are: (1) there exists a circadian-like modulation in the firing rate of the PS1 and PS2 activity both during the control and the latent time periods; (2) there is no observed drift in the firing rate of the PS1 and PS2 activity in the data obtained from control rats (Fig. 2A and C); (3) during the latent period there is a marked upward drift in the firing rate of PS1 and a corresponding marked downward drift in the firing rate of the PS2 (Fig. 2B and D); (4) the circadian-like modulation of firing rates of PS1 and PS2

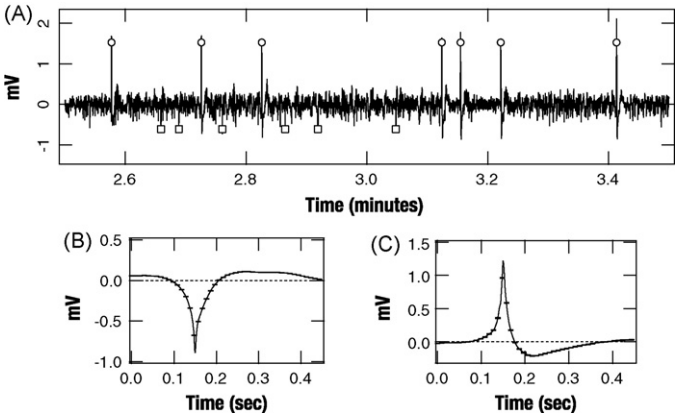

Fig. 1. (A) Sample 1 min trace of extracellularly recorded brain electrical activity from the hippocampal CA1 area. Overlayed on the trace are the times of occurrences of spontaneous population spikes, squares representing the type 1 population spikes (PS1) and circles representing the type 2 population spikes (PS2), (B) mean shape profile of PS1 and (C) mean shape profile of PS2.

are locked in-phase during the control period (Fig. 2E), while during the latent period the two PS oscillate anti-phase with respect to each other (Fig. 2F), with a marked shift in the rhythmic activity of PS1; (5) the average number of PS1 events per hour recorded during the latent period in the three epileptogenic rats are significantly greater ($p \approx 0.0026$; two-sample t-test) than that recorded during the control period, while the average number of PS2 events per hour are less ($p \approx 0.058$; two-sample t-test) during the latent period as compared to the pre-status epilepticus control period in these rat (Fig. 2G and H).

In Fig. 3, we summarize the results on the phase shift in the circadian-like firing activity of the two PS and the imbalance in their firing rates during the latent period from the PS data obtained from 3 epileptogenic (E1, E2, E3) and 2 controls (C1, C2). The imbalance in the firing rates is quantified by estimating the drift $D = \langle df/dt \rangle$ (f: firing rate) in the firing activity of both PS1 and PS2 through a least-squares fit of the drift in the baseline-firing rate to a straight line, $\Delta f = D\,\Delta t + c$. In Fig. 3A, we plot the mean value of D (with error bars representing the standard error corresponding to 95% confidence interval). From Fig. 3A, we see that, while the firing rates are in balance ($D \approx 0$) in controls, $D > 0$ during the latent period in epileptogenic rats ($p \approx 0.0044$, two-sample t-test). This implies an evolving imbalance in the firing activity of the two PS. The phase relationship between the circadian like firing activity of the PS1 and PS2 is quantified through a least squares-fit of the detrended-modulo 24 firing rate data (detrending implies the removal of the drift in the baseline of the circadian-like rhythm of firing rate) with a sinusoidal function $f(t) = a\sin(\omega t + b)$, with $\omega = 7.2722 \times 10^{-5}$ Hz. The phase is associated with the time T_X (X = PS1, PS2) of maximum value obtained by $f(t)$ and is given as: $\Phi_X = 2\pi T_X/24$. The mean value of phase for the two PS (with standard error corresponding to 95% confidence interval) is shown in Fig. 3B. The relative phase difference is quantified as $\Delta\Phi = |\Phi_{PS1} - \Phi_{PS2}|$. In-phase firing activity of the two PS is considered to occur when $\Delta\Phi \leq \pi/2$. We see that during the control period, the two PS events are phase-locked with a lag of around $\pi/4$ radians, however during the latent period, the phase lag increases to approximately $3\pi/4$ radians. The phase shift $\Delta\Phi$ in the relative phase for the epileptogenic rat is significantly greater than that for the control rat ($p \approx 7.3775 \times 10^{-5}$, two-sample t-test).

We have proposed a CC hypothesis, which suggests that the evolving imbalance in the PS1 and PS2 firing rates is the result of an abrupt phase-shift in their circadian activity. In order to study the implications of this hypothesis in the context of our experimental results as presented above, we consider a simple two-dimensional

Please cite this article in press as: S.S. Talathi, et al., Circadian control of neural excitability in an animal model of temporal lobe epilepsy, Neurosci. Lett. (2009), doi:10.1016/j.neulet.2009.03.057

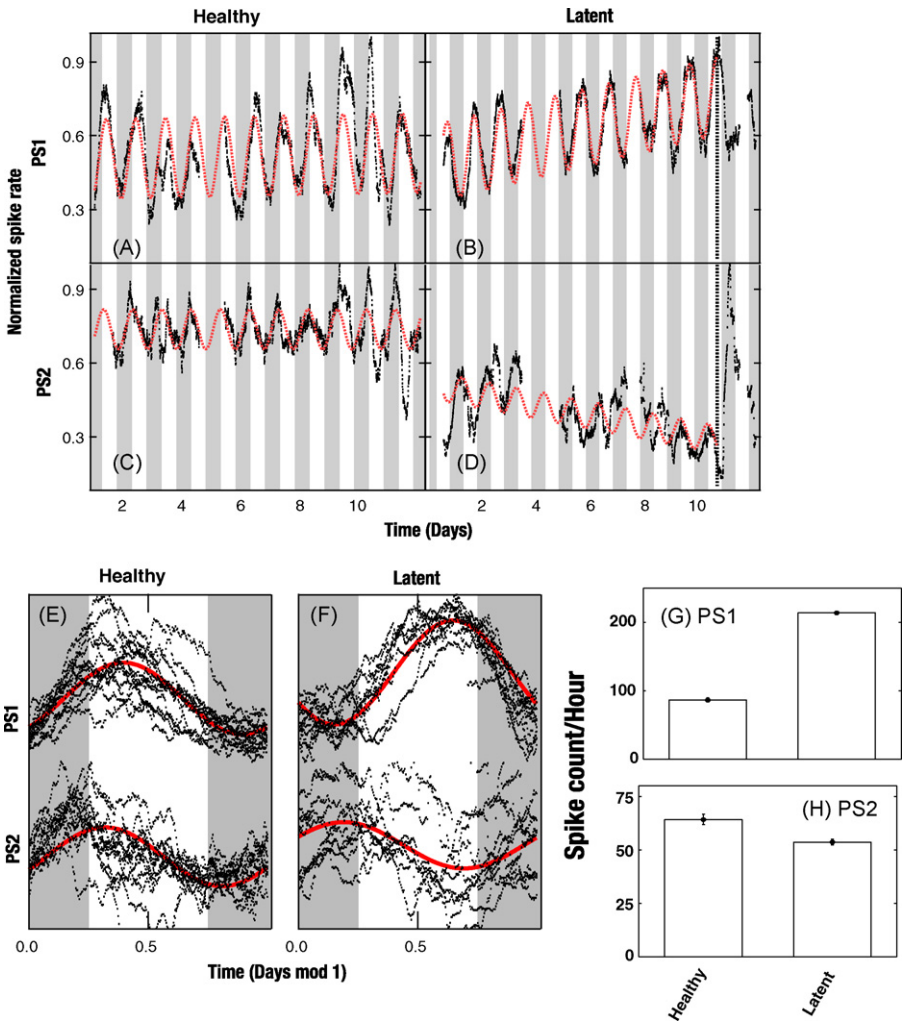

Fig. 2. In A–D we shown the firing rates of type 1 (PS1) and type 2 (PS2) population spikes recorded from a control rat (C1) and an epileptogenic rat (E2) during the latent period. Red dotted lines represent the least-squares fit of the firing rate data to a function $f(t) = at + b\sin((t + c)$ where $\omega = 7.2722 \times 10^{-5}$ Hz. The fitted line is shown as a guide for the eye to follow the circadian pattern in the firing activity of PS. The gaps in the firing rate data (around day 5 in both control and latent period) reflect the absence of recordings on those days due to technical problems. The phase of circadian oscillations of PS1 and PS2 from the control rat and the epileptogenic rat are shown in (E) and (F), respectively. The red line is a least squares fit to the phase data with a function $f(t) = \alpha\sin(\omega t + \beta)$, where $\omega = 2\pi$. The diurnal day–night cycle is shown in the background. The dotted line in (B) and (D) shows the time of occurrence of the first spontaneous epileptic seizure. The average number of PS1 and PS2 events observed per hour during the pre-status epilepticus control time period and the epileptogenic latent period in rat E2 are shown in (G) and (F), respectively.

Wilson–Cowan model for the interaction between the PS1 and PS2 activity. The Wilson–Cowan model describes the dynamics of interaction firing activities of populations of excitatory and inhibitory neurons [23]. In the Fig. 4A and B, we show the schematic diagram of the interactions between the PS in controls and the epileptogenic rats under the assumption that PS1 and PS2 represent the synchronous firing of populations of excitatory and inhibitory neurons, respectively. We have made two specific assumptions in the development of our modified version of the Wilson–Cowan model for PS1 and PS2 interactions. (1) PS1 represents the synchronous firing of populations of excitatory neurons. This assumption is based on the observation that the firing rate of PS1 during the latent period of epileptogenesis increases as one gets nearer in time to the first spontaneous seizure. (2) PS2 events represent the synchronous firing of population of inhibitory neurons. This assumption is based on the observation that the firing rate of PS2 decreases during the latent period of epileptogenesis. These assumptions allow us to incorporate anatomical connectivity patterns within the CA1 region [10,13,14] into the model to test our hypothesis that the relative shift in the circadian phase results in a sustained increase in the firing rate of PS1, and a concurrent decrease in the firing rate of PS2. However, we note that our experimental approach of continuous long-term *in vivo* recording using a chronically implanted microwire electrode array precludes us from conclusively demonstrating the synaptic origin of the population spikes reported here. In summary, epileptic seizures are known to be associated with increased excitability within the CA1 pyramidal cells. Thus, the association of PS1 patterns with excitation and the PS2 pattern with inhibition conforms to the notion of increased excitation within the hippocampus resulting in the development of spontaneous epileptic seizures. If, then, within the framework of our modified Wilson–Cowan model, we take a coupled pair of ordinary differential equations (ODEs) governing the evolution of $X(t)$ and $Y(t)$ representing the firing rates of PS1 and PS2, respectively, we have:

$$\begin{aligned} \tau_x \frac{dX}{dt} &= -X + S(A\ \sin(\omega t + \Delta\Phi) + c_1 X - c_2 Y + P) \\ \tau_y \frac{dY}{dt} &= -Y + S(B\ \sin(\omega t) + c_3 X - c_4 Y + Q) \end{aligned} \tag{1}$$

where $\tau_x \ll \omega^{-1}$ and $\tau_y \ll \omega^{-1}$. $S(x) = [1 + \exp(-\alpha x)]^{-1}$ is the response function [23]. c_j ($j = 1 \ldots 4$) represents the strength of local interactions between the population of excitatory and inhibitory

Please cite this article in press as: S.S. Talathi, et al., Circadian control of neural excitability in an animal model of temporal lobe epilepsy, Neurosci. Lett. (2009), doi:10.1016/j.neulet.2009.03.057

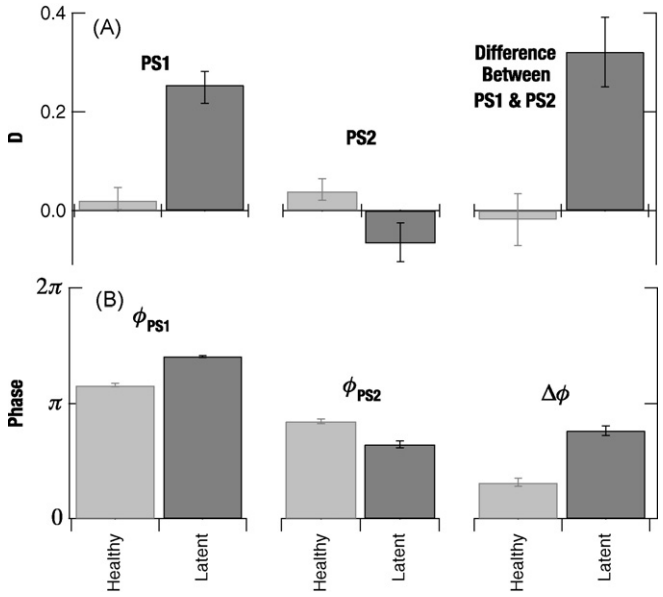

Fig. 3. The mean amplitude of the drift in the firing rate, D and the circadian phase shift in the relative firing activity of the type 1 (PS1) and type 2 (PS2) population spikes during the control and the latent periods are shown in (A) and (B), respectively.

neurons in the CA1 area. The necessary condition for the coupled pair of ODEs in Eq. (1), to exhibit intrinsic stable limit cycle in absence of external sinusoidal driving ($A = B = 0$) is, $c_1 \neq 0$ [17]. However, based on our assumptions (See Fig. 4A and B), c_1 represents the recurrent interaction between populations of excitatory

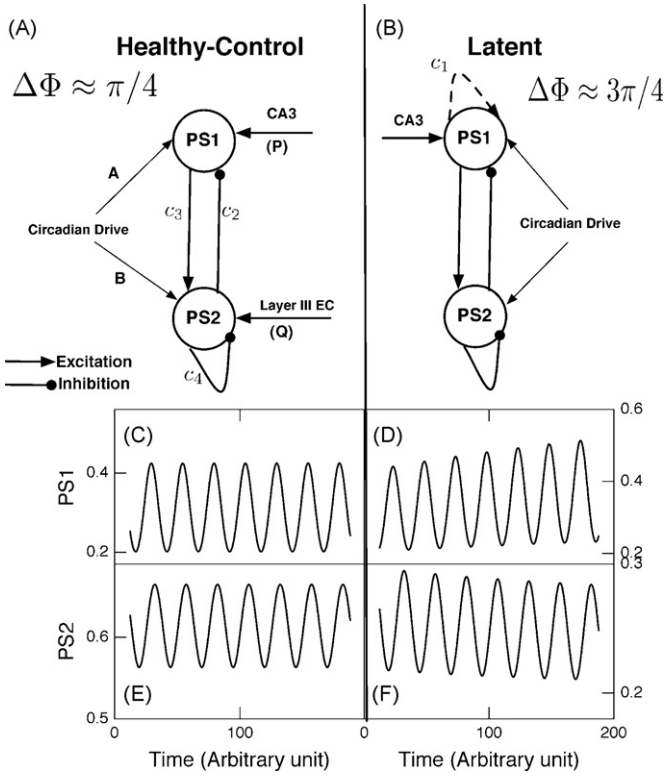

Fig. 4. In A and B we present the schematic diagram of the interaction between the type 1 (PS1) and the type 2 (PS2) population spikes in control and the latent period. The PS1 and PS2 firing activity generated by the model (Eq. (1)) for the control and the latent period are shown in (C) and (D). The model parameters are, $A = 0.5$, $B = 0.25$, $\omega = 2\pi/25$, $\tau_x = \tau_y = 1$, $\tau_L = 200$, and $p = 0.025$ for both the control and the latent time periods. $Q = 1.9$ for control period and $Q = 0$ for the latent time period.

neurons in the CA1 area that give rise to the PS1 activity. Moreover, it is known from the anatomy of network connectivity within the CA1 network, there are sparse recurrent connections between the CA1 excitatory neurons [13]. Additionally, the synaptic time scale of interaction between the populations of neurons in the CA1 is much faster than the circadian-like activity of PS (Fig. 2). Therefore, in our modeling of the firing activity of the two PS through Eq. (1) above, we assume that the origin of circadian-like oscillations in the hippocampal CA1 is from an external source. Although we are not aware of any direct anatomical pathway into the CA1 through which the circadian drive can influence the CA1 activity, there is evidence for the influence of a circadian cycle or drive on synaptic activity within the CA1 [2,6].

Accordingly, the circadian influence in Eq. (1) is modeled through an external sinusoidal input to X and Y. A and B represent the strength of external circadian drive onto both PS1 and PS2 activity, respectively, and $\Delta\Phi$ represents the phase difference in the time of circadian drive to the two classes of population spikes that are modulated following brain injury. P represents the excitatory input from the hippocampal CA3 Shaffer collateral–commissural projections onto the CA1 excitatory neurons [1]. Q represents the excitatory input onto the CA1 interneurons via the temporoammonic pathway from the layer III of the entorhinal cortex [14]. Finally, according to the CC hypothesis, the asymptotic strength of interaction between the PS1 and PS2 activity, c_j^∞ is considered to be dependent on the phase-lag $\Delta\Phi$ of the circadian input that drives the PS1 and PS2 firing activity. The asymptotic strength of the interaction terms is modeled through a linear dependence on $\Delta\Phi$, $c_j^\infty = \alpha_j + \beta_j \Delta\Phi$ and the differential equation governing the evolution of c_j is given by $dc_j/dt = (c_j^\infty - c_j)/\tau_L$, where $\tau_L \ll \omega^{-1}$. The parameters used in our simulation example are $(\alpha_1, \alpha_2, \alpha_3, \alpha_4) = (0.65, -0.015, 0, 0.32)$ and $(\beta_1, \beta_2, \beta_3, \beta_4) = (0, 0.05, 0.1, 0.5)$. In Fig. 4C–F we show the output from our model, simulating the conditions from our experimental findings (Figs. 2 and 3). For $\Delta\Phi = 3\pi/4$, representing the condition observed in controls (Fig. 2A and C), we see from Fig. 4C and E that the firing rates of both PS1 and PS2 exhibit circadian rhythmicity with the maintenance of balance in the relative firing rate of two patterns. During the latency period, there is a sudden shift in the phase of circadian drive onto two populations of interacting neurons resulting in $\Delta\Phi = 3\pi/4$. This, in turn, results in modulation in the interaction terms c_j through the homeostatic learning rule. Additionally, due to the selective loss of neurons in layer III of the entorhinal cortex in the animal model of limbic epilepsy [10], parameter $Q = 0$. As a result, there is a sudden decrease in the firing rate of PS2 activity. The non-linear interaction between the firing rates of PS through Eq. (1), then results in further decrease in firing activity of PS2 and a corresponding increase in the firing rate of PS1 activity (Fig. 4D and F). Thus, using the constraints imposed through the CC hypothesis and the anatomy of network connectivity within the CA1, this simple model (Eq. (1)) is able to replicate our experimental finding of evolving imbalance in firing activity of the two PS following brain injury.

All the simulation results presented above were performed using a 4th order Runge–Kutta method for differential equations. The source code will be made available from SST upon request.

In conclusion, we present experimental evidence for an evolving imbalance in brain excitability following injury, as characterized by the firing activity of the two distinct classes of PS. We note that the synaptic origin of these PS events cannot be discerned in the context of the experimental paradigm of continuous long-term *in vivo* recordings of extracellular activity within the hippocampus. We have shown that the imbalance in the PS firing rates is accompanied with a phase shift in the circadian rhythm of their relative firing activity. Based on this experimental observation we have proposed a circadian control mechanism for the phase-induced

Please cite this article in press as: S.S. Talathi, et al., Circadian control of neural excitability in an animal model of temporal lobe epilepsy, Neurosci. Lett. (2009), doi:10.1016/j.neulet.2009.03.057

imbalance in the observed firing activity of the two PS. We test the implications of the circadian control of PS activity using a modified two-dimensional Wilson–Cowan model. Two key assumptions: the recorded PS events in the hippocampal CA1 area represent interaction between excitatory and inhibitory population of neurons, and the firing rate of these PS is under circadian control, allowed us to model the observed temporal dynamics of PS within the framework of the Wilson–Cowan model, under the two conditions of control and epileptogenic state of the brain, in order to elucidate the circadian influence on the pathophysiology of an evolving brain disease.

Acknowledgements

The National Institutes of Biomedical Imaging and Bioengineering (NIBIB) through Collaborative Research in Computational Neuroscience (CRCNS) Grant Numbers R01 EB004752 and EB007082, the Wilder Center of Excellence for Epilepsy Research, and the Children's Miracle Network supported this research. SST was partially supported through fellowship award from the Epilepsy Foundation of America.

Appendix A. Supplementary data

Supplementary data associated with this article can be found, in the online version, at doi:10.1016/j.neulet.2009.03.057.

References

[1] P. Andersen, T.V.P. Bliss, K.K. Skrede, Lamellar organization of hippocampal excitatory pathways, Exp. Brain Res. 13 (1971) 222–238.
[2] C.A. Barnes, B.L. McNaughton, G.V. Goddard, R.M. Douglas, R. Adamec, Circadian rhythm of synaptic excitability in rat and monkey central nervous system, Science 197 (1977) 91–92.
[3] A. Bragin, G. Jando, Z. Nadasdy, M. van Landghem, G. Buzsaki, Dentate eeg spikes and associated interneuronal population bursts in the hippocampal hilar region of the rat, J. Neurophysiol. 73 (4) (1995) 1691–1705.
[4] R.P. Brenner, Eeg in convulsive and nonconvulsive status epilepticus, J. Clin. Neurophysiol. 21 (2004) 319–331.
[5] G. Buzsaki, Hippocampal sharp waves: their origin and significance, Brain Res. 398 (1986) 242–252.
[6] D. Chaudhary, L.M. Wang, C.S. Colwell, Circadian regulation of hippocampal long term potentiation, J. Biol. Rhythms 20 (2005) 225–236.
[7] H. Cline, Synaptogenesis: a balancing act between excitation and inhibition, Curr. Biol. 15 (2005) R203–R205.
[8] R. Cossart, C. Dinocourt, J.C. Hirsch, A. Merchan-Perez, J. De Felipe, Y. Ben-Ari, C. Esclapez, M. Bernard, Dendritic but not somatic gabaergic inhibition is decreased in experimental epilepsy, Nat. Neurosci. 4 (2001) 52–62.
[9] G.W. Davis, Homeostatic control of neural activity: from phenomenology to molecular design, Ann. Rev. Neurosci. 29 (2006) 307–323.
[10] F. Du, R. Schwarcz, Amino-oxyacetic acid causes selective neuronal loss in layer iii of the rat medial entorhinal cortex, Neurosci. Lett. 147 (1992) 185–188.
[11] L. El-Hassar, M. Milh, F. Wendling, N. Ferrand, M. Esclapez, C. Bernard, Cell domain-dependent changes in the glutamatergic and gabaergic drives during epileptogenesis in the rat ca1 region, J. Physiol. 578 (2007) 193–211.
[12] M.S. Fee, P.P. Mitra, D. Kleinfeld, Automatic sorting of multiple unit neuronal signals in the presence of anisotropic and non-Gaussian variability, J. Neurosci. Methods 69 (1996) 175–188.
[13] W.B. Knowles, P.A. Schwartzkroin, Local circuit synaptic interactions in hippocampal brain slices, J. Neurosci. 1 (1981) 318–322.
[14] J.C. Lacaille, P.A. Schwartzkroin, Stratum lacunosum-moleculare interneurons of hippocampal ca1 region. ii. Intras-matic and intradendritic recordings of local circuit interactions, J. Neurosci. 8 (1988) 1411–1424.
[15] R.R. Llinas, U. Ribary, D. Jeanmonod, E. Kronberg, P.P. Mitra, Thalamocortical dysrthythmia: a neurological and neuropsychiatric syndrome characterized by magnetoencephalography, Proc. Natl. Acad. Sci. 96 (1999) 15222–15227.
[16] E.W. Lothman, E.H. Bertram, J.W. Bekenstein, J.B. Perlin, Self sustaining limbic status epilepticus induced by continuous hippocampal stimulation; electrographic and behavioral characteristics, Epilepsy Res. 3 (1989) 107–119.
[17] L.H.A. Monteiro, M.A. Bussab, B.J.G. Chaui, Analytical results on Wilson–Cowan neuronal network modified model, J. Theor. Biol. 219 (2002) 83–91.
[18] J.L. Rubenstein, M.M. Merzenich, Model of autism: increased ratio of excitation/inhibition in key neural systems, Genes Brain Behav. 2 (2003) 255–267.
[19] J.C. Sanchez, T.M. Mareci, W. Norman, J. Principe, W.L. Ditto, P.R. Carney, Evolving into epilepsy: multiscale electrophysiological analysis and imaging in an animal model, Exp. Neurol. 198 (2006) 31–47.
[20] H.S. Singer, K. Minzer, Neurobiology of tourette's syndrome: concepts of neuroanatomic localization and neurochemical abnormalities, Brain Dev. 25 (2003) S70–S84.
[21] S.S. Talathi, D.U. Hwang, M.L. Spano, J. Simonotto, M.D. Furman, S.M. Myers, J.T. Winters, W.L. Ditto, P.R. Carney, Non-parametric early seizure detection in an animal model of temporal lobe epilepsy, J. Neural. Eng. 5 (2008) 85–98.
[22] A. Wassef, J. Baker, L.D. Kochan, Gaba and schizophrenia: a review of basic science and clinical studies, J. Clin. Psychopharmacol. 23 (2003) 601–640.
[23] H.R. Wilson, J.D. Cowan, Excitatory and inhibitory interactions in localized populations of model neurons, Biophys. J. 12 (1972) 1–24.

Please cite this article in press as: S.S. Talathi, et al., Circadian control of neural excitability in an animal model of temporal lobe epilepsy, Neurosci. Lett. (2009), doi:10.1016/j.neulet.2009.03.057